Alma Mater Studiorum – Università di Bologna

DOTTORATO DI RICERCA IN

Ingegneria civile, chimica, ambientale e dei materiali

Ciclo 35

Settore Concorsuale: 09/D2-SISTEMI, METODI E TECNOLOGIE DELL'INGEGNERIA CHIMICA E DI PROCESSO

Settore Scientifico Disciplinare: ING-IND/24-PRINCIPI DI INGEGNERIA CHIMICA

Chemical looping reforming from methane to syngas: investigation on CeO_2 oxygen carrier lifetime and optimal process times

Presentata da: Alba Storione

Coordinatore Dottorato

Prof. Alessandro Tugnoli

Supervisore

Prof. Ferruccio Doghieri

Correlatori

Prof. Matteo Minelli
Eng. Francesco Miccio

Esame finale anno 2023

Abstract

Emissions of CO_2 are constantly growing since the beginning of industrial era. A historical value of 33.1 Gt CO_2 emitted per year was reached in 2018, while a slight decrease of this value was observed during the covid pandemic.

Trend monitoring suggests the occurrence of a scenario where the carbon budget necessary to stay within the 1.5° C warming will be sufficient for 9.5 ± 0.1 years (2031) or 6.6 ± 0.1 years (2028) depending on the estimated likelihood level, of 67% and of 83%, respectively.

Interruption of the production of major emitters sectors (energy and agriculture) is not a viable way and reducing all the emission through carbon capture and storage (CCS) is not economically viable and little publicly accepted, therefore, it becomes fundamentals to take actions like retrofitting already developed infrastructure employing cleanest resources, modify the actual processes limiting the emissions, and reduce the emissions already present through direct air capture.

The present thesis will deeply discuss the aspects mentioned in regard to syngas and hydrogen production since they have a central role in the market of energy and chemicals.

Together with an overview of the main advantages and limitations of the processes actually employed for their production, the discussion will consider which steps are critical from an emission perspective, and the mitigation strategies commonly adopted.

Among the strategies discussed, greater emphasis is given to the application of looping technologies and to direct air capture processes, as they have been the main point of this work.

Particularly, chemical looping methane reforming to syngas was studied with Aspen Plus thermodynamic simulations, thermogravimetric analysis characterization (TGA) and testing in a fixed bed reactor.

The process was studied cyclically exploiting the redox properties of a Ce-based oxide oxygen carrier synthetized with a simple forming procedure. The two steps of the looping cycles were studied isothermally at 900 °C and 950° C with a mixture of 10 %CH_4 in N_2 and of 3% O_2 in N_2, for carrier reduction and oxidation, respectively.

The effect of the process times on carbon deposition, specific syngas yields, and selectivity, was inspected, together with the investigation of best conditions to fully regenerate the carrier, adjust the syngas final ratio, and ensure stable performances.

During the stay abroad, in collaboration with the Swiss Federal Institute of Zurich, a CO_2 capture process in presence of amine solid sorbents was investigated, studying the difference in the performance achievable with the use of contactors of different geometry (pellet, monolith at closed and open channels).

The process was studied at two concentrations (382 ppm CO_2 in N_2 and 5.62% CO_2 in N_2) and at different flow rates, to understand the dynamics of the adsorption process and to define the mass transfer limiting step.

The study confirmed the closed-channel monolith as the most promising contactor for the adsorption stage, among those explored, with a productivity per unit of sorbent mass greater than 100% and a decrease in energy penalty of 68% when compared with pellets.

Contents

1 Introduction

In daily life, huge amounts of carbon dioxide are continuously emitted to the atmosphere, to meet the needs of humankind. Indeed, the demand for energy and chemicals is constantly increasing, largely driven by the economy and the population growth, started after the pre-industrial era. As a consequence, an extensive amount of CO_2 is released in the atmosphere, causing a rise in the concentration of CO_2 in air that determines a change in CO_2 composition from value around 250ppm with periodic fluctuations, never exceed 300 ppm, to the actual 420ppm. [1,2]

Fig. 1 shows the impact on the emission brought by several countries, and it evidences among them the larger emitters in China and United States.

These two countries are identified to be part of the ten main emitters together with India, Russia, Japan, Germany, South Korea, Iran, Saudi Arabia, and Indonesia, and all of them are estimated to be responsible for over the 68% of the global CO_2 emissions. [3]

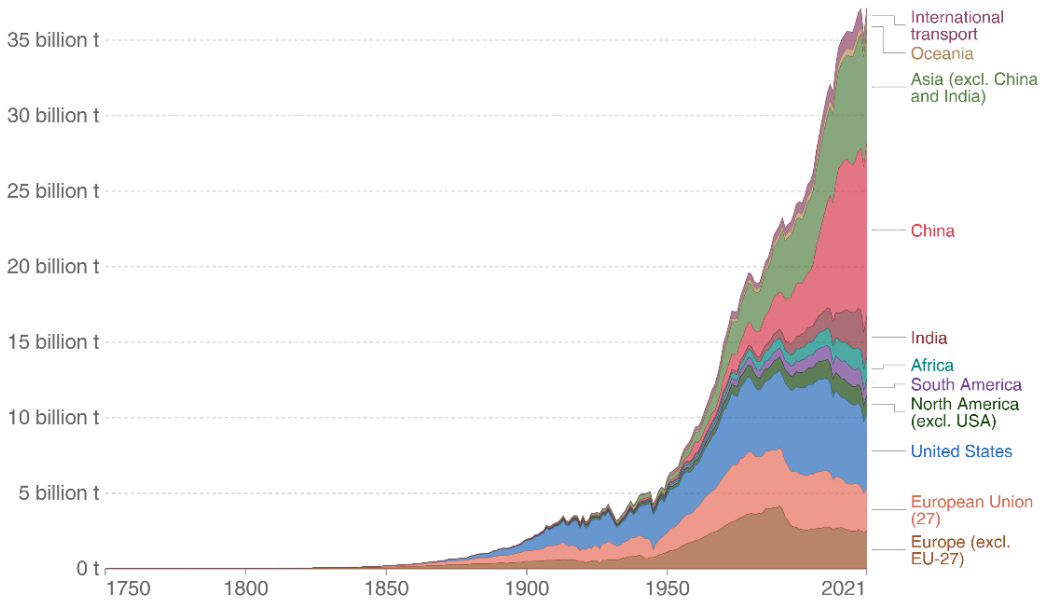

Figure 1: Annual CO_2 emissions by world region. Here are reported fossil fuel and industry emissions without considering fossil emissions derived from land use change, deforestation, soils, or vegetation.[4]

Fig. 2 displays how these emissions are distributed on the various sectors; energy accounts for almost three-quarters of the overall emissions balance, while the other quarter is occupied by agriculture, industry, and wastes. The share for transport (rail, aviation, shipping) and for energy use in industry (mainly heating), has the highest weight on the total energy emissions, and this is related to the difficulty to electrify these two sectors. This is, in part due, to the fact that the electricity system has not the capacity to cover the heating demand; indeed, in most European countries, the demand factor for heating and cooling is 2.5 times higher than the current rate of electrification. [5]

In addition, at the present time, only one third of the total electricity production relies on renewables and, being far from being fully decarbonized, electricity cannot reasonably be considered as a backbone for the heating sector. Also until the electricity is not fully carbon free, it could not support properly even the transport sector because the deployment of electric vehicles could imply a large increase in the energy demand to power their batteries and even if direct emissions from transport can be reduced, without a strong system which regulates the equilibrium between transport and energy sector, these emissions would be shift from the transport sector to the power sector.[6]

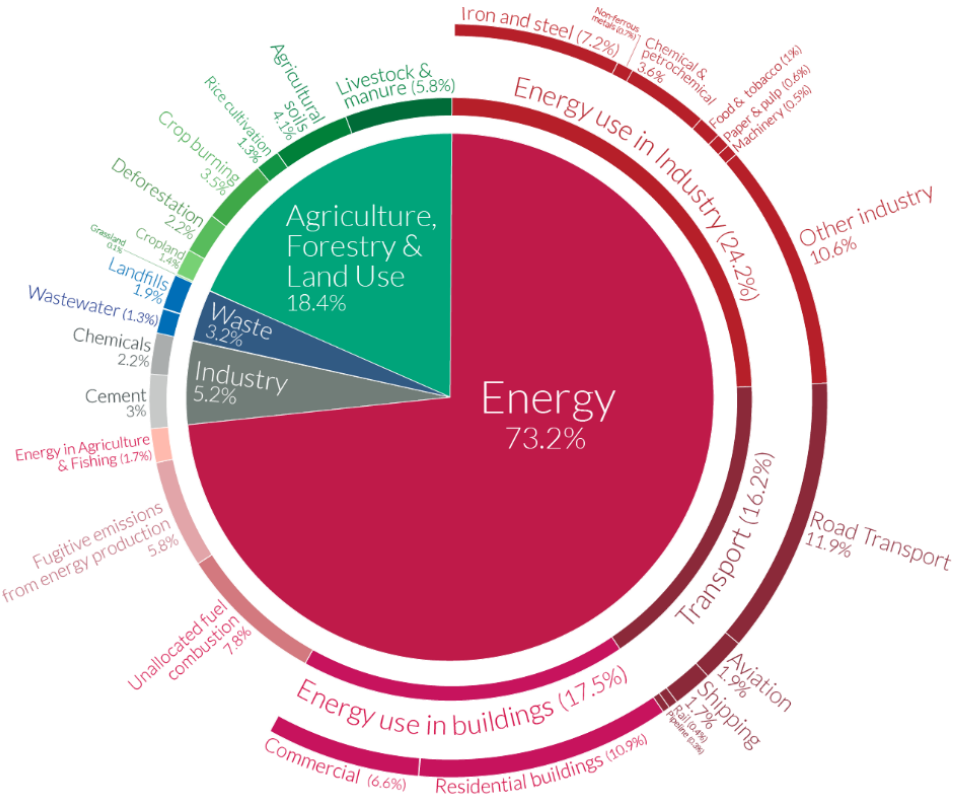

Figure 2: Global greenhouse gas emissions by sector for the year 2016. [4]

According to International Energy Agency (IEA) data, yearly CO_2 emissions around the world increased from 20.5 Gt/a to 32.8 Gt/a in the years between 1990–2017.[7]

The CO_2 emissions reached a historical value of 33.1 Gt CO_2/a in 2018, [8] while they exhibited a reduction in 2020, due to the restrictive policies applied as a consequence of the global pandemic caused by COVID-19, followed by an increase of 4.8% in the 2021 (between 34.6–35.2 $GtCO_2$/a). At this latter estimate, if no notable action is taken, the carbon budget to stay within the warming of 1.5° C might be used within 9.5 $\pm$ 0.1 years (2031) or 6.6 $\pm$ 0.1 years (2028) depending on the likelihood level, respectively of 67% and 83% for the two cases. The same calculations done to predict the scenario to contain the earth's warming within 2°C shows the probable end of carbon budget to occur in 31.0 $\pm$ 0.3 years (67% likelihood) or in 23.8 $\pm$ 0.3 years (83% likelihood).[9]

This implies an urgent need to switch from fossil fuels to renewable resources, and to retrofit the actual plants to make renewable energy an alternative profitable.

Currently, the market is still dominated by fossil usage, Fig. 3 and Fig.4 shows the actual global trend in the usage of available resources, reported on an open-source database. The imagines clearly show the dominance of the fossil fuels utilization on renewables. However, in the last years an increase in the utilization of the low carbon sources (which is the sum of nuclear and all the renewables) has been recorded. Nevertheless, further efforts are still necessary to fully implement processes based on renewables, due to their novelty respect to the proven knowledge on the mature technologies employed in the processing of fossil fuels.

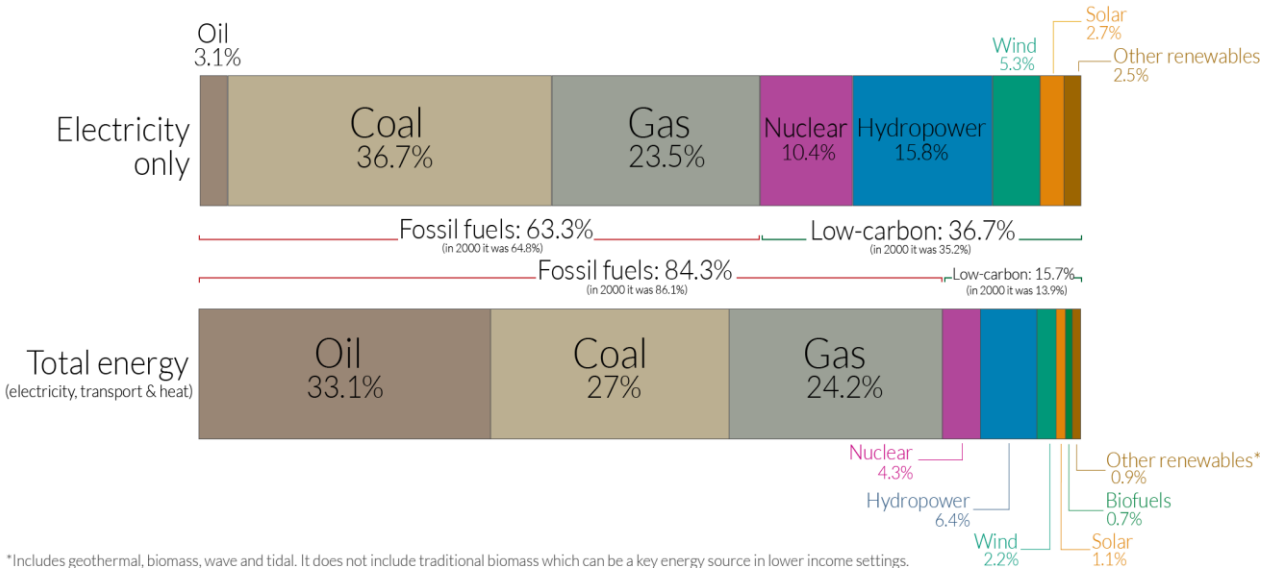

Figure 3: Global energy and electricity breakdown of the employed resources. [10]

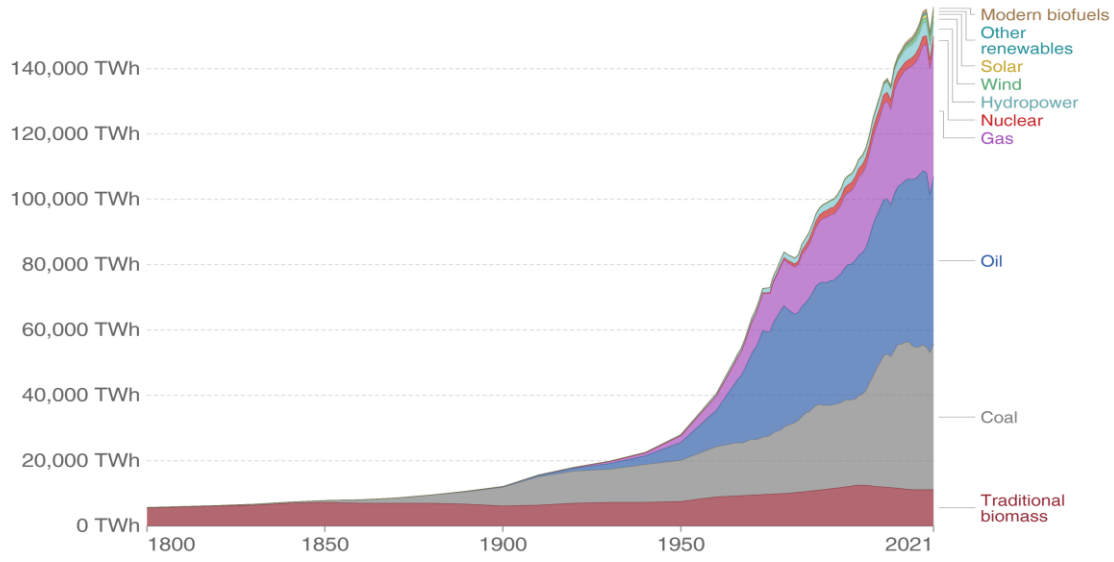

Figure 4 Global direct primary energy consumption: contribution of renewable and fossil resources. [10]

Renewables cannot represent alone an immediate solution in the supply of energy, and a diversification of the resources employed is necessary to find a trade-off between environmental requirements and the needs of humankind.

In this prospective, there are several possible strategies to mitigate the negative effect related to the utilization of fossil fuels, and between them one accepted compromise is offered by the switch from coal to natural gas, which is largely available, cleanest, and it offers comparable performance to coal. Therefore, it can be a bridge in the transition toward a sustainable economy.[11]

Natural gas reserves are derived from reservoirs that contain water, carbon dioxide, crude oils, and other substances.

The principal component is methane that has the highest heat of combustion per CO_2 emitted, compared to other hydrocarbons.[12]

It also has a higher hydrogen to carbon ratio thus bringing a greater yield of higher hydrocarbons and high processes efficiency. Together with these advantages, natural gas is recognized to be a less impacting source for air pollution with respect to bioenergy and the common fuels (Fig. 5).

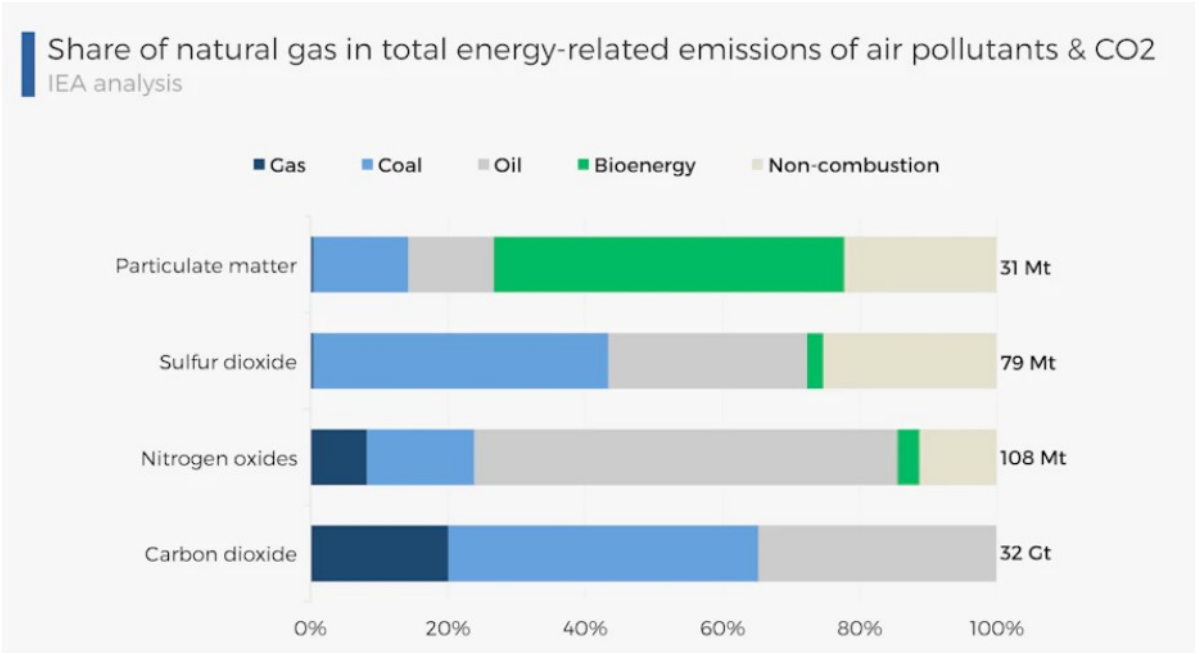

Figure 5: Share of natural gas in total energy-related emissions of air pollutants and CO_2 (one year reference).[13]

As evident from the contaminants breakdown, natural gas is the earth's cleanest burning hydrocarbon: from its combustions is produced 10% of nitrogen oxide (NO_x), virtually no SO_2 emissions and negligible levels of particulate matter (PM) being comparable the amount of energy produced from oil, coal and natural gas as previously reported with Fig. 3.

The US Energy Administration frequently reports on its distribution and gives information on which reserves are recoverable based on current technology and prices.

Fig. 6 shows the distribution of natural gas reserves in the world in both convention and unconventional form, (coal bed methane (CBM), tight and shale gas).

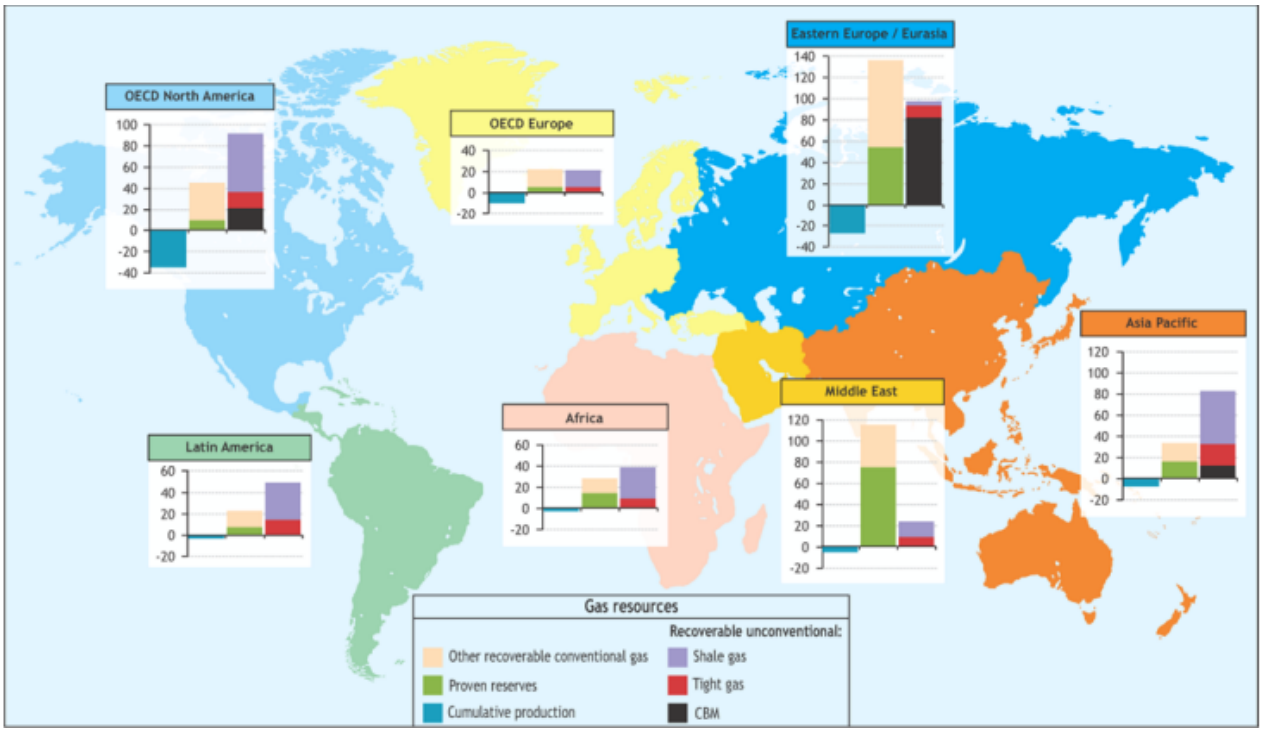

Figure 6: World natural gas resources by major region.[14]

Conventional recoverable resources are estimated to be equivalent to more than 120 years of current global consumption, while total recoverable resources could sustain today's production for over 250 years.[14]

For all these reasons, in this work has been chosen to study methane as feedstock rather than renewables resources.

1.1 Energy and syngas: role on the market

As emerged from an analysis carried out by Global Industry Analysts, two-thirds of the global syngas are consumed by Asia-Pacific, Middle East, and African countries with the Asia Pacific accounting for more than 48% of the market share of syngas and its derivatives market in 2020 (Fig. 7)

In this latter year, globally, syngas and its related market recorded volumes of 180,000 MWth, and it has been estimated to expand at a compounded average growth rate (CAGR) of 9.1% from 2021 to 2031 approaching volumes of production around 469,000 MWth. [15]

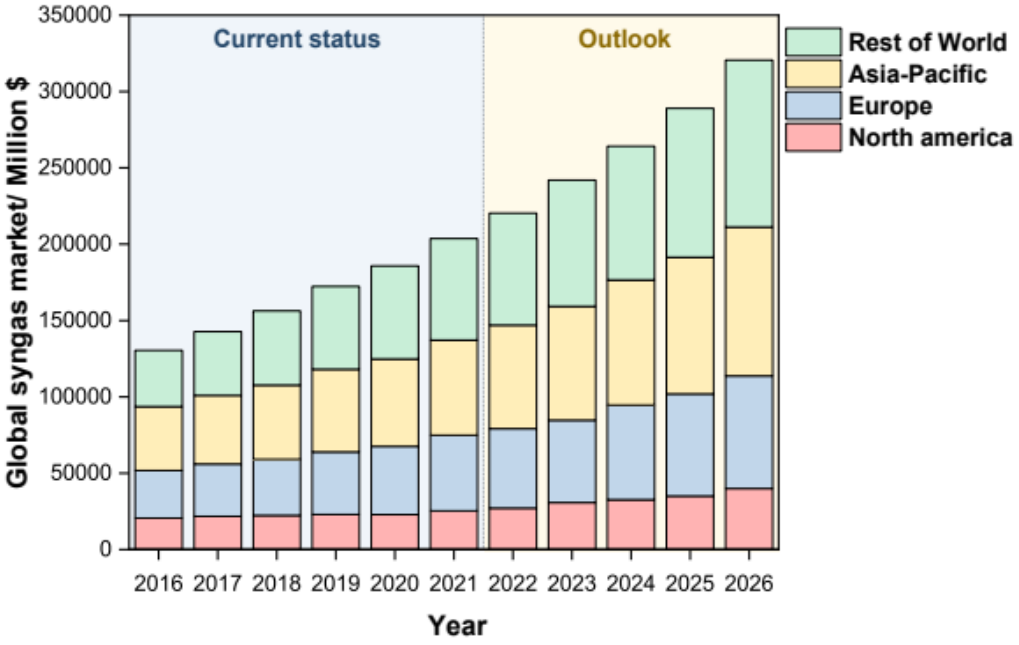

Figure 7: Market trend of syngas.[15]

One clear advantage to investing in this market is the versatility associated with the syngas downstream processing; chemicals, power generation, liquid fuels, and gaseous fuels are the major end-use industries where syngas is used.

Their use ranges from the obtainment of energy to pharmaceutical and cosmetics, with applications also in the food chain and in the polymer industry (Fig. 8).

The possible application is strictly related to the H_2/CO ratio; synthesis gas at high hydrogen content and molar ratio over 50 are more often involved in the energy generation, while if the syngas is further purified to hydrogen, this latter found different uses in the energy field, among which common example are ammonia synthesis, fertilizers production and pre-treatment of raw compounds for refinery (hydrotreating and hydrocracking).

Mixtures at low ratio H_2/CO ratio, instead, are generally utilized for methanol and dimethyl ether (DME) production, which are important industrial feedstocks employed as transportation fuels.

A syngas ratio close to two results particularly suitable for the Fisher-Tropsch synthesis to achieve liquid hydrocarbons at high molecular weight.

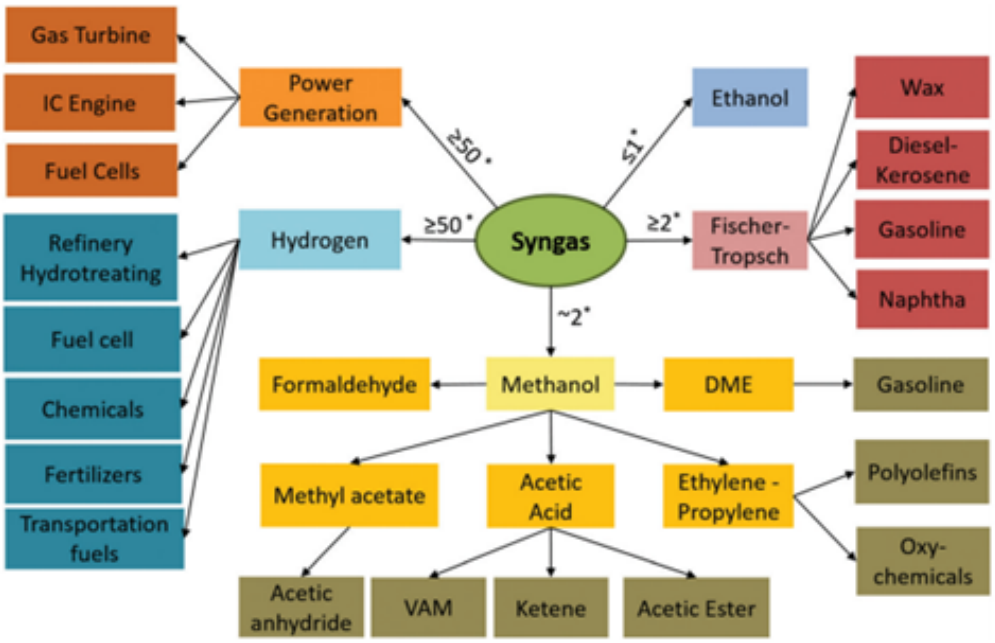

Figure 8: Syngas derivatives with reference to their composition (H_2/CO molar ratio).*[16]

Hydrogen and syngas market are strictly interconnected, and so are the processes applied for their production, indeed in most cases the syngas is an intermediate. Specifically, around 96% of hydrogen is currently generated together with the syngas from fossil fuels, 49% of which from natural gas, 29% from liquid hydrocarbons, and ca. 18% from coal, with just a minor share obtained from water electrolysis (4%), due to economical constrains [17].

These numbers suggest that a huge amount of energy is consumed, and they highlight the urgent need to deeply investigate in detail syngas production routes to identify successful strategies to contain the emissions without compromising the market and the economic growth.

1.1.1 Production from renewable resources

At the present time, renewable resources cannot cover chemical and energy needs, so they were not investigated in this thesis work. Nevertheless, for completeness of the discussion, the main processes and limitations associated with the use of renewables are presented.

Resources, which could be classified as renewables, are the ones able to naturally replenish themselves and to provide energy and chemicals without intervening negatively on the carbon cycle. Known examples of them are wind, hydro and solar energy, and biomass. This latter is easily available and reliable, with respect to most of the renewable resources, since it can be stored, transported, and utilized in different locations. However, it has low power density: 0.5 W/m^2 of biomass crops, respect to the wind power (2 W/m^2) and photovoltaic power (10 W/m^2) [8].

The processing of biomass could occur through both thermochemical conversion and anaerobic digestion, widening the range of routes and technologies available for the obtainment of bioenergy and chemicals.

The thermal conversion of biomass through pyrolysis and gasification is a mature technology, as witnessed by the presence of several commercial plants based on their utilization. A recent report drawn up by the International Energy Agency (IEA, 2016) states that most of them is dedicated to the production of liquid fuels (mainly Fischer-Tropsch liquids, methanol, and ethanol), while just a small percentage of the facilities plan to direct the production towards gaseous synthetic natural gas for applications involving its injection in the natural gas grid.

Despite the integration in the chain is viable, the feasibility of this path depends on the ability to further upgrade the synthetic natural gas to fit the quality requirements imposed by the legislation.

Indeed, it is difficult with a process of this type to achieve pure synthetic natural gas (SNG), and impurities and co-products are typically present, instead; Among them H_2 represents a greater problem, since it increases the risk of embrittlement of the piping lines and of leakages, and it also negatively affects the transport capacity due to its lower heating value (approximately 13 MJ/nm^3 vs 40 MJ/nm^3 of natural gas). Indeed, only a content of hydrogen by volume between 5% and 15% is accepted for injection in the United States while a content not exceeding 12% it is allowed in Europe. [8]

Alternatively, to thermochemical treatment, biomass (agricultural wastes, livestock production, landfills) can be transformed into biogas through anaerobic digestion done by microorganisms able to live and reproduce in oxygen free environment (bacteria and methanogens).

The digestion process involves several stages, which end in the obtainment of a mixture of methane, carbon dioxide, number of trace gases, and a digestate, which represents a natural soil conditioner and fertilizer that even the latest regulations equate with the traditional use of chemical fertilizers.

The technology used for the biogas upgrading affects the purity of methane obtained, therefore different technologies will be preferred depending on the application.

Water scrubbing and physisorption separation bring high methane loss (3-5%) in fact, even if the solubility of methane and carbon dioxide in water is quite different, some methane dissolves and it is lost. This limitation is partially solved through the utilization of chemical sorbent, since they can react selectively with CO_2, however the stronger interaction solvent-molecule implies the utilization of heat at higher temperature for the regeneration of the solvent, and this increases the costs.

Chemical absorption technology also has high maintenance costs, especially for larger plants, although it has high energy efficiency, and it allows to obtain methane at high concentration. Cryogenic separation allows for high methane purity, but it has high costs, due to low efficiency.

In almost all the upgrading procedures, it is necessary to remove H_2S. In case of using water scrubbing ,e.g., H_2S dissolves in water which, in turn, becomes corrosive to pipes, while in pressure swing adsorption PSA unit's, its adsorbs irreversibly onto the solid.[18]

When the requirement on CH_4 purity is high, chemical absorption and PSA are appropriate choices.

For applications in combined heat and power generation (CHP), there is no specification on the concentration of methane and thus on the level of biogas upgrading. However, the reduced calorific value of biogas is the main limitation to fully implement it for power and electricity generation from gas turbines.

On the other hand, CHP systems have been in operation for a longer time than the majority of biomethane production plants and they are therefore likely to have reached full depreciation, therefore retrofitting CHP plants can be cheaper than the retrofit of biomethane plants.[19]

The Upgrading process simultaneously generates a CO_2-enriched stream that can be used in enhanced oil recovery (EOR) to reduce emissions. To serve EOR CO_2 must come from upgrading processes that ensure high levels of purity to allow for a good miscibility with oil and to reduce costs of transportation to recovery wells.

EOR accounts for approximately 50 million tons of CO_2 utilization annually, of which around 40 million tons are supplied from natural CO_2 reservoirs at a price generally in the order of 15–19 US$.

The CO_2 stream can also be used as a nutrient for the growth of biomass for other biogas production or exploited to decrease pH in the aluminum extraction process (with minimum CO_2 concentration of 85%).[18]

The interest in biogas is still growing, and it is already widely commercialized; Italy, alone, counts for 2000 plants spread throughout the country with an annual national production, estimated by the Italian consortium for biogas (CIB), of 2.5 billion cubic meters and a prospective to reach 4 billion by 2026. [20]

1.1.2 Syngas production from renewables

From this section on, an in-depth analysis of syngas production will be addressed, due to its strategic role.

Among the renewable alternatives, one of the most travelled roads, is the gasification of biomass which allows to achieve syngas of different quality and composition depending on the operating modes. The main problems encountered during the use and testing of such plants are due to reactor clogging from high tars production and subsequent system shutdown.

Biomass syngas is a combustible gas that can be used to produce electrical energy in turbines and fuel cells. However, it needs several stages of cleaning to be competitive with the common fuels since bio-syngas contains alcohols, ammonia, olefins, natural gas, and many other aromatic compounds. Also, similar to the coal derived syngas, bio-syngas generally contains contaminants among which hydrogen sulfide is the main component, which, despite being present in lesser extent (commonly 0.01 wt.% in biomass against 0.1e5 wt.% of coal), is a hazardous substance that generates acid rain and corrosion. [21]

The final composition determines the heating value contained by the syngas, that is different as shown in table 1, for the different feedstocks: oil refining by-product (pet coke), coal, biomass, and municipal solid waste (MSW).

Feedstock	H_2 (% mol)	CO (% mol)	CH_4 (% mol)	CO_2 (% mol)	HHV (MJ/m^3_n)
Coal	25–30	30–60	0–5	5–15	7–15
Petcoke	22–30	39–48	0–1	18–34	8–11
Biomass	5–16	10–22	1–6	8–20	4–7
MSW	8–23	22–24	0–3	6–15	3–7

Table 1: Syngas composition obtained by gasification of different raw materials.[22]

Due to these reasons, an easy way to exploit bio-syngas is as second fuel in co-firing applications, where it could be used for energy production without any need to retrofit the existing equipment. However, even in this case it is necessary to limit the number of ashes, often present in the biomass, to avoid damage of some components of the burner.

For the case in which the synthesis gas, out of the indirect gasifier, still presents higher amount of methane (10% vol), the production of bio-methane could be the final application since some methane is already present in the mixture to be converted.

Therefore, the efficiency achievable for the methanation process is higher than if the syngas mixture contained only CO, H_2, CO_2, for the same amount of stream to be processed.

Despite the processing of biomass is the most investigated production alternative to fossil resources, several studies also focus on the electrochemical routes. Indeed, if driven by renewable energy, the electrochemical reduction of CO2 can also be attractive to produce syngas.

This approach is based on the co-electrolysis of H_2O/ CO_2 towards H_2/CO to produce syngas or eventually hydrogen. However, there are several limitations which obstacles the commercial implementation of the process, such as the dominance of noble metals-based catalysts and the lack of data on the long-term performance achievable with the employment of the most promising catalysts. [16]

1.1.3 Syngas production through conventional routes

Traditionally, synthesis gas comes from natural gas, residual oils, petroleum, and coal (carbon containing fuels).

The most studied technologies for its production are partial oxidation, dry and steam reforming, and mixed processes where both water and CO_2 can be co-fed as oxidant agents.

Among all, steam methane reforming (SMR) is the only process widely commercialized, indeed from its utilization comes the greater share of the world's hydrogen and syngas production.

The overall process involves different stages (Fig. 9). The first step is the natural gas pre-treatment to convert the organic sulfur into H_2S, which is later absorbed. The cleaned gas is sent to the main reformer, heated by direct or indirect combustion of an external fuel. This stage is responsible for a greater part of CO_2 emissions; it is enough to say that in the whole process about 9 to 12 tons of CO_2 are released per ton of hydrogen produced. [12,23]

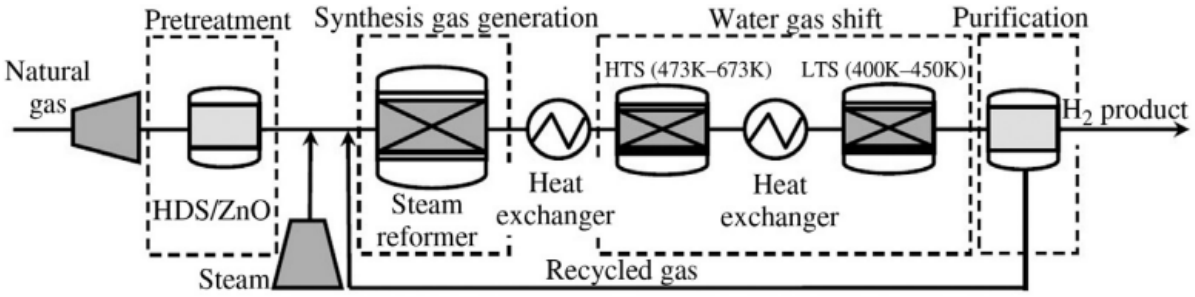

Figure 9: Stages of production of hydrogen and syngas for the traditional steam methane reforming.[24]

In the reformer, methane conversion is required to operate at a high-temperature range of 650–1000 °C and a pressure range of 5–40 bar. These conditions are necessary to have considerable methane conversions (> 90%) since the main reaction is highly endothermic (R1). [17]

$$CH_4 + H_2O \rightleftharpoons CO + 3H_2 \qquad \Delta H° = +206\ \mathrm{KJ/mol}\ (R1)$$

At the reformer outlet, the gases are mainly constituted of syngas, that could be enriched in hydrogen when sent to the water gas shift units and separated by pressure swing adsorption (PSA) for purification.

The SRM is catalyzed process, and typically supported nickel is used as catalyst, due to its low cost and high activity. However, the use of nickel favors the carbon formation and makes it necessary to significantly increase the steam to carbon ratio at the inlet; typically, S/C molar ratios of 2.5-3 are employed to avoid an excessive deposition of carbon. Therefore, to generate high-pressure steam, considerable amount of heat is consumed, thus decreasing the overall efficiency of the process.

Several alternatives to this process are studied to limit the emissions and decrease the energetic demand.

One of them is the methane dry reforming (DMR) which is based on the reaction with carbon dioxide to give syngas in equal ratio (R2).

Methane dry reforming is often accompanied by secondary reactions from which the most common is the reverse water gas shift (R3), responsible for a decrease in the syngas final ratio, inadequate for most of the uses.

$$CH_4 + CO_2 \rightleftharpoons 2CO + 2H_2 \qquad \Delta H° = +247.3\ KJ/mol \qquad (R2)$$

$$CO_2 + H_2 \rightleftharpoons CO + H_2O \qquad \Delta H° = +41\ KJ/mol \qquad (R3)$$

The efficiency of reforming and the overall productivity are in all the cases limited by carbon deposition, which is thermodynamically favored both at high and low temperatures according to reaction 4:

$$2CO \rightleftharpoons C + CO_2 \qquad \Delta H° = -172\ KJ/mol \qquad (R4)$$

The presence of carbon is unavoidable, and it has been found to be more present among 560 to 700 °C.[25]

Not surprisingly, the extent of these reactions is, in the general case, more pronounced when the feedstock employed contains more C atoms, making the coke deposition an unsolved problem that especially affects the implementation of dry reforming, but also obstacles the utilization of high hydrocarbons like ethane, butane, and pentane. The latter are presents together with methane in several extraction sites like the shale gas reserves.

Carbon formation can be disfavored by changing the feed ratio, e.g., by introducing larger amounts of CO_2, the equilibrium is shifted according to Le Chatelier' s principle to the left of the disproportionation reaction of CO.

However, the reverse reaction is another endothermic reaction, and it is necessary to introduce an alternative way that allows a thermal recovery to place dry reforming in economically viable processes.

Catalytic and non-catalytic partial oxidation is an exothermic process, and it has the advantage of not needing any heat provided. On the other hand, heat recovery at high temperature is not very efficient and the gas temperatures reached (1200-1400°C) are difficult to be kept homogeneous thus decreasing the security of the process.

Catalytic studies have been carried out to reduce the operative temperature. However, non-catalytic processes have several advantages. Indeed, they allow to deal with raw feedstock, even containing sulfur, that would poison most of the catalyst, decreasing the costs generally required for the gas cleaning and increasing the possibility of utilizing materials not acceptable in the strictest operative condition of SMR and DMR.

Partial oxidation allows to obtain the exact ratio of H_2 to CO with high selectivity at low contact time enabling the utilization of smaller reactors. However, the high capital and operating costs of air separation units (ASU) reduce its competitiveness.

Autothermal reforming is a self-sustaining process where methane, oxygen and water are fed in ratio suitable to utilize the energy released by the oxidation to run the steam reforming. It stands as a process that allows us to overcome the limitations of expensive heat supply and recovery, but it still requires high costs for the air separation unit for its functioning.

1.1.4 Looping configuration

In recent years, a lot of attention has been given to the study of transport properties of solid compounds, to the chemical looping technologies and their mutual integration, to overcome the limitation of the traditional processes.

The looping concept is based on a two-step mechanism that exploits the redox properties of a transporter material, often oxygen carrier, to ensure a controlled release of the oxygen species and to guarantee high level of selectivity through the tuning of the reduction degree.

In this application the transport of oxygen from air is indirect; indeed, the carrier allows the oxygen storage bringing to the inherent separation of nitrogen and oxygen, without the need of expensive air separation units.

The source of oxygen could be flexible, making it possible to exploit water and carbon dioxide splitting to provide oxygen and paving the path to hydrogen and syngas production at reduced emission.

Among a variety of options, thermochemical water splitting (TCWS) offers hydrogen at high purity and high conversion. When practiced in association with the utilization of a fuel, the temperature and energy demand considerably decrease, due to the enhanced reactivity of the oxygen carrier in presence of a reductant agent.

The fast kinetic achievable with an appropriate choice of carrier allows to increase the productivity and to reduce the overall costs achieving the co-production of hydrogen and syngas. Also, it permits to replace high-quality heat supply with isothermal redox operation improving the system efficiency[26].

To go in further details, Fig. 10 shows the configurations that can be assumed by the conventional processes when run in looping. The looping offers many combinations and, among all of them, the ones reported in the figure below are some of the most investigated. For example, chemical looping dry reforming (CLDR) could be performed utilizing the first stage for methane cracking or as alternative for selective partial oxidation; if the cracking route is adopted, the material acts as carbon carrier and distinct streams for H_2 and CO are produced.

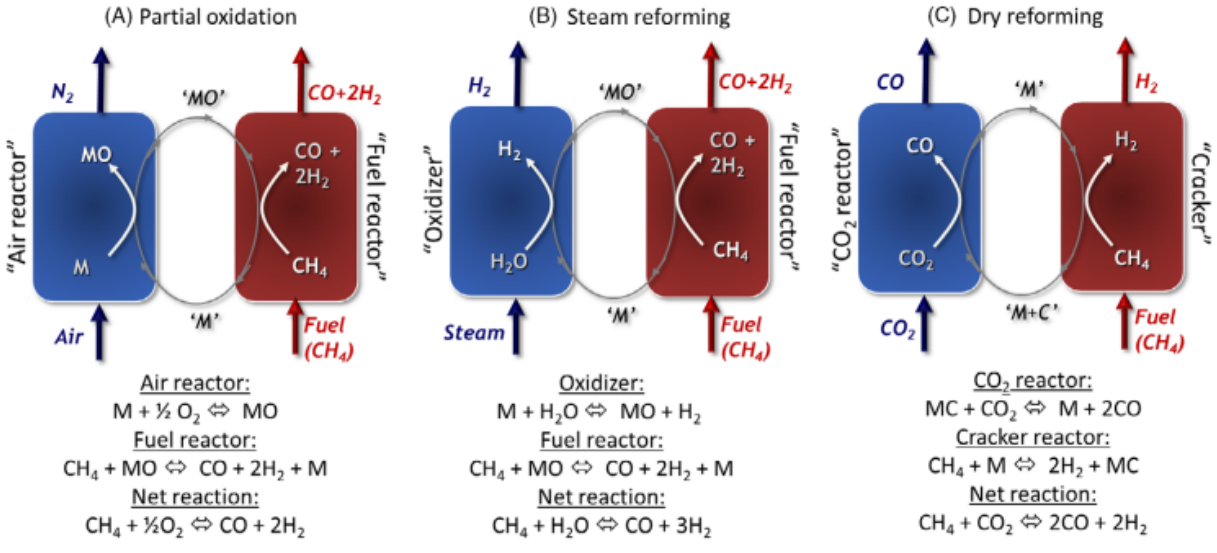

Figure 10: Looping process for syngas production: a) partial oxidation, b) steam reforming, c) dry reforming.[27]

The main advantage of preferring the configuration where only methane thermolysis occurs finds explanation on the possibility to achieve pure streams.

Indeed, the result of CLDR run with carbon carrier is hydrogen and carbon monoxide, the two components being produced in separates reactors, where the overall product can have the same characteristics of a syngas achieved by conventional DRM except for the fact that in this case the two streams achievable are both pure.

CO could be used for carbonylation reactions to produce chemicals, it could be sent in the water gas shift unit to increase the hydrogen production, as the downstream processes are the same employed in conventional reforming process, or it could be mixed in flexible ratio with the hydrogen to be employed in a wide range of applications.

In the case, instead, in which an oxygen carrier is employed, on contact with methane, oxygen is released to give a mixture of syngas, while carbon dioxide is used for carrier regeneration to provide the oxygen back and additional CO.

The main limitation of steam and dry reforming remains the substantial energetic demand to guarantee the reaction temperature. However, there are several strategies applicable to reduce the overall demand that are function of how the heat is supplied.

In the conventional approach the reactor is located inside a furnace where additional fuel is burnt, generally methane. As alternative, in process like di CLDR, CO could be used as fuel but, in this case, more gas needs to be processed due to its lower heating value (CO 280 kJ/ mol vs CH4 891 kJ/mol) and less CO remains available for syngas and hydrogen production.[27]

As an alternative to external combustion, other routes are investigated for the looping configurations, like to directly exploit the combustion of the carbon deposited inside the main reactor with pure oxygen or air. The utilization of oxygen brings to the production of pure CO_2 that can be usefully employed in reaction, but it involves the utilization of air separation unit, which is energetic less promising, while the oxidation with air is less effective, and it causes the dilution with nitrogen of the off gases, which cannot be recycled into the reactor, but can alternatively be fed to an expander for energy recovery.

In general, looping technologies offer a new path for process integration and optimization and add flexibility to the process industry. Selection of the best option, among all routes described, is not univocal and it strictly depends on the market demand.

During this thesis work, it was decided to investigate methane reforming to syngas in a looping technology because of the great flexibility it offers in varying the output ratio of the desired products.

Indeed, the products that can be obtained from syngas change significantly depending on the starting syngas ratio, and so it becomes critical to be able to act on this parameter as needed.

1.2 CO_2 emission mitigation strategies

The processes described so far, despite being of great importance, are often accompanied by CO_2 emissions that must be managed to safeguard the environment.

Two of the main institutions responsible for the CO_2 level monitoring, namely, International Energy Agency (IEA) and the Carbon Sequestration Leadership Forum (CSLF), have stated that, for the energy sector, in order to achieve net zero emissions by 2050, the global scale of CCS must be increased by 10-15 times in 2030 and by 100 times in 2050, with respect to 2020, when 40 Mt/year were sequestered.[28]

Currently, the geological sequestration of carbon dioxide is economically viable only if CO_2 is used for enhanced oil recovery (EOR), an extraction process that allows to store carbon dioxide exploiting its solubility properties and recovering additional crude oil.

The geological sites for CO_2 storage are generally oil and gas reservoirs, already connected with the existing infrastructure, or deep saline aquifers found in sedimentary basins.

Large-scale CO_2 storage requires strict conditions, among which critical steps are the assessment of the underground capacity and the safety for long-term storage. Indeed, leakages would affect the groundwater potability causing the return of CO_2 in the atmosphere. In this respect, storage in the open sea can reduce the risk for human health, but a release of gas would result in water acidification with possible damage for the animals.

However, the procedures for secure storage are well established and to keep practicing CCS is stated as one of the mandatory lines to be adopted to reach the environmental goal declared by the Paris agreement. Nevertheless, CCS as unique measure is not sufficient, and it is required to increase the valorization of carbon dioxide into useful chemical through the deeper implementation of CCU, indeed only 0.2 Gt. of CO_2, over the 32 Gt produced by humans' activities, are used annually by industrial activities.[29]

In several applications, carbon dioxide must respect purity standard to be used as feedstock. A purity index is provided by the sulfur oxide to carbon dioxide ratio since the separation of sulfur compounds is normally necessary before CO_2 can be used.

This ratio is 100 times lower if the carbon dioxide is captured from the air or from the biogas upgrading, which provided CO_2 with limited amounts of sulfur compounds, even though for the case of biogas the purity is difficult to predict due the wide difference in the origin of the starting biomass.

Together with the purity standard, other parameters that need to be considered are the cost of conversion and transportation, which participate to further emissions, and force to carefully evaluated the effective convenience of CO_2 utilization. Indeed, in most cases, severe operative conditions are needed, such as high temperature and pressure, to run the process and to produce the co-reagents.

A typical example of this is the large utilization of water for hydrogen production, the main reagent involved in the carbon dioxide conversion processes. In this contest, the utilization of renewable energy would make these processes more viable, and this is the scenario where the bioenergy with carbon capture and utilization (BECCU) is being developed.

This application has the great advantage of being able to use the same technologies and supply chain already developed for fossil fuels. On the other hand, its full implementation finds several obstacles among which one the mains are land degradation, threat to biodiversity, and food competition.[30,31]

The production on a wide scale raises concerns about intensive farming with large use of fertilizers and the risk of water unavailability.

Carbon dioxide coming directly from air (DAC) avoids any competition with the food industry and allows flexibility on the location avoiding the costs for transportation, however the development of the technology still requires time due to the high energetic costs resulting from the capture at low concentrations.

The highest energetic consumption is related to i) the electricity that must be provided by the fan that forces air through the capture modules and ii) the use of heat and/or electricity to operate in high vacuum, depending on the regeneration method chosen for the adsorbent material.

Due to this, decreasing energy consumption, has been one of the main aspects considered during the part of the thesis carried out abroad, where the performance of different contactors has been evaluated in terms of the specific energy demand of the fan as a function of CO_2 capture rate.

1.2.1 Storage and utilization: Capture from source point

Capture at large point sources refers to a process which develops carbon dioxide streams at high concentrations, like the flue gases of industrial sources (e.g., power plants, cement, or steel factories). The field is dominated by oxy and pre-/post-combustion technologies.

Pre- and post-combustion capture processes employ amines and ammonia liquid solvent for CO_2 absorption and differ in the concentrations of CO_2 treated; pre-combustion deals with more concentrated stream, often coming from integrated gasification combined cycle (IGCC). The process has higher efficiency respect to post-combustion, where the CO_2 is more diluted, however IGCC plants are not so many, and the adsorption costs are substantial.[32]

Post-combustion is the most employed solution for carbon capture. The world's first post-combustion CO_2 capture facility is in Canada, and it has captured and sequestered more than 4.5 million tones since operations began in fall 2014. The technology exploits a liquid solvent based on amine, which requires high costs for regeneration, that often are the greatest expense in capture process. [28]

The oxy fuel processing uses pure oxygen in combustion, to obtain a pure CO_2 stream. The absence of nitrogen improves the separation of the CO_2 in the flue gases, and it avoids the formation of NO_x compounds. Before to be compressed and transported, particulate matter is removed from the CO_2 purified stream through electrostatic separation, while sulfur dioxide is removed through desulfurization.[33]

The next stages of CCS involve compressing and transforming CO_2 into a fluid so that it can be transported by pipelines, ships or other vehicles to a storage site or being utilized and therefore stored.

As already mentioned, one of the main applications for CO_2 is in the enhanced oil recovery. EOR has been carried out in the United States and Canada since the 1960s. The US always dominated this application, indeed the world's first large-scale process with the utilization of CO_2 for EOR has been conducted in Texas using CO_2 from natural fields of Colorado. Throughout the duration of the project (1972-2009) more than 175Mt of CO_2 have been injected.

However, natural CO_2 source fields (reservoirs of carbon which can be drilled out of ground) are not sources which can participate per se in decreasing the emissions, but they have introduced the concept of utilize waste CO_2 to enhance the oil extraction.

CO_2 EOR forces more of 8-20% than the original oil out of the well, and it extends the lifeline of an oil well for an additional 20-25 years or more, allowing a longer utilization of fossil fuels which, despite to be the major cause of the global warming, also ensure the security and stability of the energy system. [34]

Similarly, to the EOR, calcium looping also stands as an intermediate technology between use and storage. Indeed, it could be placed downstream of high-emission processes for post-combustion capture (Fig. 11) or integrated in the production of hydrogen enhancing its production in pre-combustion application.

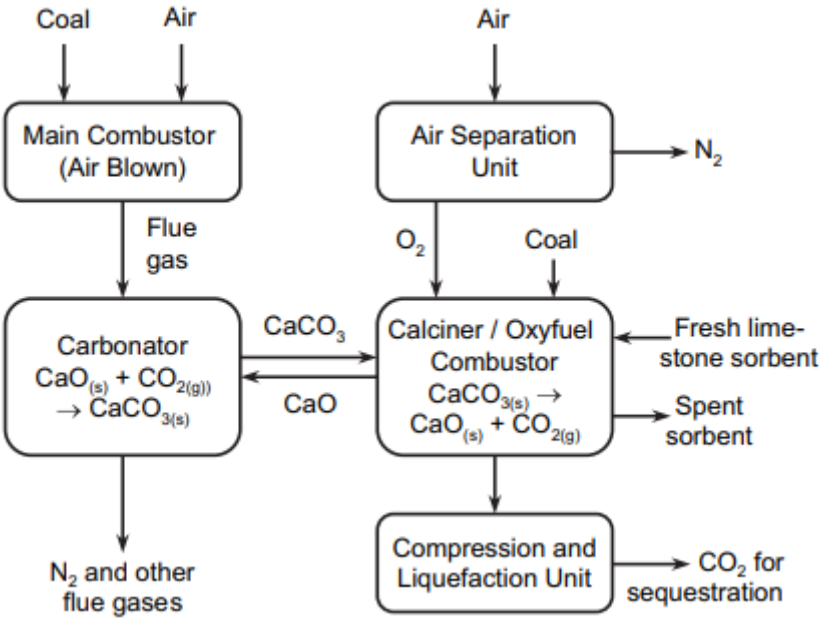

Figure 11: Calcium looping integration in CO_2 capture.[35]

In a typical cycle, fresh calcium oxide, also known as limestone, is made to react by carbonation reaction and it is after sent to a second unit to regenerate the adsorbent.

The process could be run for several cycles obtaining carbon dioxide separation with a high level of purity, while the spent carrier could instead be utilized by the cement industry increasing the amount of CO_2 that can be handled by this technology, potentially decarbonizing both industries.[35]

Technology development and process integration can reduce process costs. Another example of this is the development of chemical looping combustion (CLC), where it is possible to achieve an inherent separation of the carbon dioxide, producing energy while reducing the CO_2 capture costs.

Indeed, CLC cooperates for CO_2 valorization since it exploits the same principle of the oxy fuel combustion, but utilizing oxygen provided by solid carrier, instead of air separation unit, producing a high purity CO_2 stream suitable, e.g., for extraction of aromas and production of carbonated beverages etc.

1.2.2 Storage and utilization: Capture from the atmosphere

In recent years many fundings has been directed to the companies to address the climate crisis, and due to this, always more enterprises are starting to find solutions to adjust their activities in a way to protect the environment.

The paths that pass through renewable resources are also more publicly accepted. However, from the perspective of land use, CCS is an underground-space utilization technology, and coal-fired power plants plus CCS require a much smaller land area than solar and wind power plants. [28]

Clean sources are more challenging to implement, due to lower levels of technological maturity and economic viability.

Vegetable biomass is one of the most employed renewable resources, since it is directly synthetized from the natural process of photosynthesis, where the CO_2 present in the atmosphere is absorbed and converted into nutrients, while O_2 and water are released back to the environment as non-polluting gases.

The origin and typology of biomass could be very diverse and so the elemental composition which defines the properties of the obtained products.

The most employed biomass for energy purposes belongs to the second-generation category, to avoid the competition with the food industry, however the production of first-generation fuels is also practiced, most notably in Brazil and in United States, to obtain bioethanol, employed in internal combustion engine (Fig. 12).

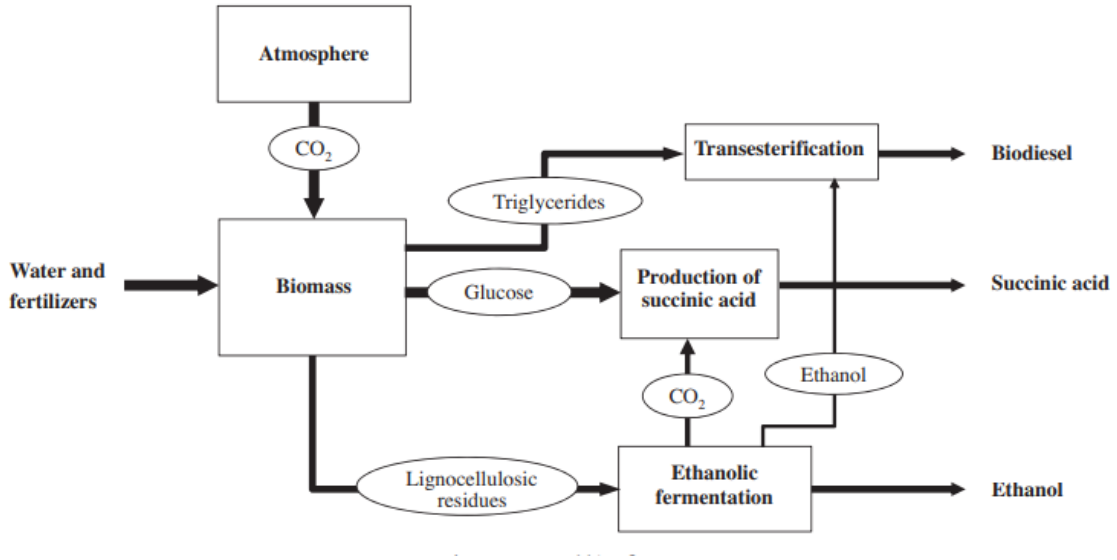

Figure 12: Biomass valorization for green production of fuels and high value chemical compounds. [29]

Ethanol fermentation brings to the production of pure and cheap carbon dioxide (6–12$/t CO_2), which can be further utilized to obtain succinic acid. [29]

The most interesting aspect of this cycle relies on the fact that CO_2 is sequestered from the atmosphere, and it is incorporated into a useful production.

This process is part of a broader category, known as bioenergy with carbon capture and utilization (BECCU), and, along with other capture technologies could play an essential role in the mitigation of CO_2 emissions. Indeed, in this case not only the process does not produce new emissions, but it also consumes the CO_2 already present in the atmosphere.

The same principle has led to the development of materials suitable to capture CO_2 from air to increase the benefits that can be achieved thanks to the synergy of more techniques and to overcome the general limitations associated with the extensive use of biomass.

Direct air Capture (DAC) allows to address diffuse sources, like the ones coming from aviation and agriculture sectors, from which 25% of total greenhouse gases emissions derive.[36]

DAC also presents challenges; indeed, it requires more energy than capturing CO_2 from flue gases and the processing of considerable volumes of air. Additionally, the poor concentration of CO_2 in air makes direct air capture a challenging and highly expensive approach. [37,38]

It is enough to say that in a process with 100% recovery, approximately 1400 m^3 of air at normal conditions need to be processed in order to capture 1 Kg of CO_2.[36]

The large volumes that need to be treated impose to work with significant flow rates to achieve appreciable productivity, also because the low concentration of the solute causes slow kinetics of the adsorption process.

Regardless of these limitations several companies (Carbon Engineering (Canada), Climeworks (Switzerland) and Global Thermostat (USA)) already operate with DAC plants looking for improvements of their technologies, particularly aimed at reducing costs.

Typically, the adsorption process is run in packed bed column, but the strict requirements imposed by the direct air capture applications, have led to study the process even in presence of other structures, such as honeycomb monolith, foam and laminates. [39–41]

Indeed, the configuration of the gas solid interface plays a significant role in the determination of relevant process parameters such as the flow regime that is being established and the pressure drop along the column.

Therefore, the understanding of the optimal design and operation achievable with different contactors is crucial to be able to place DAC between the affordable and effective technologies in the reduction of CO_2 emissions.

Several possibilities are available for the end use of this CO_2. For example, It could be reduced by renewable hydrogen via the Sabatier-reaction to synthetic natural gas for use in power to gas applications (PtG)[42–44], even though this field required further development to overcome the low efficiency achievable when coupling electrolysis and methanation (< 40%). [17] Alternatively, it could be sent to greenhouses to faster growth of plants, algae, or others biomass. [45,46]

1.3 Materials for methane reforming

Reforming reactions can be performed through thermochemical process, where the chemical reaction occurs when a determined temperature is reached or be catalyzed by species that increase the reaction rate, promoting more efficient reaction mechanisms, that can also bring to operate at mild conditions.

These two approaches can also be combined. This is the case with most of the looping processes, where carrier compounds interconvert between different redox stages depending on the temperature and on the nature of the reactants fed.

Reforming processes are employed on a large scale, and they have been studied for decades in the prospect of improving the global efficiency of the process and the material lifetime.

The literature available on the materials investigated is extensive.

Noble metal catalysts (Rh, Ru, Pd, Pt, and Ir) show high catalytic activity and stability for dry reforming, with scarce carbon deposition, but they cannot find application on large scale, due to their high price.

On the contrary, transition metals such as Ni, Co, Cu, Mn, and Fe based catalysts, are highly promising, due to their abundance, low cost, and good thermodynamic properties for reforming processes. [47–49]

Solid transition metal (Ni, Co, Fe, Cu)-based catalysts interact with hydrocarbons, breaking the C-H bond and favoring the thermolysis reaction at lower temperature, thus increasing the possibility of carbon deposition.

The management of this carbon, despite not being trivial, could also be in part beneficial, since it allows us to produce part of the hydrogen from a less energetic demanding reaction than steam or dry reforming (R 1,2). These materials can also be suitable for the direct production of hydrogen if mixed in alloy and applied molten [23].

Nickel supported over alumina catalysts is the most popular choice for syngas produced from methane dry and steam reforming (DMR-SMR). Despite their toxicity, Ni based materials are the focus of multiple studies because of their high catalytic activity toward methane and other light hydrocarbons.

However, while allowing a conversion of methane almost complete, Ni-based oxygen carriers are susceptible to deactivation by sulfur poisoning and elemental carbon deposition. In addition, disposal of the spent catalysts represents a problem, because of their toxicity.

Cu-based oxygen carriers show suitable redox behavior to ensure a good oxygen transfer capacity along with good reactivity for the reforming reaction. They are also capable of directly releasing oxygen by thermal decomposition at medium-high temperatures (800- 1000 °C). Also playing in favor of these systems is their low price and limited toxicity, but they can give rise to sintering and melting even at temperatures below 800°C [50], and be subjected to friction due to limited mechanical strength.

These limitations are partially overcome employing support like on γ-Al_2O_3, MgO, SiO_2, CeO_2, and ZrO_2, or promoters such as alkaline and alkaline earth metals, as well as rare earth metals, which remarkably improve catalytic performance and reduce coke formation, especially in dry reforming processes.[51,52]

Features required by an oxygen carrier (OC) are excellent fluid dynamic properties, such as resistance to friction and mobility within the reactor, low cost , resistance to C formation and other fouling elements (sulfur, ash, etc.) and chemical and thermal stability following multiple redox cycles. [53]

Therefore, it is also important to identify the best physical characteristics, such as particle size and shape, material structure, and pore size, as they concur in the determination of process kinetic, thermal stability, and reversibility of the carrier i.e., lifetime without undergoing deactivation.

Since the use of suitable materials determines the sustainability, cost-effectiveness and durability of the process, further investigations are needed to design a material that can replace those currently used at the industrial level.

1.3.1 Ceria-based oxygen carriers

This sub-chapter will go into the details of Ce-based oxygen carrier properties, since they are among one of the main materials considered in the current state of the art for methane looping.

Cerium oxide offers high melting point (> 1960K) and does not give rise to carbide formation. In addition, it offers faster kinetics of water splitting with its transition state Ce(III) oxide, which is normally reached after reaction with methane, positioning it as a viable material for the synthesis of both syngas and hydrogen. [54]

The oxidizing properties of ceria can be attributed mainly to two electron exchange zones: the surface zone of the material and the innermost (bulk) zone. It has been observed that oxygen exchange on the oxide surface exhibits an activation energy 30% lower than that in the bulk, thus suggesting an easier redox exchange on the surface in the initial stages. [55]

Ce- based carrier are often studied in association with other oxides, where ceria can be the support, it can be supported or be bind in a mixed phase, like the case of mixed oxide and perovskite-type oxides.[56]

Support CeO_2 on high temperature-stable ZrO_2 allows a good dispersion of the ceria particles improving its resistance to sintering during repeated cyclic operations[57], while the incorporation of ZrO_2 into CeO_2 lattice occurs when they are combined as mixed oxide, on one hand enhancing the formation rates of H_2 and CO, on the other hand undermining the syngas selectivity. [58]

Other strategies to improve cerium oxide performance rely on the introduction of different porosities through forming procedures followed by thermal treatments. Indeed, pressing the cerium oxide powder at different pressure values introduces porosities of different shape and dimensions, changing the kinetics and selectivity, while the further treatment enhances thermal resistance. [59]

However, a pre-treatment at high sintering temperature (1400 °C) can decrease the solid-gas interface area and lattice oxygen mobility, thus negatively affecting the syngas yield and methane conversion.[60]

The loss of surface area and the decrease in porosity must be considered when choosing the heat treatment. Indeed, in the absence of adequate porosity, it may not be possible to have proper oxygen mobility, going to worsen the re-oxidation of carbon deposited.

The utilization of ceria for methane chemical looping has been deeply studied and relevant information is available in literature, examples of which includes the effect of temperature on carrier reduction and regeneration and the relationship between reactants flow rate, conversion achievable and syngas selectivity.

Ceria reduction has been found to be strongly dependent on temperature or methane flow rate.

Particularly, an increase of temperature from 900 to 1000 °C increases the conversion of methane but working at 1100 °C leads to methane cracking, indicating that 1000 °C is near the upper limit on operating temperature for the cycle.[61]

A too high flow rate makes methane cracking prevails on the partial oxidation, while limiting the flow rate can favor the oxidation reaction and enhance methane conversion but at the expense of syngas selectivity. Therefore, a trade-off in methane flowrate needs to be considered to achieve high syngas yield while preserving maximal methane conversion.[60,61]

On the other hand, fast and full regeneration are guaranteed with CeO_2 (between 900 °C and 1050°C), which means the carrier re-oxidation is not kinetically limited by temperature changes and isothermal

operation can be carried which avoids sensible heat losses occurring during temperature-swing cycle and eliminates the need for heat recovery.[60]

Due to the various advantages listed above, ceria is still under investigation in the most recent works, with the prospective to overcome the limitations that obstacles its commercialization as carrier for chemical-looping methane reforming.

1.3.2 Ongoing challenges in the use of CeO_2

Carbon deposition, oxygen carrier lifetime and process's energy penalty are some of the main limitations for the full implementation of methane chemical looping.

Carbon formation is often responsible of decreasing catalyst/ oxygen carrier lifetime due to the occlusion of the porosity and/or to the formation of phases that disfavor reactivity toward methane, therefore, its removal is investigated by all the studies that aim to scale the process at an industrial level.

One widely used strategy to deal with carbon formation is optimizing the cut-off time of the reforming step, to limit methane cracking, and to employ an oxidant to re-oxidize the residue carbon during carrier regeneration.

For the case of cerium dioxide, this approach was found to be effective for samples of different morphology (foam, pellets, fibers) and rapid overall cycle (reforming-regeneration) were achieved thanks to the fast kinetics provided by Ce-based materials.[62]

However, pure cerium oxide required operating temperatures between 900-1100 °C to react with methane, which in turn implies a high energy demand, typically met by combustion of additional natural gas, and even if there are already works[63] which proved the feasibility of employing concentrated solar heat, as alternative and renewable energetic resource, the solar to fuel efficiency reached to now is still low.

The energy to fuel efficiency is one of the most relevant indices for the evaluation of the efficacy of solar energy utilization and it is defined as the ratio of the higher heating value of the syngas produced over the sum of the solar radiative power input through the solar reactor's aperture and the higher heating value of CH_4 fed to the solar reactor.

The highest efficiency (solar-to-fuel) observed to-date for chemical looping reforming methane (CLRM) it was found to be 10.06%. and it was recorded by Warren et al. at 1150 °C and feeding CH_4 at 25%.

The study employed commercial cerium oxide on large scale (300-350 g), calcined at 1200°C for 10h, ground and sieved till particles of dimensions < 500 μm. The methane conversion and syngas selectivity achieved in these conditions were found to be equal to 69% and to 93%, respectively.

Also, Chuayboon et al tested pure ceria employing solar energy and even if they reached a lower solar to fuel efficiency (5.22%), they confirmed the success of employing pure ceria as a reticulated foam for methane reforming. Indeed, they tested 18.37 g of carrier reaching stable performance for ten cycles, methane conversion of 60% and syngas yield around 8.08 mmol/g CeO_2.[64]

Other works tried to enhance process performance, through the incorporation of noble and transition metals in the composition of the carrier, with the aim of reducing methane activation energy, and so the reforming temperature. Among the transition metals nickel is the cheapest option and therefore its reactivity has been deeply investigated.

Ni decorated CeO_2 was found to exhibit high methane conversions of 65–90% at 700-800 °C[65] while conversions of ~99% were observed at increased temperature (900°C) and for extended cycling (50 cycles).[66]

The two studies, based on nickel utilization, have been carried out with a low carrier loading (0.2-1 g), testing the reactivity in presence of dilute methane (5-10%).

However, comparable performance in terms of syngas production and methane conversion was found with CeO_2 (working at: 1000-1100 °C) and with Ni-CeO_2 (working at: 700-800 °C).

Both materials offer very promising results, indeed pure cerium oxide is effective on higher carrier scale, while cerium oxide doped with metallic catalyst allowed for milder operating temperatures.

However, even though the development of a suitable carrier for methane chemical looping is at a very advanced stage, several points still need to be addressed before getting the material commercialized.

On this prospective the current research is focus on i) increasing the energetic efficiency achievable with the employment of concentrated solar heat as source of energy, ii) decreasing the methane activation energy through the utilization of catalysts (transition and noble metals) and/or by increasing the methane concentration.

1.4 Aim of the work

The objective of this work is to study methane looping reforming employing pellets made of pure commercial ceria as oxygen carrier.

Previous study based on the utilization of CeO_2 demonstrated that its suitability for syngas production could be comparable with that of more complex redox catalysts, even if higher operating temperatures are required when pure ceria is selected.

The encouraging results obtained on a larger loading scale than those normally used using catalyst-doped carriers have been the main reason which also prompted this work to expand the database of data obtainable employing ceria as a carrier for syngas production.

The starting idea have been to treat a commercial ceria powder with a simple forming procedure followed by a thermal treatment at 900°C, to testing it in a fixed bed rig and to provide a detailed description of how to optimize process times (reforming, oxidation) to increase products productivities and exploiting deposited carbon to increase syngas specific yields while modulating the output ratio.

The solid- gas reactivity, in the range of interest (800-950°C), has been verified through the thermodynamic tools of Aspen Plus software simulator, while the carrier reactivity and cycling stability on small scale have been verified by thermogravimetric characterization at the institute of science and technology for ceramic (ISTEC-CNR).

For the testing at higher scale, an experimental rig has been built specifically for the project, and a trustable analytical method have been put in place for the interpretation of all the relevant metrics which concur to establish the efficiency of reforming processes (e.g., specific productivities, product yields and purity).

2 Process simulation: Aspen Plus

2.1 Aspen Basis

ASPEN stands for Advanced System for Process Engineering, and it is a software used to simulate a chemical process scheme and to quantity model chemical plants, perform sensitivity analyses, check process safety, and economic.

It is normally employed for complex process schemes constituted of main units preceded and followed by up and down stream treatment stages.

It works by solving:

- Extensive property balances such as mass, moles, and energy.
- Thermodynamic relationships for reacting and nonreacting systems such as phase equilibria and chemical equilibria.
- Empirical correlations for velocity, momentum, heat transfer and mass transfer.
- Reaction stoichiometry and kinetic data.

Aspen incorporates several features such as Aspen Plus, Aspen Adsorption, Aspen Custom Modeler, Aspen Dynamic, and many others.

Aspen plus is normally used for thermodynamic assessment of many processes equipment where stationary variables are involved since it does not consider temporal variation.

The temporal dynamics could be eventually described with Aspen Custom Modeler which gives the possibility, once a time-dependent model of a system has been run, to export it as an Aspen Plus block if a steady state exists.

Aspen tools are very flexible, and they can often communicate between them if determined conditions are respected. Also, they can be integrated with external code, generally Fortran, to increase the level of details required for a specific case.

2.2 Thermodynamic assessment

In this work the thermodynamic tools of Aspen Plus were used to assess the performance of the CeO_2 carrier for methane reforming.

All the simulations were set up in steady state input mode with the optional stream class MIXCISLD for the introduction of vapor components and conventional solids.

Process analysis was performed within the RGIBBS reactor which predicts the gas phase composition once the minimum of the Gibbs free energy is reached, and an equation of state Is provided for calculations.

Such an approach does not need to input reaction stoichiometry, indeed all the components are equally specified by the user distinguishing only their physical state.

The simulator searches within all the possible set of reactions the ones which allow to get an overall minimum energy and when a minimum of the Gibbs free energy function is reached, it determines the equilibrium composition of the gaseous phase only providing the composition at the chemical equilibrium with unit activity of the solid reactant.

Simulations were performed on cerium oxide (CeO_2) at atmospheric pressure to evaluate the effect, of change in the feed composition and operating temperature, on the extent of the gas–solid reaction, heat duty and syngas selectivity and purity.

A sensitivity analysis was run in the temperature range framed as necessary for the reaction to occur, namely 860 °C to 950°C, with a stoichiometry feed of CH_4 to CeO_2 (1 kmol/h CH_4; 2 kmol/h CeO_2).

At the ideal temperature provided by this analysis, an isothermal regeneration with air was evaluated as represented in the scheme below (Fig. 13).

At the inlet of the first RGIBBS reactor the reactants are fed, therefore separated though a cyclone that sends the solid into a second RGIBBS reactor where air is co-fed for regeneration.

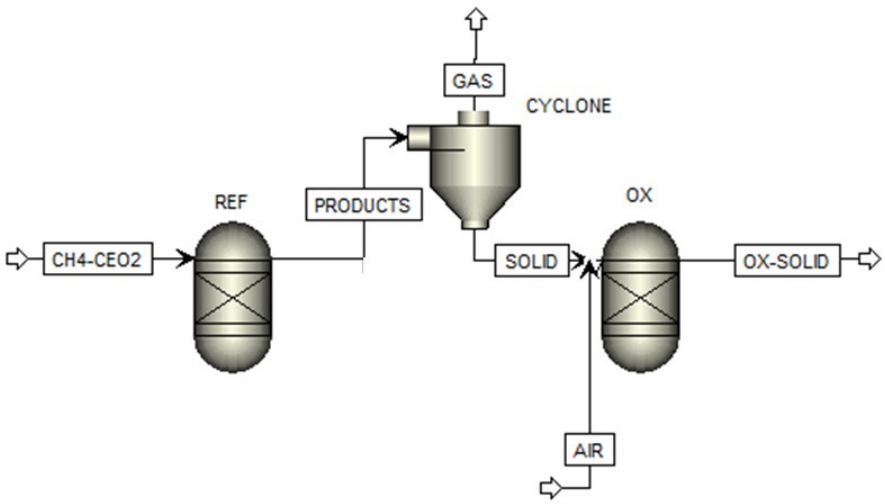

Figure 13:Scheme of a complete redox cycle of reduction with CH_4 and oxidation in air.

From the sensitivity analysis is expected to observe a relationship between the operating temperature and the favored reactions (methane cracking, methane partial and total oxidation) and to being able to evaluate the feasibility of working isothermally.

The analysis also aims to verify reactants conversion (CH_4, CeO_2) over reforming (REF unit) and over oxidation (OX unit) and to check the feasibility of regenerating the spent carrier.

3 Material and characterization

3.1 Carrier preparation

The oxygen carrier was prepared through a simple methodology of forming starting from a commercial material provided by a UK company.

Cerium oxide powder (PIKEM, purity 99.9%) was formed by a hydraulic press, imposing a pressure of 250 MPa, and then sieved to a fraction of 0,595-0,841 mm.

The resulting pellets were thermally treated in the furnaces of the ISTEC-CNR facilities.

The treatment was carried out in air with a heating ramp of 30 °C/min and left in isothermal condition at 900°C with a dwell time of 1h.

It was used then as it is for the testing phase and for TGA characterization.

3.2 Thermogravimetric Analysis (TGA)

3.2.1 Principle

Thermogravimetry is an analytical technique in which the mass of a sample is constantly monitored to record any change in weight that occurs over the time as the temperature changes.

The measurement can provide information on physical phenomena like phase transition, adsorption and desorption and chemical processes such as thermal decomposition or solid-gas reactions. Kinetic parameters, material stability, and changes in the composition are some of the most relevant aspects definable with this type of analysis.

TG is a simple technique able to work with low amount of sample in the order of 10^{-3}g. In the figure is reported how a typical instrument looks like, model STA449 C Jupiter, employed for TG analysis and a sketch to illustrate the main components (Fig. 14).

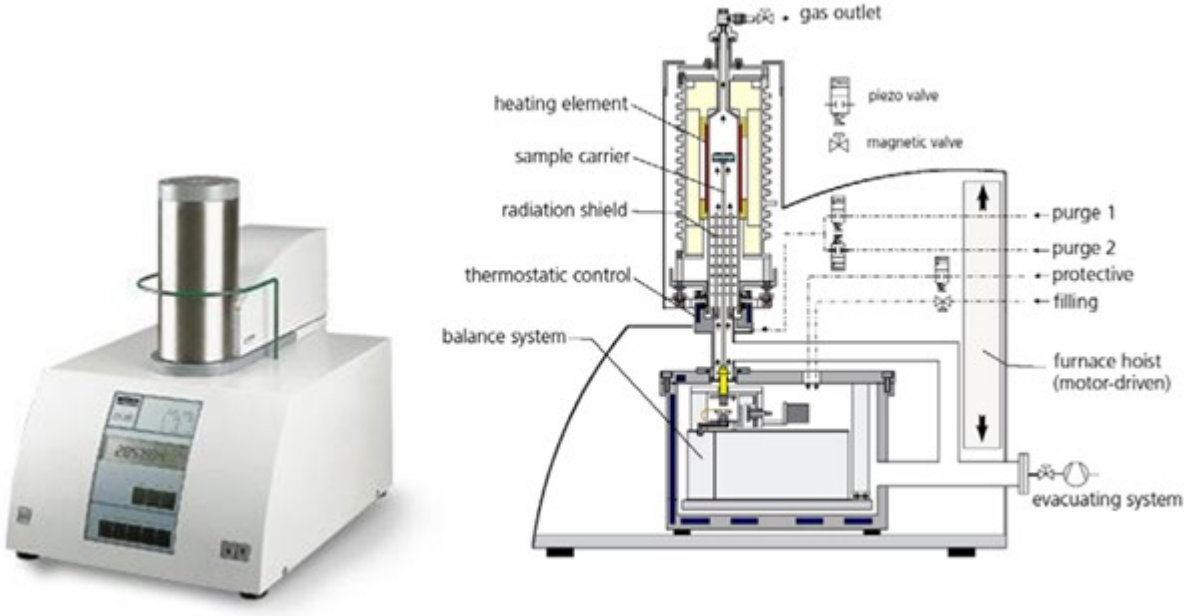

Figure 14: Scheme of Netzsch-STA-449C Jupiter device.

The TG sample carrier is equipped with a thermocouple for the direct measurement of the temperature at the sample crucible. Gases of different nature can be sent through the chamber to allow for measurements in inert or reactive atmosphere.

The measuring unit of the balance is maintained at a constant temperature while the heating element can provide temperature up to 1500 °C, allowing for measures in different temperature ranges, according to the application of interest.

Additionally, many instruments designed for TG are also able to serve for differential scanning calorimetry (DSC) and simultaneous TG with quantitative differential thermal analysis (DTA).

The instrument is normally connected to a computer which can collect, store and process data returning the trend of mass variation as a function of time and temperature.

3.2.2 Analysis carried out

The ability to work as an oxygen carrier is related to the internal structure of the oxide and to its redox potential.

One way to analyze redox behavior is to subject the material to cyclic temperature changes to induce its change in oxidation state.

The oxygen released is driven by the temperature and it is often induced by the utilization of reductant compound, able to activate redox reactions and to mitigate the conditions otherwise required for oxygen release.

Thermogravimetric analyses in air and in inert atmosphere were carried out to assess the oxide stability in absence of reductant agent, at the higher temperature required in the calcination pre-treatment, and during the inert purge step required in the looping process.

The measurement was collected by employing air during the heating till 1000°C, and Argon for cooling to room temperature.

The characterization with reductant gas was carried out to check the solid-gas reactivity and quantify the oxygen releasable from the reaction.

The ability of the carrier to recover the oxygen was also verified since the re-oxidation capacity is a property which strongly determines the number of cycles that a carrier can guarantee without loss performance.

The analysis was conducted in a way useful to simulate what occurs in a looping process.

In a typical test the sample was heated in an inert atmosphere up to the temperature desired and when a stable value was reached a reductant mixture was sent on the sample.

The reductant atmosphere was kept until the temperature conditions chosen for oxidation were reached and the oxidation was performed with air till its completion.

Lastly, the same oxidant atmosphere was kept up to the moment the reduction temperature was reached again.

In all the analysis a flow rate of 180 ml/min at 4% CH_4 in Ar and a flow rate of 100 ml/min of air were used for the reduction and oxidation respectively.

4 Testing

4.1 Set up description

The test rig, specifically designed for this experimental campaign, consists of three main parts: feeding system, reaction area, gaseous stream detection (Fig. 15).

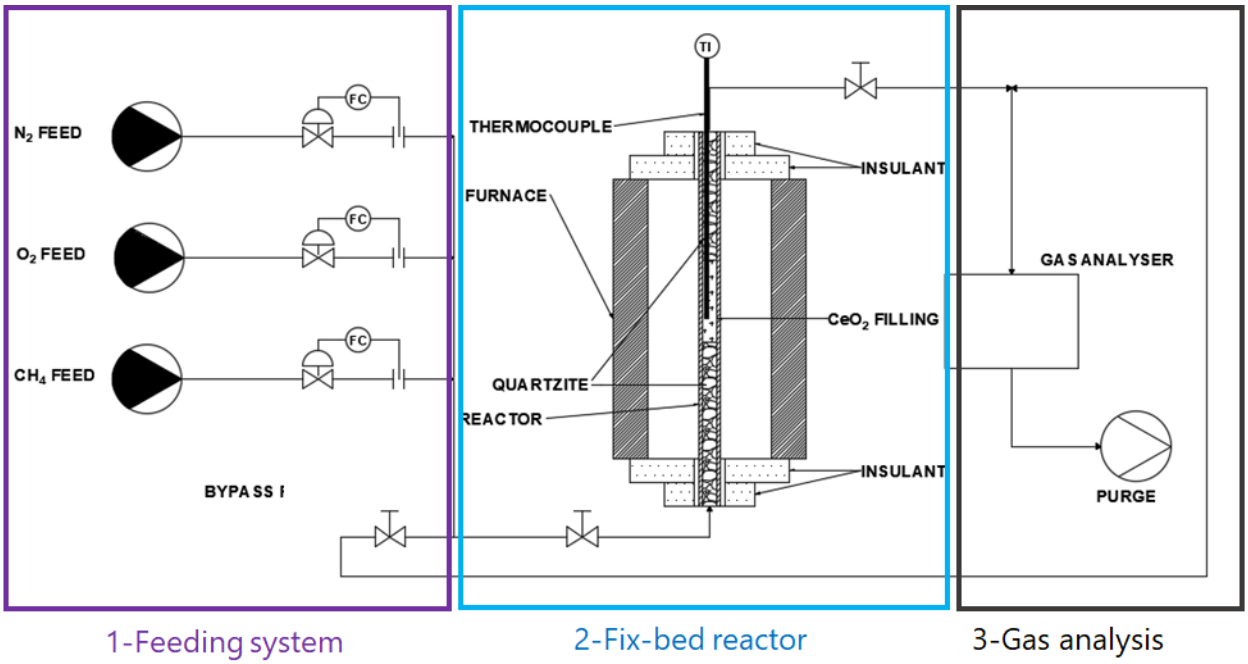

Figure 15: Set up employed for the experimental campaign.

The feeding system is made of several Bronkhorst mass flow controllers, while the outlet gases are analyzed continuously by means of an online analyzer (GEIT 3100 P+ Syngas) equipped with a thermal conductivity detector (TCD) for the detection of hydrogen, an infrared detector (NDIR) for CH_4, CO, CO_2, and an electrochemical sensor for oxygen.

The flow meters scheme is organized in a way to easily switch between the gaseous atmosphere, with each flow meter dedicated to a single, different gas.

The mixed gas feed stream is connected both to the bypass and to the reactor inlet to allow checks of the composition before starting a new experiment and to account for the actual reagent contribution eventually removing instrumental errors.

The reactor zone consists of a stainless-steel fixed bed reactor (AISI 316 with an inner diameter (ID) of 10 mm) enclosed in a tubular furnace and perfectly insulated, with external layer of quartz wool, to guarantee a constant working temperature.

The furnace temperature is set and checked on a Carbonite oven, while the internal temperature of the carrier is measured with a K-type thermocouple located at the bed mid-length.

The reactor outlet is connected to the analyzer which in turn communicates with a computer for data collection. Fig. 16 shows real pictures of the overall apparatus.

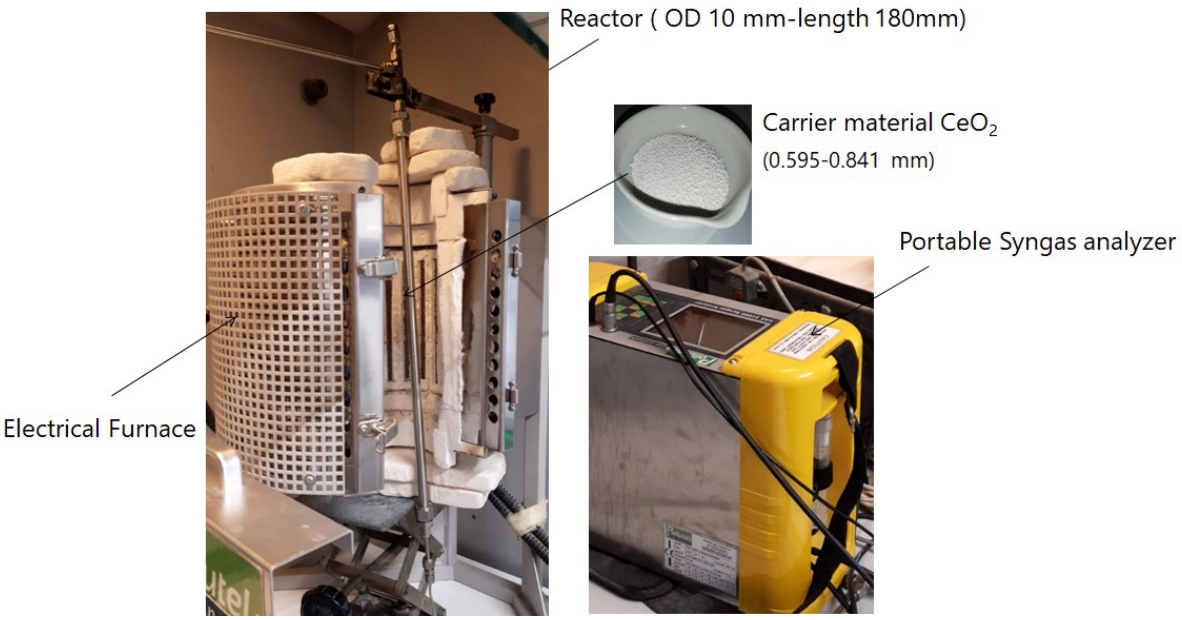

Figure 16: Experimental set up as it is in DICAM laboratories.

The rig was used in cyclic mode for the execution of consecutive cycles of CH_4 reforming and carrier re-oxidation at isothermal condition, while keeping constant the reagent partial pressure and the carrier loading.

The load of carrier was decided in relation to the instrumental needs; indeed, the analyzer required a minimum flow of 1 NL/min for its correct operational, therefore, ~15 g of reactant was employed to avoid an excessive dilution of the output gases that could have caused a low accuracy in their measurement.

In a typical experiment, the reactor was loaded with ~15 g of cerium oxide oxygen carrier prepared as previously described and employed without any further treatment.

The sample was heated up at atmospheric pressure and the temperature within the reactive bed was monitored and recorded approximately every two minutes, while the composition of the gases evolved during the reaction was analyzed continuously.

The looping was obtained through the switch of the reductant/ oxidant stream with a purge with nitrogen as intermediate step to ensure the cleanliness of the reactor from the previous flow.

4.2 Rationale experiments

In the initial phase of the experimental campaign preliminary assessments were done on the system to check its operability, and to be able to elaborate a reliable analytical method that would rule out false contributions to the process.

The insulation quality was checked heating up the reactor to the reaction temperature and monitoring the ability to reach the set temperature value without straining the oven's controlling resistors within the scheduled ramp times.

The dead volume and the sensors delay time were calculated measuring the response time from valve opening till gas full breakthrough, at the reaction temperature.

The time at half breakthrough was considered as the time that must be subtracted from the overall time in each experiment (lag time), to gain accuracy in the description of the initial stage of the reaction.

The subtraction of this delay time is indeed necessary to avoid counting delay time as already part of the reaction time (thus going to overestimate values of conversions and yields).

Fig. 17 shows the breakthrough curve obtained for each single gas flow. Each curve was recorded employing 5% in vol. of the gas to be measured mixed with N_2 and with the reactor only filled with the inert material.

Same criteria were used for products and reactants, since the sensor response time was estimated to contribute more to the overall lag time than the time spent in the pipeline from valve opening to reactor inlet.

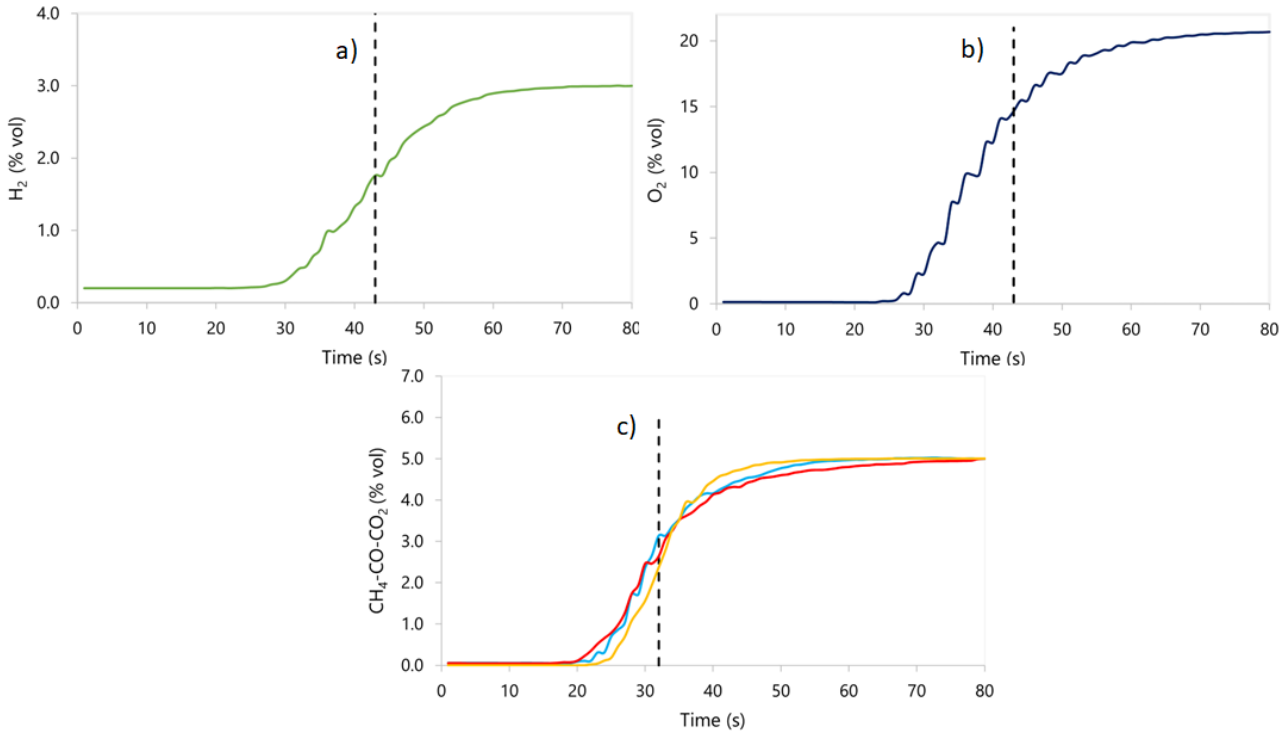

Figure 17: Overall delay time at 900° C for sensor typology a) TCD, b) electrochemical, c) NDIR (red for CH_4, blue for CO, yellow for CO_2)

The breakthrough curve appears to be sharp for all gases proving the fast response time of the syngas online analyzers. The slight differences visible in the results are related to the different sensors type used for detection. Electrochemical and TCD sensor requires more time for the measurement than NDIR sensor.

Once rig operational and analyses response were defined, blank experiments were performed in presence of only the filler material (quartzite sand) to confirm its inertia during the chemical reaction.

Finally experiments in different conditions were started to find the ideal conditions to run the two stages of reforming and oxidation of the looping process.

4.2.1 Experiments at long times

The initial experiments were conducted to explore the solid- gas reactivity and to frame the trends achievable in presence of the selected carrier.

The first test was carried out at 900°C (CH_4 10% in N_2, 1 NL/min) and lasted until no more gaseous products were detected waiting for the full breakthrough of the reagents at this operational condition. Absence of gaseous products at the reactor outlet means that is not useful to exceed this time and it shows the maximum reaction time achievable in the explored condition.

The selectivity for the reaction of interest and the extent of competitive reactions, namely, methane cracking and total combustion, was quantified and monitored over time.

Isothermal regeneration was also checked. In this stage the effect of change in oxidant composition and flow rate was evaluated to determine the possibility to work with simple air, without excessive overheating of the reactor trying the following oxygen content in nitrogen: 3%, 5%, 21%.

The effect of the overall flow rate variation was checked at three different values: 1,3,5 NL/min.

Reproducibility and performance maintenance were verified through duplication of experiments and testing for several cycles.

The same procedure was applied varying the reforming temperature, but keeping all the other parameters constant, to evaluate the differences caused by an increase in temperature.

4.2.2 Experiments at fixed times

The first set of experiments was used to study the system, understand its limitations, and identify suitable times for the conduction of the two looping stages.

In the second part of the testing, the most promising temperature was used for isothermal experiments at fixed time.

The shorter experiments made it possible to verify performance and reproducibility for a greater number of cycles, therefore they were used to further optimize the process looking at the details of cracking contribution, carbon accumulation and degree of carrier reduction.

The data were analyzed looking for the condition necessary to work in absence of carbon or, in case, adding its value through the re-conversion, in additional CO which can enhance the syngas yield.

A summary of the experiments done is reported in table 2.

Test motivation	T [°C]	t. reforming [min]	t. oxidation [min]
Effect of temperature	900	60	5
	950	60	5
Effect of time	950	30	5
	950	60	5

Table 2: Time and process temperatures employed for methane chemical looping over CeO_2 oxygen carrier.

4.3 Data processing

The method for data analysis was developed together with the verification of the proper operation of the system. The reaction involved in the two stages of the process were assumed to be the following:

Reforming step

$CH_4 + 2CeO_2 \rightleftharpoons CO + 2H_2 + Ce_2O_3$ (Partial oxidation) $\Delta H° = +332.3$ KJ/mol (R5)

$CH_4 + 8CeO_2 \rightleftharpoons CO_2 + 2H_2O + 4Ce_2O_3$ (Total combustion) $\Delta H° = +670.7$ KJ/mol (R6)

$CH_4 \rightleftharpoons C + 2H_2$ (Methane cracking) $\Delta H° = +75.0$ KJ/mol (R7)

Oxidation step

$Ce_2O_3 + ½\ O_2 \rightleftharpoons 2CeO_2$ (Carrier regeneration) $\Delta H° = -368.3$ KJ/mol (R8)

$C + ½\ O_2 \rightleftharpoons CO$ (Carbon oxidation) $\Delta H° = -110.5$ KJ/mol (R9)

$C + O_2 \rightleftharpoons CO_2$ (Carbon oxidation) $\Delta H° = -393.5$ KJ/mol (R10)

The excel file for data processing was developed with the following corrections and assumptions:

I. The behavior of gases was assumed to be ideal and ideal gas law was used for all calculations.

II. Changes in the flow rate were corrected with a mass balance on the inert gas.

III. Correction coefficients estimated through an initial check of the composition, in the bypass, was applied to consider instrumental error.

IV. The lag time was subtracted from the total reaction time.

The amount of each gaseous species in the outlet stream was obtained from direct measurement, except for water, which was instead inferred by balances.

Differential and integral mole balances were calculated, as following, to obtain production rate and total yield respectively:

$$\frac{1}{RT}\frac{\partial y_{CO2,out}\,\dot{V}_{out}}{\partial t} \quad ; \quad \frac{1}{RT}\int_0^t \dot{V}_{out}\; y_{CO2,out}\; dt$$

For hydrogen, the distinct contributions obtained from the two reactions (R5, R7) were calculated thanks to the knowledge of the extent of the partial oxidation reaction and of the value of total hydrogen produced, being the first calculated from the amount of CO produced and the second obtained by direct measurement of the TCD sensor:

$$\dot{n}_{\mathrm{g,H_2}}^{\mathrm{ox}} = \; 2\xi_{ox} \; = 2\,\dot{n}_{g,CO} \qquad ; \qquad \dot{n}_{g,\mathrm{H_2}}^{\mathrm{cracking}} = \frac{\dot{n}_{\mathrm{g,H_2}}^{\mathrm{tot}}}{2} - \dot{n}_{\mathrm{g,H_2}}^{\mathrm{ox}}$$

The entity of methane cracking was inferred by stoichiometry of reaction R7 while the extent of the total combustion was derived from the measurement of the overall CO_2 produced (R6).

The carrier conversion was calculated assuming partial oxidation and total combustion as the only reactions where the oxygen is transferred:

$$\chi_{\mathrm{CeO_2}} = \left(\frac{2n_{\mathrm{CO}} + 8n_{\mathrm{CO2}}}{n\mathrm{CeO}_{2,\mathrm{in}}}\right)\cdot 100$$

While the success of carrier regeneration (R8) was checked with a balance on the oxygen, where its recovery by the carrier is calculated subtracting, from the overall oxygen supplied during the oxidation step ($n_{\mathrm{O_2}}^{\mathrm{reg}}$), the contributions needed for the formation of CO_x species (R9; R10):

$$n_{\mathrm{O_2,reg}}^{\mathrm{CeO_2}} = n_{\mathrm{O_2}}^{\mathrm{reg}} - \frac{1}{2}n_{\mathrm{CO}}^{\mathrm{reg}} - n_{\mathrm{CO_2}}^{\mathrm{reg}}$$

The carbon generated in the first step of reforming was quantified with a balance of any compounds containing carbon, as:

$$n_{\mathrm{C}} = \; \mathrm{n_{CH4,g}} - n_{\mathrm{CO2,g}} - \; n_{\mathrm{CO,g}}$$

While the re-oxidizable carbon was obtained for direct measurements of the CO_X species in the following regeneration phase:

$$n_{\mathrm{C}}^{\mathrm{reg}} = n_{\mathrm{CO}}^{\mathrm{reg}} + n_{\mathrm{CO_2}}^{\mathrm{reg}}$$

The difference between the latter two quantities was used to evaluate carbon accumulation for the single cycle:

$$\mathrm{n}_{\mathrm{C}}^{\mathrm{acc}} = n_{\mathrm{C}}^{\mathrm{ref}} - n_{\mathrm{C}}^{\mathrm{reg}}$$

The calculations explained so far were used to define the main parameters sought by the process, namely:

Selectivity for the partial oxidation:

$$selectivity^{ref} = \frac{n_{\mathrm{CO}}^{\mathrm{ref}}}{n_{\mathrm{CO_2}}^{\mathrm{ref}}}$$

Syngas ratio for reforming and for the overall process:

$$syngas^{ref} = \frac{n_{H_2}^{\mathrm{ref}}}{n_{\mathrm{CO}}^{\mathrm{ref}}} \; ; \quad syngas^{tot} = \frac{n_{H_2}^{\mathrm{ref}}}{n_{\mathrm{CO}}^{\mathrm{ref}} + n_{\mathrm{CO}}^{\mathrm{reg}}}$$

Specific syngas yields (mol · g^{-1}) for reforming and for the overall process:

$$yield^{ref} = \frac{n_{H_2}^{\mathrm{ref}} + n_{\mathrm{CO}}^{\mathrm{ref}}}{\mathrm{CeO_2, g}} \; ; \quad yield^{tot} = \frac{n_{H_2}^{\mathrm{ref}} + n_{\mathrm{CO}}^{\mathrm{ref}} + n_{\mathrm{CO}}^{\mathrm{reg}}}{\mathrm{CeO_2, g}}$$

5 Results

The thermodynamic analysis, carried out on Aspen Plus, provided useful insights on the potential use of CeO_2 as oxygen carrier for the selective oxidation of methane, suggesting the best working temperature for the stage of reduction, at least from the equilibrium point of view.

The sensitivity analysis reported in Fig. 18 shows the results in the range from 860 to 950 °C, recognized to be the area in which the reactivity towards methane is more significant.

As evident from the plot a), the oxygen release occurs already at 860 °C, but at such temperature less than 40% of the oxide may be converted, and at least 900°C must be reached to get completion. From this temperature onward, it is possible to achieve 98% of methane conversion and 100% of oxide conversion.

Additionally, the analysis of the outgoing products pointed out Ce_2O_3 as reduced product of CeO_2 conversion while no metallic Ce formation was detected in all conditions explored.

When the carrier completely undergoes in the reduced form, very low carbon deposition is favored together with a syngas ratio of 2 (Fig. 18b), proof of the high selectivity for the partial oxidation over the methane cracking.

Interestingly, working with CeO_2, in all cases, guarantees a very high CO/CO_2 ratio, suggesting a negligible contribution of the complete combustion to the reaction scheme.

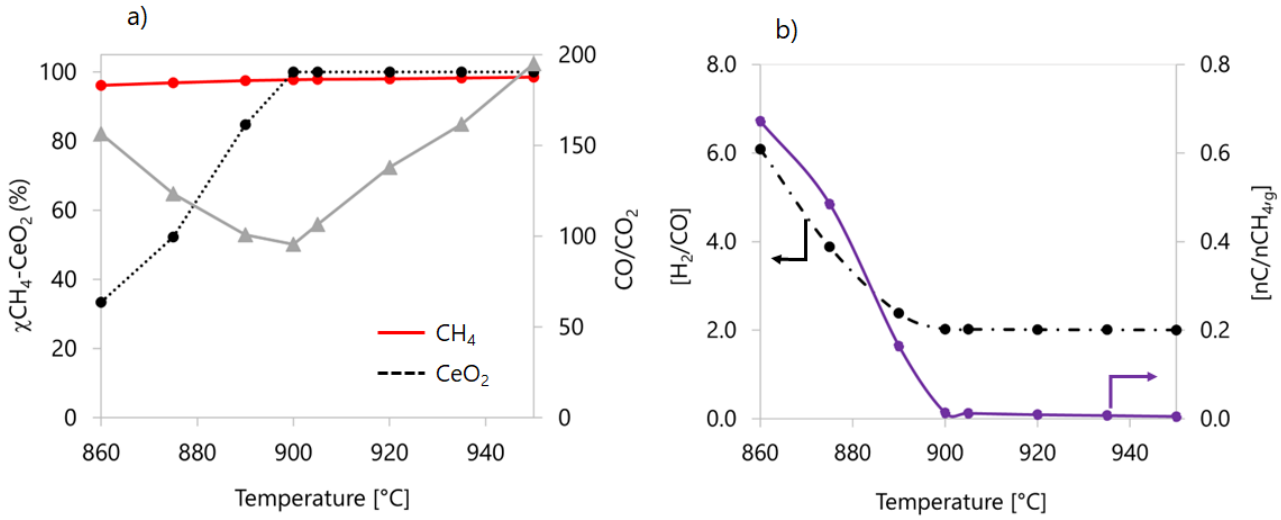

Figure 18: Sensitivity analysis results, collected between 860°C and 950°C for a stoichiometric [O/CH_4] ratio, of a) reactants conversion and reaction selectivity, b) carbon deposition and syngas ratio.

The performance was also checked through a simulation of the overall cycle (reforming, gas-solid separation, oxidation) to verify the carrier regeneration and the possibility to fully remove the residual carbon, to avoid its accumulation. Table 3 shows the simulation output achieved at both temperatures, 900°C and 950°C, with air as oxidant agent.

Temperature (°C)	χCe_2O_3 (%)	CeO_2 (Kmol/h)	C (Kmol/h)	CO (Kmol/h)	CO_2 (Kmol/h)
900	98.7	1.97	0	0.013	1e-04
950	99.5	1.99	0	0.005	9e-5

Table 3: Aspen plus results for the carrier regeneration carried out at the following ratio CH_4:CeO_2: air = 1:2:2.38.

The material results re-oxidated at both temperatures, reaching almost completion at 950°C, and so the carbon, despite a high temperature is generally not suitable for conducting exothermic reactions as the carbon re-oxidation.

Interestingly, the presence of Ce_2O_3 determines a preferentially formation of CO, with respect to the product of complete oxidation, CO_2, which is beneficial, both considering the syngas yield achievable and the environment concerns related to CO_2 management.

These results make ceria an interesting material, potentially convenient and feasible for the process, at least from the thermodynamic point of view; however, this type of analysis does not provide any information on material durability or syngas production rates, which in turn require the determination of kinetic data.

For this reason, in this work, the possibility of simulating the kinetics of the process was evaluated by exploiting literature data, as starting point for assessing the validity of the kinetic simulations achievable using the Aspen Plus package and their ability to describe simple experimental conditions.

The reaction between a carrier in a fixed position continuously flown by a gas stream, it is classified as a pseudo-stationary process/ transient process, where the oxide can be consumed and regenerated cyclically depending on the temperature applied.

In this regard, Aspen Plus presents two fundamentals' limitations. One is the impossibility to represent a time-dependent semi-batch process in an environment of stationary variables, the second is the absence of a section for the description of the reactivity for an immobilized catalyst/reactant.

These limitations could be partially overcome through the integration of an external code describing the temporal dynamics of the system with Aspen Custom Modeler, which is commonly done in literature when also a process integration must be evaluated.

However, this is beyond the scope of this work since a process integration assumes advanced knowledge of the operation of the individual fixed bed unit and to have already identified a suitable material.

Therefore, it has been decided to focus the work on thermodynamic assessment and on verifying the carrier performance through experimental testing.

In parallel with the simulation activity, to gain useful information about the material behavior and deeply investigate its reactivity in the process envisaged, the carrier was characterized by thermogravimetric characterization (TGA) at the institute partner of the project (ISTEC-CNR of Faenza).

First, the cerium oxide stability in air and inert gas at the operating temperatures of the reforming in absence of reducing agent, was verified, to check the thermal resistance and to ensure that the release of oxygen depends solely on the reaction with methane (Fig. 19).

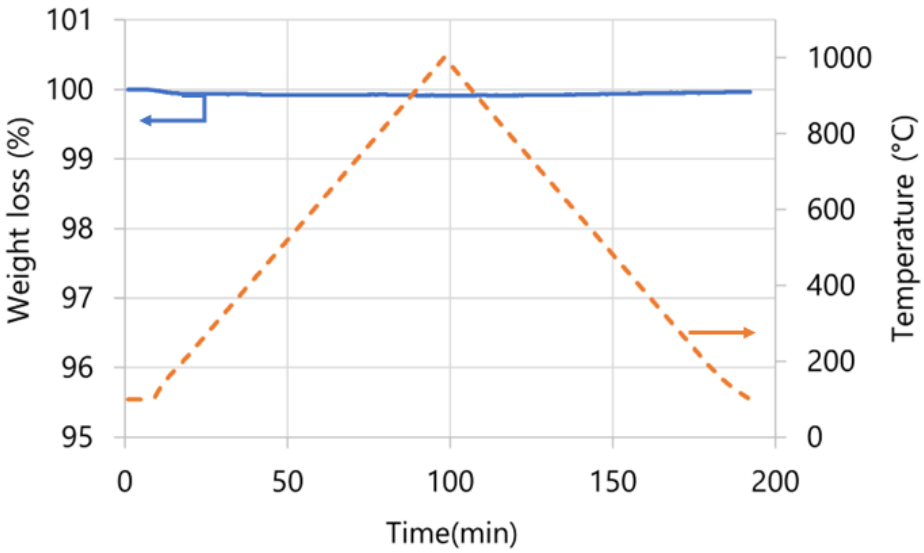

Figure 19: CeO_2 thermogram recorded in absence of reducing agent.

As clear from the solid straight line, index of changes in mass of the sample, no weight loss was observed in the investigated temperature range.

Therefore, thermogravimetric analysis was carried out at the most promising temperature values suggested by simulations, 900 °C and 950°C, in a periodic fashion, switching at controlled time the atmosphere from reductant to oxidant (CH_4 4 mol.% in Ar, and air).

The reaction occurs quite fast when methane reaches the oxide, and it gives rise to a maximum release of oxygen of 2.75 wt.% at 900°C and of 4.30 % at 950°C after 40 minutes of reduction (Fig. 20). The further regeneration appears to be completed, almost instantaneously, at all temperatures investigated (in the range 600-900 °C), proving that oxidation is not the limiting stage.

Working at 950 °C allows for faster kinetic, indeed, in comparison with the lower temperature, the same oxygen release from the OC is achieved about 20 minutes earlier, while running the stage for longer time allow to reach value close to the theoretical one for the transition from CeO_2 to Ce_2O_3 (4.75 wt.%).

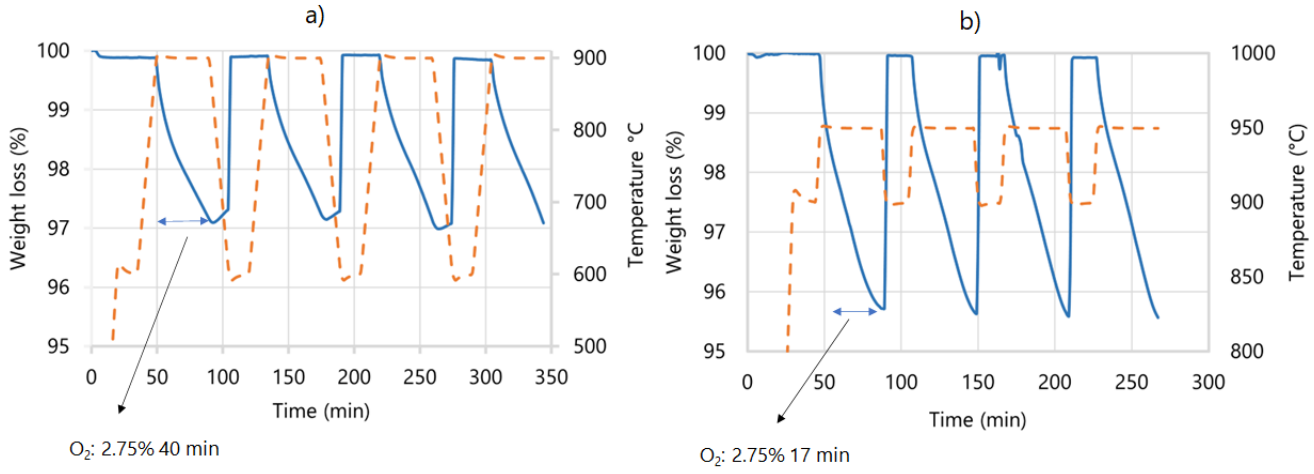

Figure 20: Thermogravimetric results for 80 mg of cerium oxide obtained at a reduction temperature of)900 b) 950 for consecutive redox cycle using CH4 4 mol.% in Argon for reduction and air for oxidation.

However, the TGA used for material characterization was not coupled with any analytical technique for the gas stream emerging from the crucible, so that it allows to compare the OC conversion and the reaction times at different temperature, but it is unable to provide any information about the actual gaseous products formed and the selectivity in the products of interest.

Experimental tests were carried out in the fixed bed reactor at the two temperatures (900°C and 950 °C) to quantify the gases produced and the data were elaborated highlighting the trends of the more relevant parameters which concur to determine the cyclic performance, namely, reactants conversion, process selectivity and yields of the products of interest.

As one can see in Fig. 21, in the fixed bed experiments, the carrier conversion is limited, similarly to what observed in TGA, and it cannot reach completion as predicted by thermodynamic simulations.

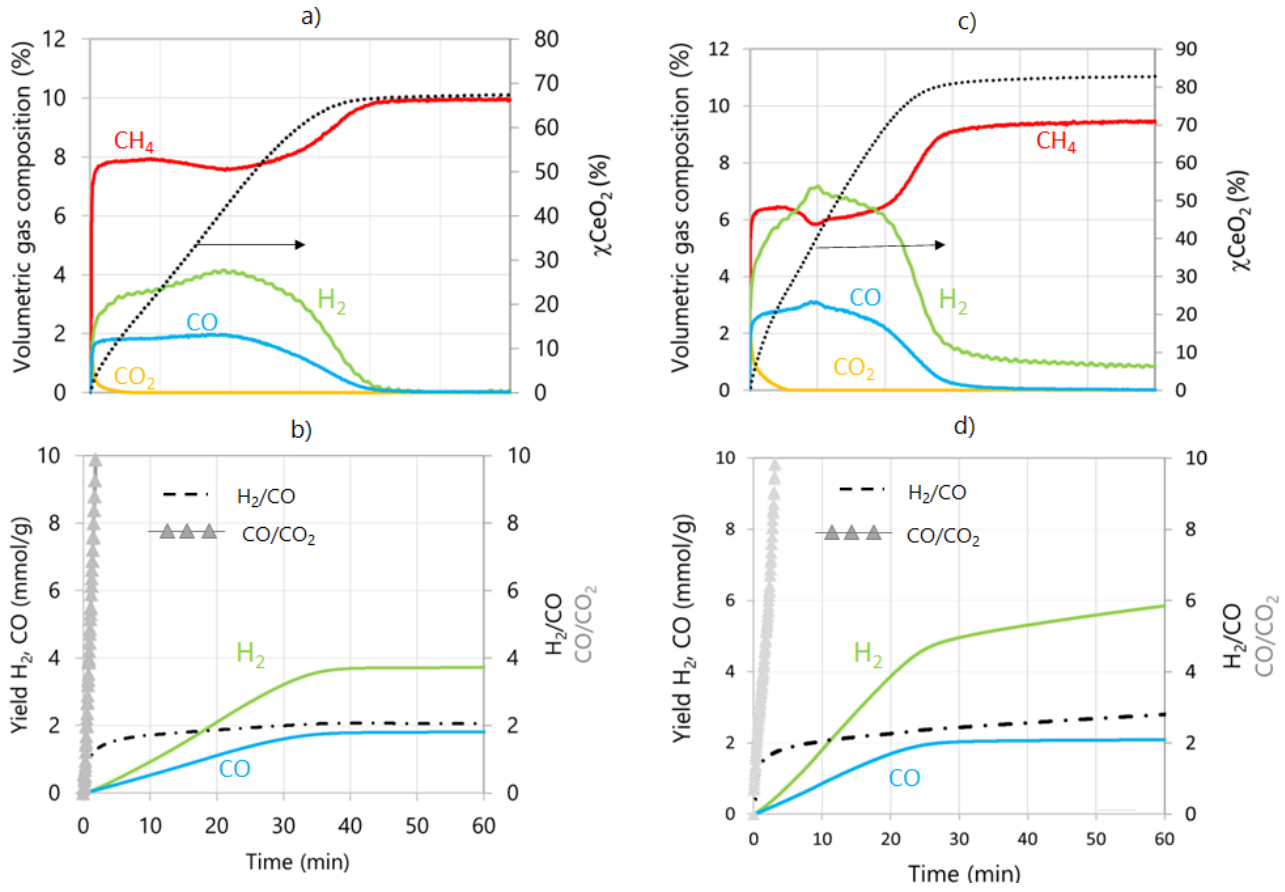

Figure 21:Reforming results of CeO_2 conversion, outgoing gases profiles, syngas yield and selectivity at a), b) 900 °C and c), d) 950 °C achieved for 10% CH_4 in N_2 and carrier load of 15.34 g.

However, the model analysis assumed ideal conditions, in which all the oxide is accessible to methane, the characteristic contact time between the two phases in the reaction environment.

Complete conversion could be hampered by the inability of methane to penetrate and diffuse into the porosity of CeO_2 under the conditions investigated so far.

Table 4 reports the amount of oxygen released, achievable in all the explored conditions over the TGA cycles and during the fixed bed experiments to show its extent respect the theoretical value for the transition from CeO_2 to Ce_2O_3 obtained from stoichiometry (maximum O_2 release of 4.75 wt.%).

However, it is necessary to point out that such data are meant to frame trends and not to draw down quantitative conclusions, since they come from different measurement techniques, in which the gas/solid contact times are not comparable.

		Temperature(°C)	
	Time(min)	900 O_2-released (wt.%)	950 O_2-released (wt.%)
Fix bed	30	2.73	3.74
	40	3.08	3.81
TGA	30	2.30	4.00
	40	2.75	4.30

Table 4: Oxygen released value for fresh cerium oxide sample achieved in TGA and for fixed bed experiments.

However, it is evident, from the large conversion values obtained, that the phenomenon is not merely superficial and both bulk and surface oxygen react.

In the same time frame, a larger working temperature (950 °C) allows for a greater release of oxygen and thus a faster rate of reaction of interest. Nonetheless, the conversion is incomplete and carbon deposits are observed in both cases.

As shown in Fig. 21 a) and c), the conversion of methane and cerium oxide reaches a maximum after 40 minutes at 900 °C, while only 30 minutes are needed at 950°C, confirming the faster kinetic achievable at higher temperature and the more efficient utilization of the reactants, even visible from the larger yields of syngas (Fig. 21 b, d). This is particularly evident for hydrogen, while the increase in CO yield is not that significant, indicating that the change in temperature has a stronger influence on the methane thermolysis than on partial oxidation.

However, in both cases, one can obtain syngas quality in the range of interest (dash black line), and the hydrogen formation continues without oxygen transfer, when the carrier stops reacting, as indicated by the non-zero value of hydrogen and the incomplete conversion of methane. Furthermore, methane cracking seems to be the only reaction that competes with partial oxidation, as the selectivity towards syngas is notable as testified by the high CO/CO_2 ratio.

The amount of carbon deposited can be inferred from the difference between the total hydrogen produced and the one generated from the partial oxidation only (R5-R7).

Fig. 22 shows how the H_2 production rate varies with the carrier conversion, and it shows the greater presence of carbon at the higher temperature, which is not surprising if one considers the endothermic nature of methane cracking.

The plot also allows to identify the extent of cerium reduction needed to avoid carbon deposition opening the path to the optimization of the reforming step.

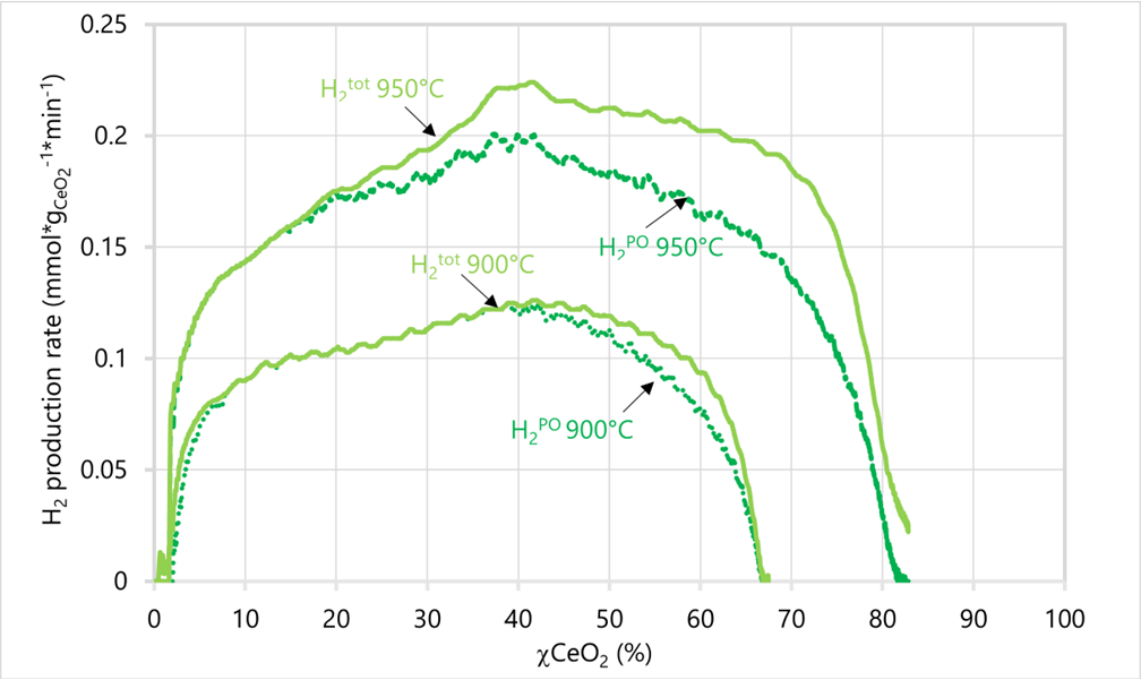

Figure 22: Different contribution to hydrogen production rate of methane cracking and partial oxidation at 900 °C and 950 °C.

Combining these results with those reported in Fig. 21, it is possible to make consideration on the ideal duration of the reforming. Indeed Fig. 22 pointed out when methane cracking starts in relation to the carrier conversion while Fig. 21 a) and c) shows at which process time a certain extent of carrier conversion is reached.

As one can see, selecting a reforming step lasting 10 minutes (χCeO_2: 40%), corresponding to maximum rate of production and negligible quantities of carbon formed, makes the regeneration easier; that represents the optimal solution as it may coincide with a considerable increase in the life of the material respect to the cases with carbon considerably build-up.

On the other hand, if the redox reaction is interrupted after 20 minutes ($xCeO_2$: 70%) or 30 min (χCeO_2: 80%) the produced syngas is characterized by an interesting ratio for the targeted use, together with a good utilization of both the reactants and a higher overall productivity.

Despite a longer reforming contributes more significantly to carbon formation, making its removal more challenging, cyclic experiments were done carrying out the reforming at a fixed time of 30 minutes and the regeneration isothermally until oxygen breakthrough was observed, to evaluate the possibility to fully remove the carbon deposited and at the same time to increase the syngas yield. Indeed, during carbon regeneration part of it can be re-oxidized to carbon monoxide.

For each redox cycle, carbon build-up and regeneration efficiency were quantified as shown in Fig. (23 and 24).

Carbon at each stage has been identified through a global balance on carbon atoms during the whole cycle, subtracting the combustible carbon from the total carbon generated by methane cracking.

Indeed, the carbon can only be originated from methane decomposition in the reforming step and when an oxidant agent is sent to the carrier, carbon is gasified into CO and CO_2 to an extent that is function of

oxidant nature and concentration. The carbon which cannot be burned during the regeneration remains accumulated on the carrier.

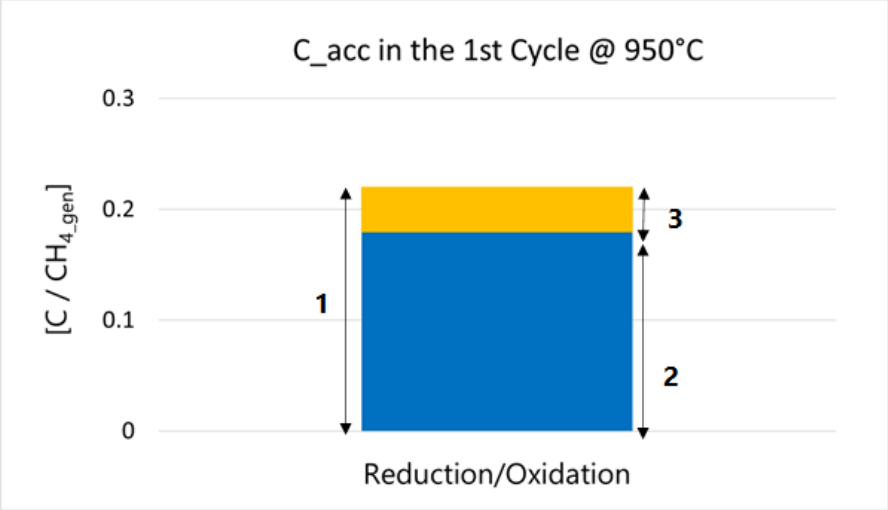

Figure 23: Carbon build-up for a reduction stage of 30 minutes and an oxidation stage of 5 where 1) is the total carbon formed in reduction, 2) the quantities combusted in the regeneration and 3) the residual carbon.

The regeneration was evaluated under different oxidation conditions by varying compositions (3-5-21% O_2 in N_2) and fluxes (1-3-5 NL/min), but it was decided to work with 3% O_2 because of the impossibility of controlling reactor overheating due to the initiation of carbon combustion reactions therefore, all reoxidations followed by a reforming time set at 30 minutes are limited to 3% O_2 and do not allow air to be used even at the highest flow rates tested, limited in turn by the flow meters available.

The efficiency of carrier regeneration was evaluated from a mass balance on the oxygen, subtracting from the overall oxygen provided during the oxidation, the one used for carbon reoxidation.

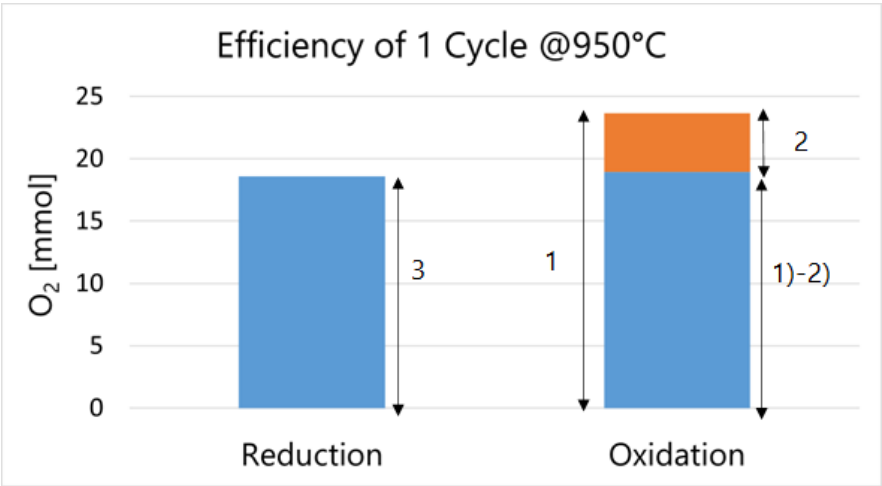

Figure 24: Oxygen balance of an overall redox cycle with a reduction time of 30 minutes and an oxidation stage of 5 where 1) is the total oxygen supplied 2) the oxygen employed in carbon re-oxidation and 3) the oxygen released during reforming.

The resulting value was compared to the oxygen released during the reforming step and the ratio of these two quantities used to define the total efficiency of oxygen regeneration (η). The stability over consecutive cycles was evaluated as well, and the efficiency was found close to the unit for eight consecutive cycles (Fig. 25).

Furthermore, the presence of carbon seems does not hinder the looping process in cyclic utilization of the OC. Indeed, even though some carbon is formed, and it accumulates during the cycles (C_{acc}), it does not seem to interfere with the ability to regenerate of the oxygen carrier, as indicated by the efficiency (η) of each cycle and from the simultaneous oxygen utilization of the carbon and the carrier (Fig. 26).

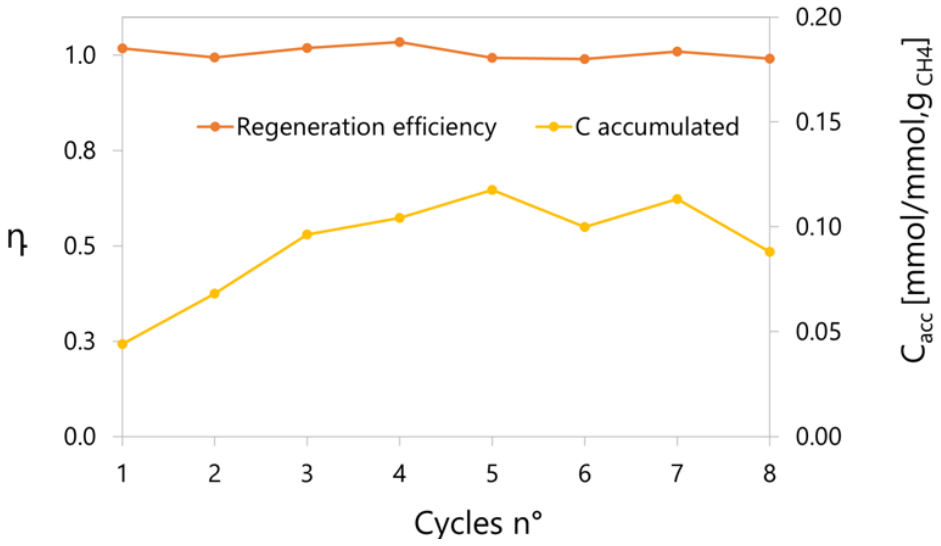

Figure 25: Evaluation of the effect of carbon deposition on the lifetime of CeO_2 carrier material over consecutive redox cycles.

The same plot shows the time required for the oxidation step, which coincides with the oxygen breakthrough reached after 5 minutes, and it highlights the faster kinetic of oxidation confirming TGA outcomes.

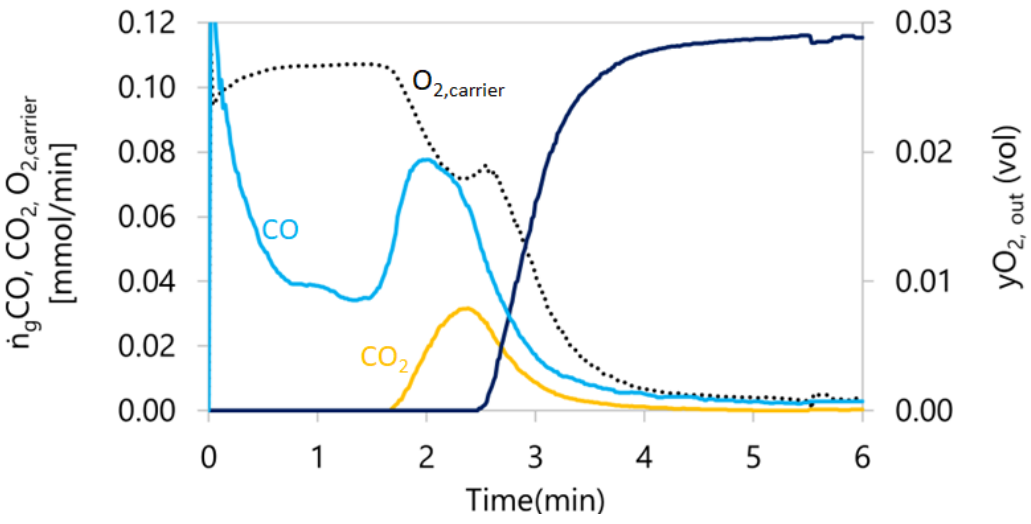

Figure 26: Average gaseous profiles obtained during eight redox cycles of carrier regeneration.

The extent of the regeneration achieved is also reflected in the stability of the production rates and yields achieved in the following reforming steps (Fig. 27). The plot reports the reforming steps with all the products detected and it evidences the predominant formation of the product of partial oxidation with only some loss in selectivity as the cycles proceed.

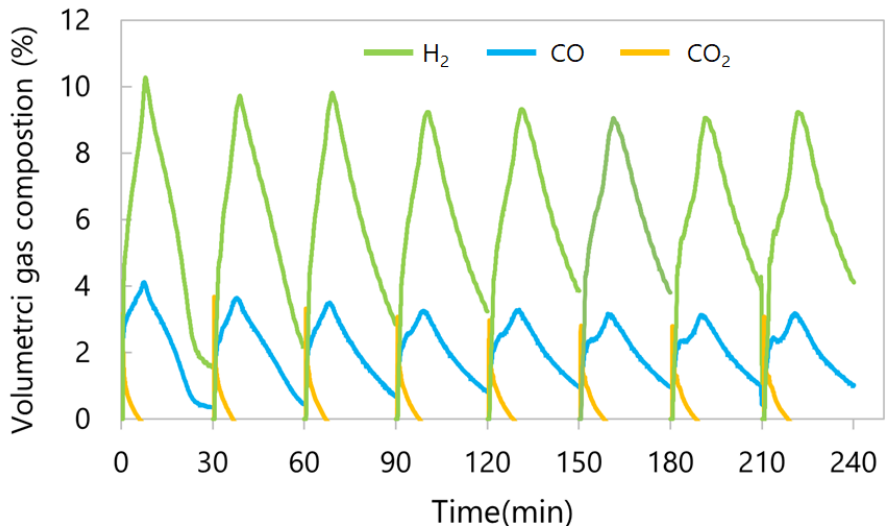

Figure 27 : Yields stability over 8 consecutive cycles.

Therefore, 950°C could be considered a viable temperature to run the process isothermally with a short overall process time of 35 minutes and no relevant change in the carrier reactivity. The carbon deposition caused by methane cracking contributed to increasing the overall syngas yield and to adjusting the final syngas ratio making it suitable for a wider range of applications (Fig. 28).

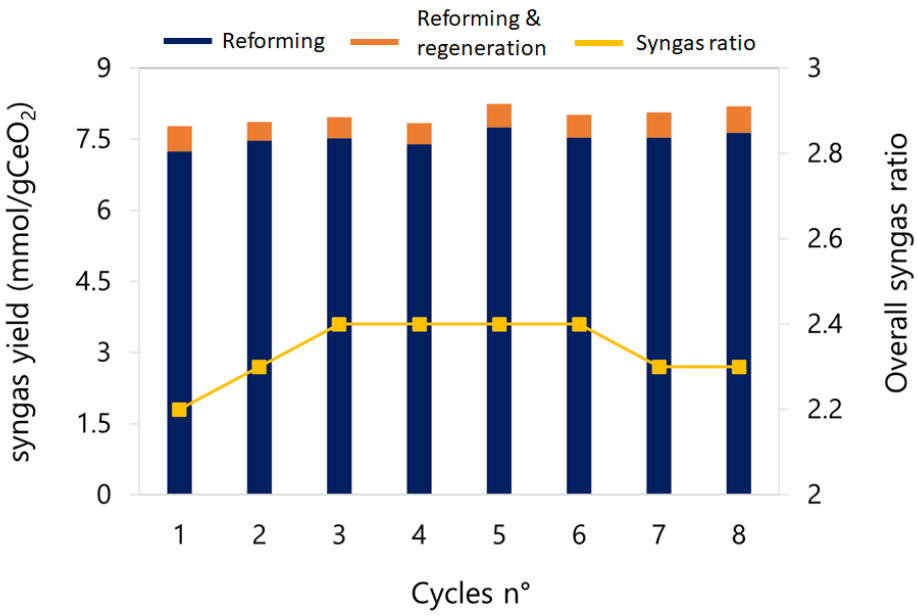

Figure 28: Syngas yield and ratio achieved after completing redox cycles.

Also, considering the results obtained, a larger number of cycles need to be carried out to evaluate optimal work conditions and guarantee the maintenance of long-term performance without recording drops in production.

6 Conclusion

Hydrogen and syngas production processes need to be further studied to overcome the limitations that still obstacles their market and ensure low environmental impact as well as cost effectiveness.

Conversion processes have been extensively studied by varying materials and process configurations but to date the only recognized process applied on appreciable scales to secure the world's need for these resources is the steam reforming of methane (SRM), a process that releases about 9 to 12 tons of CO_2 per ton of hydrogen produced.

This work set out to study a commercial material and to study it in detail by selecting for the purpose a CeO_2 oxygen carrier, known to have properties suitable for the process, to be available and cheaper than the materials generally used such as supported noble metals.

The greater advantage associated with the fact that these latter materials continue to be studied lies in their high activity toward hydrocarbons, which allows for high reactant conversions and good product formation rates.

The objective of this work was to study the limits of a commercial material processed by simple forming procedure and to increase its performance and lifetime through the evaluation of optimal process times with the future prospect of evaluating other material porosities, to overcome the kinetic limitations that obstacle the full conversion of the CeO_2 carrier.

Thermodynamic predictions obtained through simulations in Aspen plus showed that it was possible to work with ceria even at lower temperatures than those selected without negatively impact on syngas selectivity and on the desired ratio for the mixture (2-2.5).

TGA characterization provided useful information on the carrier behavior under redox looping cycles proving the solid-gas reactivity and the ease of carrier regeneration at low and high temperatures, respectively 400 °C and 900°C, highlighting how regeneration is not limiting in the process.

Fixed bed experiments carried out at different temperatures allowed testing the material at higher scale (15.34 g of CeO_2), to detect the gas evolved and to evaluate the contribution of each of the reactions involved in the process.

knowledge of the reaction pattern enabled further refinement of the data analysis by allowing a distinction to be made between the hydrogen formed by the oxidation and that obtained by thermolysis, thus giving a direct indication on the amount of carbon generated as a function of time.

From this latter data elaboration emerged that reforming test interrupt at 10 or 20 minutes could prevent carbon formation or limit it to an amount potentially easier to remove at the process conditions investigated.

However, carbon build up lasting the reforming 30 minutes did not compromise oxygen recovery by the carrier as testify by the unitary efficiency of regeneration calculated for eight consecutive cycles.

Futhermore carbon reoxidation made it possibile to increase the total syngas yield adjusting the ratio of syngas at $\sim$ 2.4, which is desired for the greater of syngas applications.

In conclusion the capability to operate the cycle isothermally at 950°C with stable performance using CeO_2 as oxygen carrier was proved under a limited number of cycles with an amount of carbon build up which did not obstacle the carrier performance. Also, the experimentally measured data reported in this work are consistent with other reported experimental values. [64]

However, the material must be tested for a higher number of cycles, to define the carrier lifetime, and the same must be done running the reforming at shorter times (10 and/or 20 minutes) to allow a complete comparison of the performance achievable employing the as prepared pellets of commercial CeO_2.

7 Research activity abroad

Part of the research activity was carried out abroad to gain new knowledge on the topics related to CO_2 capture and mitigation.

The activity took place at the Swiss Federal Institute of Zurich (ETH) from January 10th to October 14th, 2022.

Specifically, it was carried out in the separation process laboratory (SPL) of the institute of energy and process engineering under the supervision of Prof. Marco Mazzotti working on a project aimed at establishing the potential of amine-functionalized alumina pellets and monolith for Direct Air Capture applications.

The project was publicly funded, and it was direct in strict collaboration with other PhD students allowing to study the applicability of the investigated contactors from a fluid dynamic, modelling, and experimental point of view.

7.1 Materials

In this work, pellets of γ alumina and honeycomb monolith, made of mullite partially wash coat with 7.4% of γ alumina, were studied before and after an in-house functionalization with amine.

Monolith was provided by HUG Engineering while pellets came from Saint Gobain.

The aim of the study was to frame the performance achievable with the utilization of contactors of different shapes for DAC applications, where with contactor is meant the overall configuration assumed by the solid-gas interface.

One monolith corresponds to its contactor geometry, whereas for pellets the packed bed arrangement is classified as a contactor (Fig. 29).

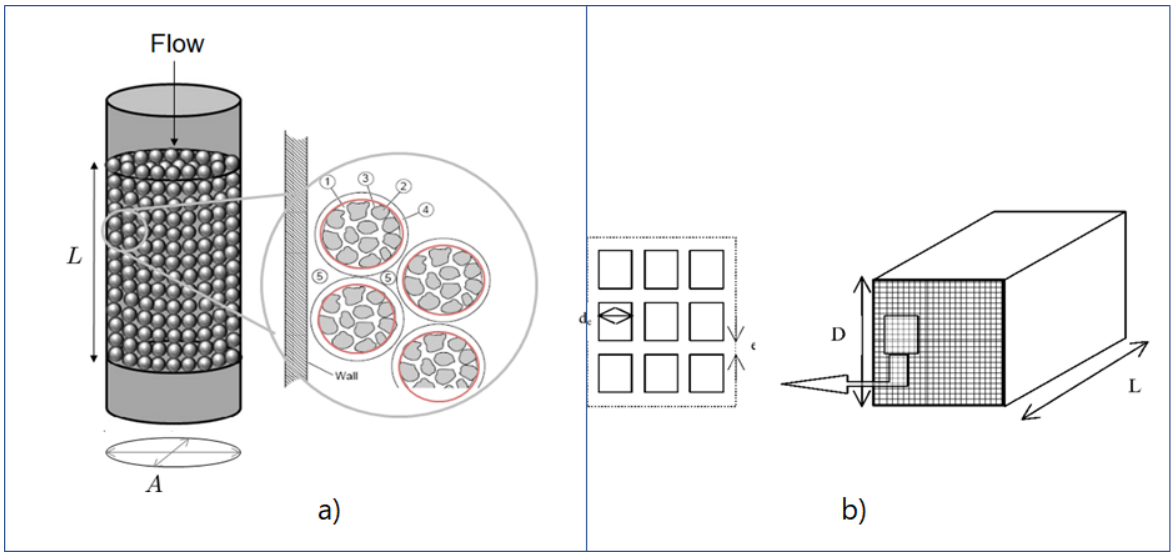

Figure 29: Details of the gas-solid interphase of pellets and monolith.

Pellets are made of 100% of γ alumina with mesopores of ~ 13nm while the basic mullite only contains macropores of ~ 22 µm, and mesopores of ~ 28nm are introduced with γ -alumina wash coat.

Mesopores are the area where the functionalization of amine occurs, therefore, they define the amount of active sorbent which is possible to deposit. Consequently, pellets allow to work with the 100% of active sorbent while monolith active sorbent is function on how much γ alumina pocket can be added inside the mullite macropores.

The relevant properties of the materials employed are summarized in table 5 and 6.

	Value
Pellet size [m]	0.003
Pore size [nm]	13.3
Material density [kg m^{-3}]	3600
Pellet density [kg m^{-3}]	1044
Pellet porosity [-]	0.71

Table 5: γ-Alumina rings properties.

	Value
Length [cm]	13
Width [cm]	2.9
Wall thickness [mm]	0.4
Mullite density [kg m^{-3}]	3030
Mullite pore size [µm]	22
γ-Alumina pore size [nm]	28

Table 6: Monolith properties.

Representative pictures of the materials are reported in Fig. 30.

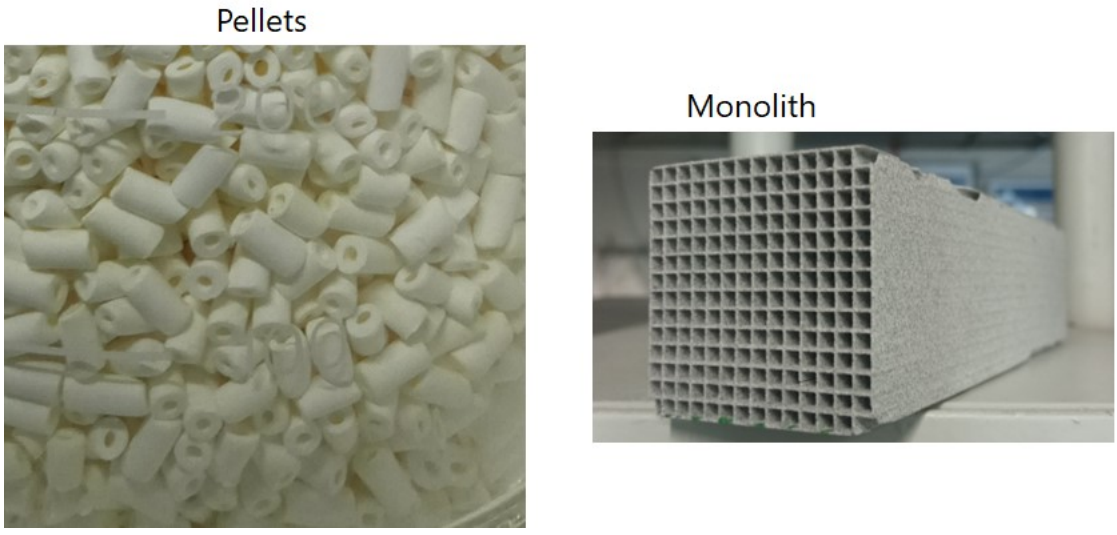

Figure 30: Contactors studied during the experimental campaign.

7.2 Set-up for testing

In the first part of the project, it was verified the operational of a set up already available, and it was modified to be able to work with two different configurations of the system.

Two heating systems were tested, one electrical heater connected to a cylindrical column surrounded by electrical coils (Fig. 31a), and one thermostat bath linked to the internal jacket of a square column, specifically designed to houses honeycomb monoliths (Fig. 31b).

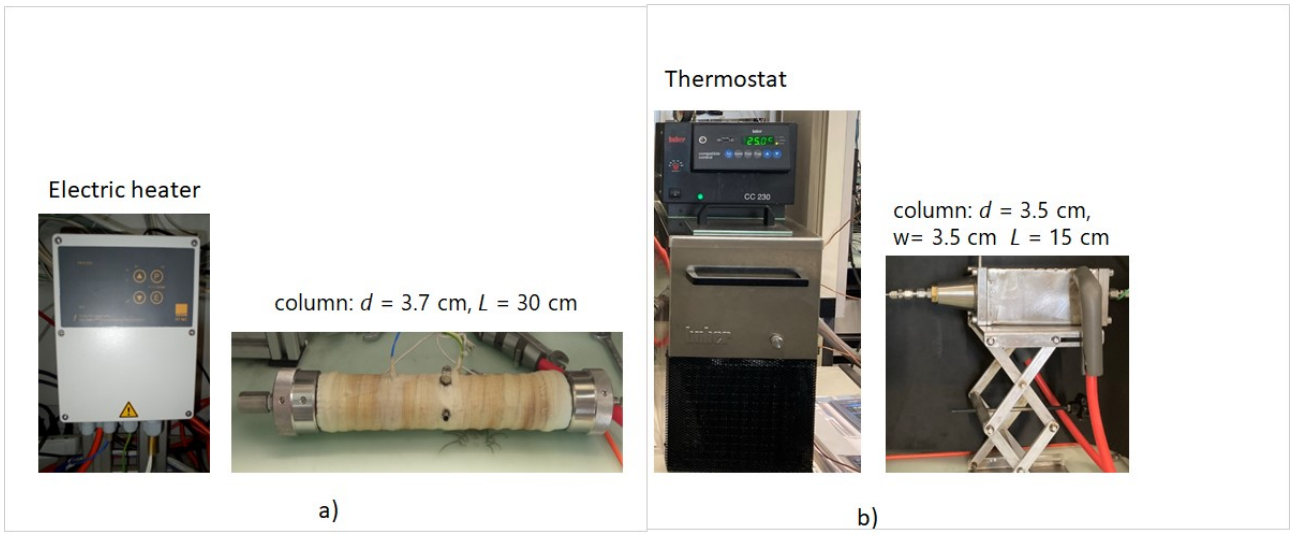

Figure 31: Equipment to carry out the testing for pellets and monolith.

The set up was designed in a way to easily switch configuration, with the first layout employed to test packed beds and the second one to evaluate monolith performance.

The overall rig is made of three main sections: a feeding system, an adsorption apparatus, and a gas analysis system.

Fig. 32 reported the rig as it was before the beginning of this experimental campaign.

As shown in the scheme the setup was already quite equipped to carry out adsorption measurement both in wet (valve V1-V3) and dry conditions (valve V2-V4).

However, it was not used for direct air capture measurement before the start of the collaboration, so it was necessary to make it suitable for the testing at low CO_2 concentrations and to adjust it in a way to be able to quantify both CO_2 adsorption and desorption to properly describe the sorbent performance.

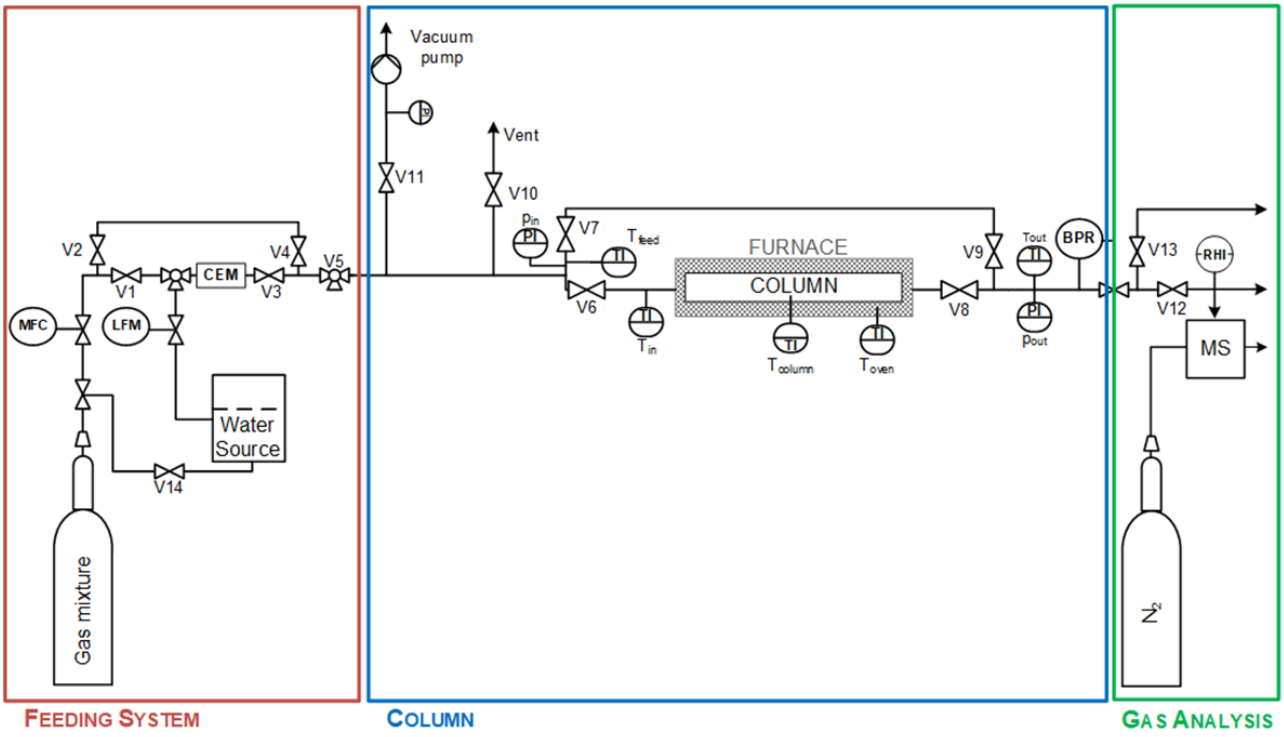

Figure 32: Set up available et SPL facilities for wet and dry adsorption testing.

Two mixtures of carbon dioxide in nitrogen [5.62% CO_2; 400 ppm CO_2] and compressed air were needed to carry out the experimental plan.

Therefore, a second mass flow controller (MFC2) was introduced for the testing at the lower composition and a tee connection was added to use compressed air coming from a closed line (Fig. 33).

Preliminary tests were performed on non-functionalized pellets to identify the feed conditions in terms of gas pressure and flowrate needed to guarantee low pressure drop and simultaneously short experimental times, at high and low CO_2 content.

Indeed, dealing with low concentration means increasing the experimental time to reach saturation therefore a higher flow rate must be fed if compared with a higher content of CO_2 to carried out tests at reasonable times.

For this reason, MFC2 and the analysis system were arranged in a way to minimize the path of the gas stream placing both closer to the column thus decreasing the pressure drop and allowing the utilization of higher flow rates.

MFC1 was left in the same position since it was employed for testing at higher composition and the pressure in the column was not particularly affected by the flow rate needed with its utilization.

A third mass flow controller (MFC3) was installed after the pump outlet to quantify the desorption.

As analytic system, a mass spectrometer (Pfeiffer Vacuum), was initially used to detect the CO_2 at the column outlet but it was then replaced with specific CO_2 sensors due to several limitations encountered with its utilization.

The main problem was the instability over time of the signal. Several strategies were adopted to account for this effect, but they could not offer the same precision achievable with the Vaisala sensor, which were

preferred since these experiments are also functional for comparison with a modeling study now ongoing and a very high quality of experimental data is therefore required.

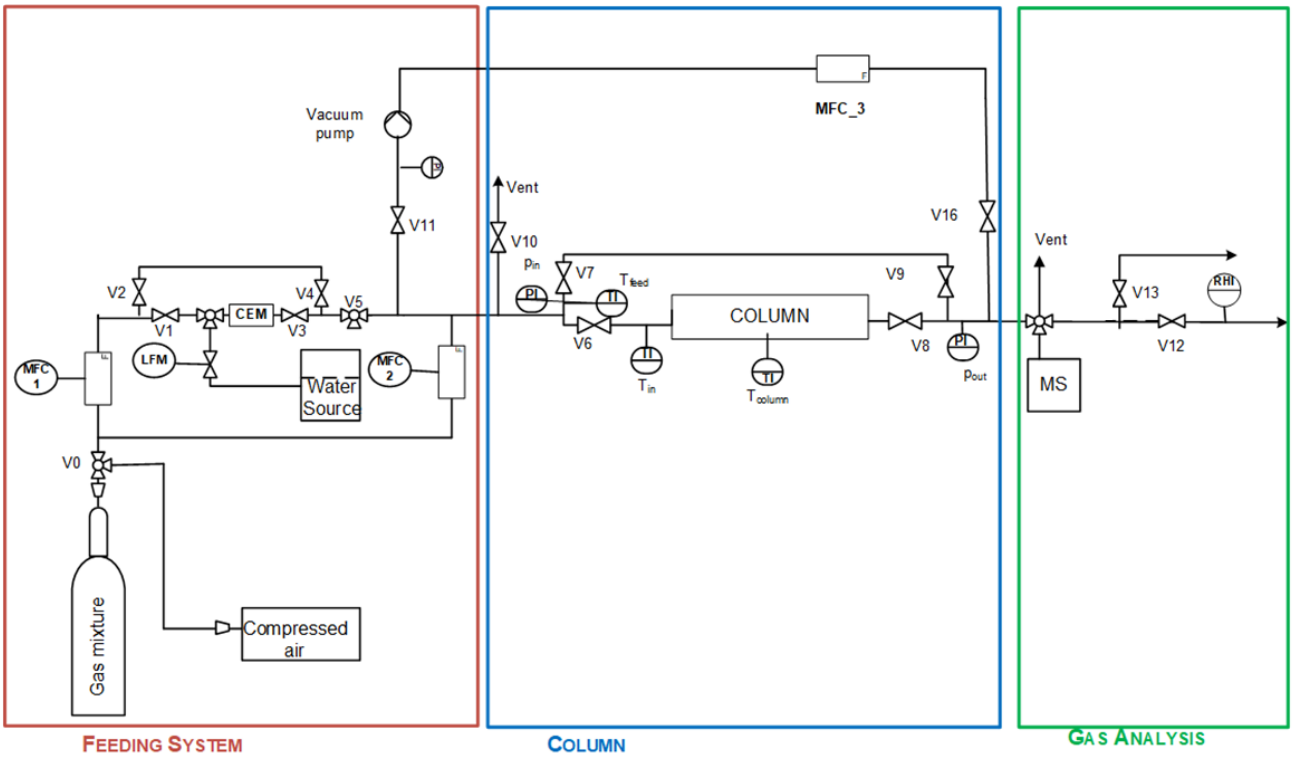

Figure 33: Set up after the first adjustment.

The adsorption was performed in dry condition, atmospheric pressure, and temperature around 23°C, while the regeneration was carried out at 100°C and under vacuum (~ 1 mbar) thus conducting the overall process in temperature vacuum swing adsorption mode (TVSA) as schematized in picture Fig. 34a.

In the TVSA cycle, for the adsorption stage, the adsorbent performances were evaluated through the quantification of the CO_2 uptake and through the analysis of the breakthrough curves, while for the desorption stage it was not possible to quantify the desorbed CO_2 for both the contactors, since the poor CO_2 flow and the proximity to the vent of the MS analysis system caused the dilution of the outlet stream.

Therefore initially, the goodness of the regeneration was evaluated indirectly, comparing the overlap of the adsorption curves achieved keeping constant all the process conditions for several TVSA cycles; while in the second part of the experimental campaign for the pure purpose of quantification the material was regenerated with a purge with N_2, and Vaisala sensors were used to quantify both the stages adopting a process configuration such as that shown in Fig. 34b.

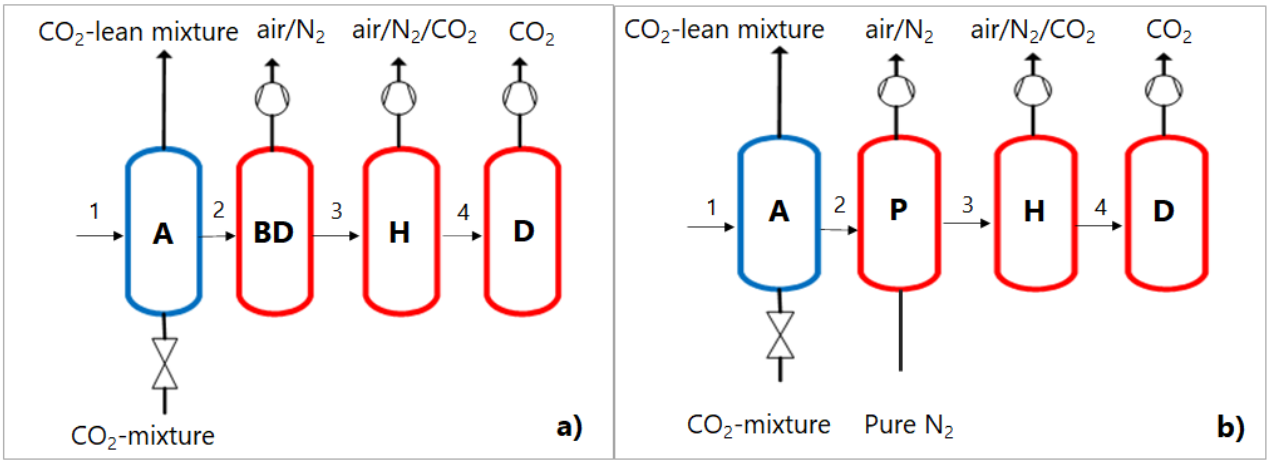

Figure 34: Stages of the process depending on the way of conducting: a) A: adsorption until saturation of the bed, BD: column evacuation down to vacuum pressure and external heating, H) external heating to fully remove air/N_2, D) desorption of CO_2 at vacuum via external heating; b) A: adsorption until saturation of the bed, P: column purge with N_2 and external heating, H:external heating to fully remove air/N_2, D) desorption of CO_2 with N_2 and external heating.

A visual sketch of the final configuration employed for this second part of the testing is provided in Fig. 35, since all the results reported from now on have been obtained with this configuration which provided the most accurate data.

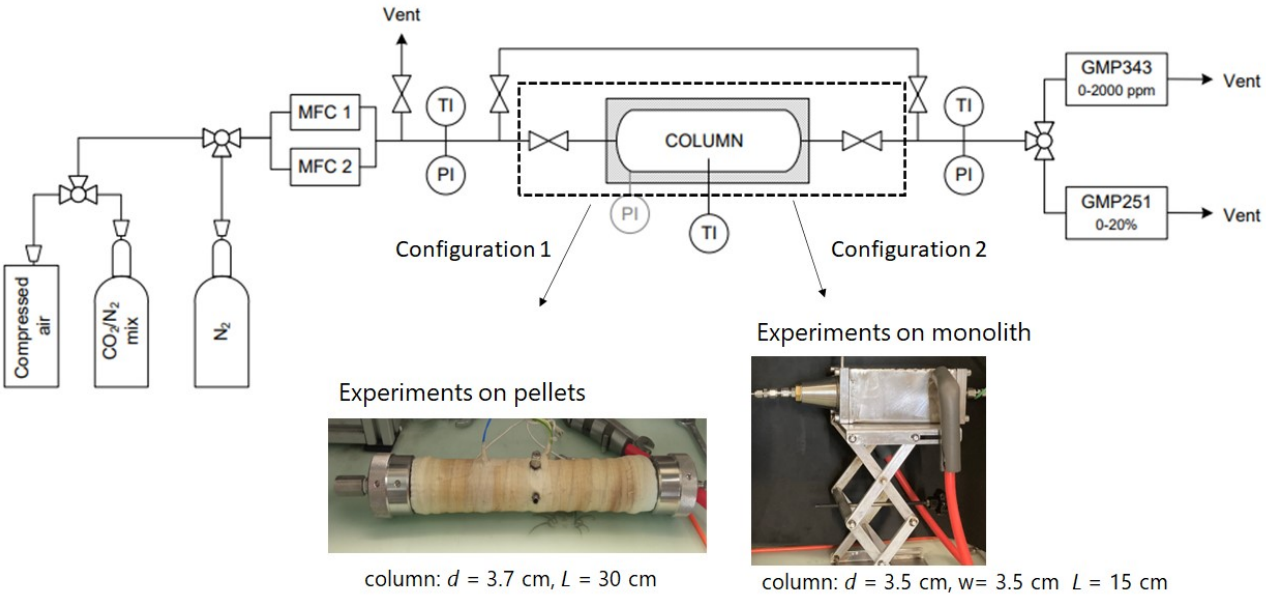

Figure 35: Experimental set up sketch of the final equipment employed for testing.

Different types of experiments were done testing the performance of pellet and monolith varying concentrations and flow rates.

For the monolith also a new design of the contactor was proposed and tested as a potential solution to improve the slow kinetic typical of the adsorption at low concentrations.

Tables 7 and 8 summarized the experimental conditions.

Test motivation	n°exp.	yCO_2[-]	Flow rate [mol/s]
Reproducibility	3	0.05	0.001
	3	0.000382	0.002
Effect of flow rate	1	0.05	0.0005
	1	-	0.001
	1	-	0.002
Effect of concentration	1	0.05	0.002
	1	0.000382	0.002

Table 7: List of experiments done on pellets.

Test motivation	n°exp.	yCO_2[-]	Flow rate [mol/s]
Reproducibility	3	0.000382	0.001
	3	0.05	0.001
Effect of flow rate	1	0.000382	0.00018
	1	-	0.002
	1	-	0.003
	1	0.05	0.00002
	1	-	0.00006
	1	-	0.00018
Effect of concentration	1	0.000382	0.00018
	1	0.05	0.00018
Effect of plug addition	1	0.000382	0.00018
	1	-	0.002
	1	-	0.003

Table 8: List of experiments done on monolith.

7.2.1 Experimental protocol

In the experimental campaign two experimental procedures were developed that differ mainly for the desorption step being the adsorption basically the same for the two cases.

The procedures were equally applied to both contactors since the couple column/heating system was interchangeable and did not require further adjustments of the rest of the equipment.

The pressured mixtures were fed to the column at ambient temperature using Bronkhorst mass flow controller of different full scale depending on the inlet concentration.

Both the mass flow controllers were designed to work with mixtures but the ones available were calibrated for a different gas combination therefore calibration factor (CF) provided on Bronkhorst website were applied for the flow rate correction.

The calculation of the coefficient required defining the inlet conditions at the MFC: temperature, pressure, and gas composition.

MFCs were controlled by LabVIEW as well as the solenoid valves that regulated the flow in the bypass and through the column.

The experimental protocol was developed twice for the need to quantify desorption.

In the first experimental procedure the analysis system employed was an MS with problems of signal stability, therefore, before and after each adsorption experiment, the signal intensity of the mixture was recorded in the bypass line to monitor signal variation over time.

At the beginning the signal in the bypass was recorded for approximately 30 minutes since the MS measured through a withdrawal valve that needed some time for stabilization.

After this step the mixture was switched through the column for adsorption at ambient pressure and temperature.

At the column opening, the LabVIEW time was written down to be synchronized with the one of MS.

At the end of the adsorption, the signal was recorded again in the bypass for some minutes while the column was heated (thermostat/ heater depending on the contactors) and vacuumed.

A similar procedure was applied in the experiments made with Vaisala CO_2 sensor.

The time for collection of the signal in the bypass was reduced to five minutes and the desorption of CO_2 was achieved by heating and purging with inert gas.

7.2.2 Adsorption response

The result of this type of experiment is a breakthrough curve. A common representation shows the outlet fraction of the gas at the column exit as a function of the adsorption time as reported in Fig. 36a.

The knowledge of the significant times of the curve, BT point and equilibria, makes it possible to estimate, respectively, the maximum time of adsorption in the column without the escape of the gas to be treated and the saturation time of the sorbent under the conditions used. The breakthrough starting point is properly quantified if the dead volume is excluded from the representation.

The area delineated by hatching highlights the extent of adsorption and through mass balance allows quantification of the maximum sorbent capacity.

Once the goodness of regeneration is validated, repeating multiple adsorption experiments allows assessments of capacity loss or conversely ensured that the material retains its characteristics the overlap of the curves obtained under the same adsorption conditions can be used to improve the regeneration conditions (Fig. 36b).

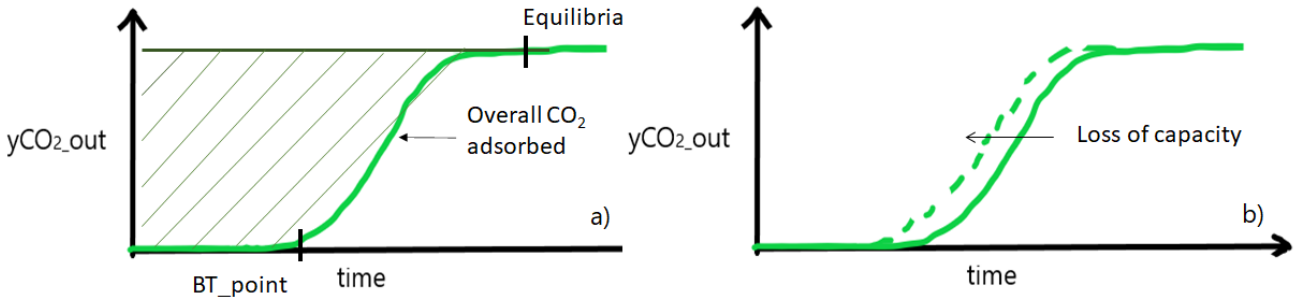

Figure 36: Main information achievable on the thermodynamic from a breakthrough curve.

The shape of the breakthroughs' curve contains kinetic information (Fig. 37). The whole zone in which the breakthrough front extends is called mass transfer zone (MTZ) and it is studied to identify the resistances to the mass transfer and to distinguish their different contributions to define the kinetic of adsorption.

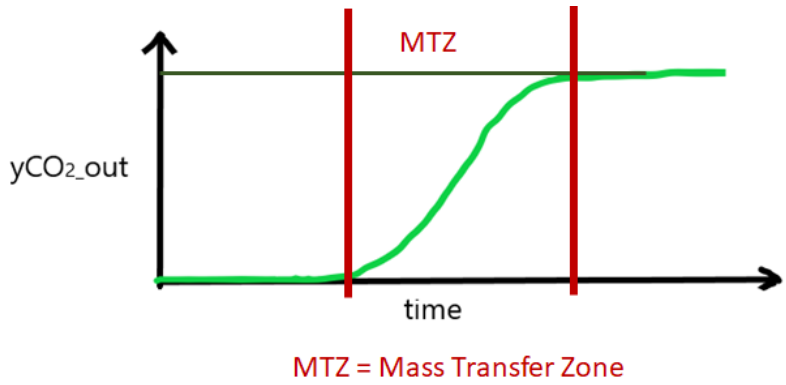

Figure 37: Area of interest for the Kinetic information achievable from a breakthrough curve.

During this work the breakthroughs' MTZ of the curves was plotted as a function of a relative time obtained as the difference of the experiment time and the time at half breakthrough (t50). In this way the time at t50 becomes the zero of each curve and it could be used for comparison.

7.3 Experiments motivation

7.3.1 Preliminary experiments

The two contactors were studied, prior to amine functionalization, to evaluate the presence and the extent of other phenomena, such as sensors response time and axial dispersion, on the shape of the breakthrough curve.

The response time was measured through the bypass connection at all the composition and velocities planned for the experiments while axial dispersion was evaluated at the same conditions but with breakthrough experiments through the column.

The volume of the bypass was not considered during response time experiments due to the short length and thin diameter of the piping line.

Axial dispersion experiments were made on monolith and pellets but in presence of these latter was not possible to properly quantify the effect due to γ alumina uptake.

7.3.2 Effect of flow rate

All other conditions being equal, variations in flow rate affect the film resistance.

Normally increasing the flow rate allows to overcome kinetic limitations related to gaseous film formation which originates to a greater extent as the adsorption proceeds.

The film is established in laminar regimes while it is less common in the presence of turbulent motions, so in the case considered this effect is more expected on experiments done with monolith.

The value of the flow rates was decided based on load of active sorbent. Monolith houses less sorbent than pellets therefore lower flow rates were employed to avoid immediate breakthrough.

On the contrary, on pellets the large presence of active sorbent prompted working at the highest flow rates achievable with the available flow meters so as not to incur in too long experiments, especially at the low concentration.

The experiments at different flow rates were done to check the presence of film resistance and eventually find the conditions to avoid its formation to increase the kinetic of adsorption.

7.3.3 Effect of concentration

The definition of the impact of the concentration of the stream to be processed on the kinetic is of fundamental importance for the development of DAC applications.

It is enough to say that, at equal amount of adsorption sites, a stream with low CO_2 concentration will take more time to occupy the same number of sites than one stream where the gas phase is richer in adsorbate.

This concept is also well visible in the adsorption isotherm, where the slope of the solid-gas ratio (q/c) decreases as the CO_2 partial pressure increases.

In the adopted linear driving force model, the mass transfer is described by a lump coefficient calculated as follow:

$$K = (K_f + K_p) \cdot \frac{C_{in}}{q^*_{in}}$$

Where K_f is the index of the transport through the film coefficient, K_p is the equivalent in the adsorbent porosities while $\frac{C_{in}}{q^*_{in}}$ consider the concentration dependency.

The investigation of the role that each of these factors plays is crucial in the definition of the kinetic of adsorption as evident from the relation existing between the adsorption capture rate and the mass transfer coefficient:

$$\frac{\partial q}{\partial t} = k(q^* - q)$$

In this work the effect of concentration on the kinetic was evaluated with testing at two compositions, namely, 5.62% CO_2 in N_2 and 382 ppm CO_2 in N_2.

In the beginning the two contactors were compared separately, testing their behavior with experiments at different composition for the same contactor.

Finally, the trends of pellet and monolith breakthrough curves were compared at the same flow rate and composition to evaluate which contactor geometry could be more competitive for the adsorption stage of a DAC process.

7.3.4 Addition of the 3D plug

The configuration of the sorbent defines the solid-gas interphase and strongly influences the interaction between adsorbate and absorbent. Therefore, customizing the design of a contactor allows to intervene in the dynamics of the adsorption process.

In this prospective during the work, a new design was proposed for the monolith with the aim of improving the performance respect those of the monolith in the traditional layout at open channels.

A 3D printed plug made of Nylon 12, was designed and applied to both the external sides of the monolith, closing each channel alternately and taking care of applying the plug complementary on the ends of the contactor as shown in the Fig. 38.

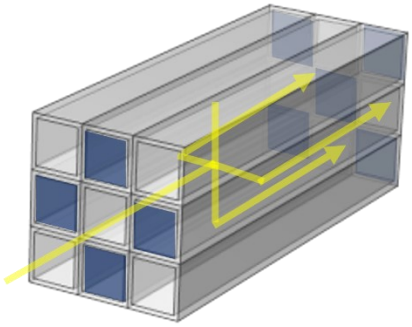

Figure 38: Flow direction for a monolith with closed channels.

The insertion of the plug blocks part of the channel varying the effective velocity within each channel and forcing the flow through the wall without bring any loss in the adsorption capacity since it does not interfere with the amount of sorbent which can be deposited but it only deals with kinetic.

In this configuration a mixture of Ergun and Hagen-Poiseuille pressure profile is expected together with an increase in the mass transfer due to a decrease of pores resistance.

The difference in the performance achievable with this new configuration is a novelty in the field of DAC, indeed in literature results of adsorption achieved with this contactor has not been found.

Experiments at the different flow rates were carried out on the monolith with open channels and the results were compared with those achievable with the plugged monolith to evaluate their difference in kinetic.

7.4 Data processing

The data analysis was made with MATLAB combining the information exported from LabVIEW with those of an external excel file which contained the MS data originally available as a text document. The properties of the column were added directly as .mat file.

Other parameters useful for calculations were retrieved from a second excel file where it was defined for each experiments the feed condition, the MFC used and the CF to be applied and the dead volume together with the LabVIEW time when the MS was start up and when the column was opened.

At each interval the inlet volumetric flow rate was calculated multiplying the flow rate set $\dot{V}_{n,cal}$ for the CF to evaluate the true flow rate. The subscript n depends on the fact that the MFC was calibrated under normal condition.

$$\dot{V}_{n,mix} = \dot{V}_{n,cal} \cdot CF \quad \rightarrow \quad \dot{n}_{in} = \dot{V}_{n,mix}\,(P, T)$$

The outlet flow rate was obtained from the molar balance on the inert species.

$$\dot{n}_{out} = \frac{\dot{n}_{in}\,(1 - y_{CO2,in})}{(1 - y_{CO2,out})}$$

Knowing the molar flow rate and the composition, CO_2 contribution was defined in each interval:

$$\dot{n}_{CO2,in} = \dot{n}_{in} \cdot y_{CO2,in}$$

$$\dot{n}_{CO2,out} = \dot{n}_{out} \cdot y_{CO2,out}$$

After integration over time the total uptake was achieved.

The processing with the Vaisala sensors was the same relative to the adsorption step.

The only difference was in the format of the file from which the data was extracted.

The desorption was quantified only in presence of Vaisala sensors considering zero the CO_2 inlet and applying the conversion factor the MFC at the column outlet.

7.5 Main contributions of this work

The experimental campaign brought new knowledge on the use of packed beds and monolith for the adsorption process at low CO_2 concentrations.

At first it evidenced the possibility to achieve reproducible results for both the contactors at different concentrations. In Fig. 39 are reported the results of the reproducibility obtained at the amount of CO_2 handled in DAC applications.

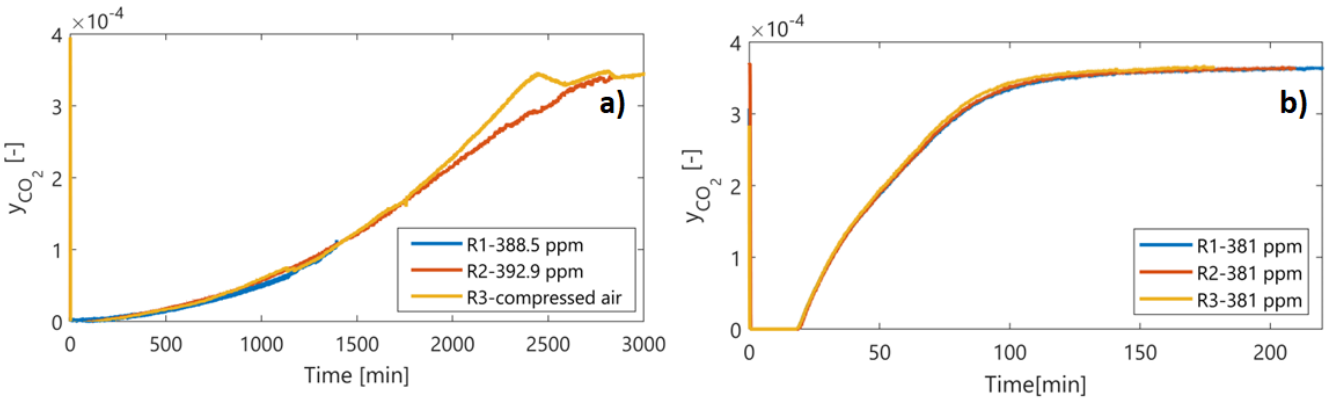

Figure 39:Reproducibility test measured on a) pellets, b) monolith.

Some discrepancy is visible in the curves profile achieved over pellet (Fig. 39a) while an almost complete overlap of the breakthrough curves is evident for the case of the monolith (Fig. 39b).

However, the experiments on pellets took so much longer due the larger sorbent loading, allowed by a packed bed configuration of the column, which made difficult to complete an entire experiment with the utilization of a single gas bottle, and brough to run experiments with tanks at slightly different compositions depending on the gas bottle availability.

The possibility to work with air was also checked and its trend over time recorded for approximately two days. The reproducibility achieved could be considered quite good in all cases considering the almost complete overlap of the curve for more than one day.

The deviation after 30h for the case of air (R3 in Fig. 40a) was attributed to the failure of the mass flow controller to stabilize change in the pressure of the compressed air, which could be quite variable for long use.

Packed beds and monoliths both showed good reproducibility. However, they required a very diverse time to complete the breakthrough curve due to different sorbent loading but also to differences in the kinetic of the adsorption process.

For the evaluation of the capture rate, a model with a linear driving force and a lump mass transfer coefficient was considered.

Preliminary experiments were done to decouple the contributions on kinetic of axial dispersion and mass transfer.

First breakthrough profiles were recorded in the bypass to exclude the dead volume and the sensor response time from kinetic evaluation (Fig. 40). Next experiments were done through a not functionalized contactor (Fig. 41).

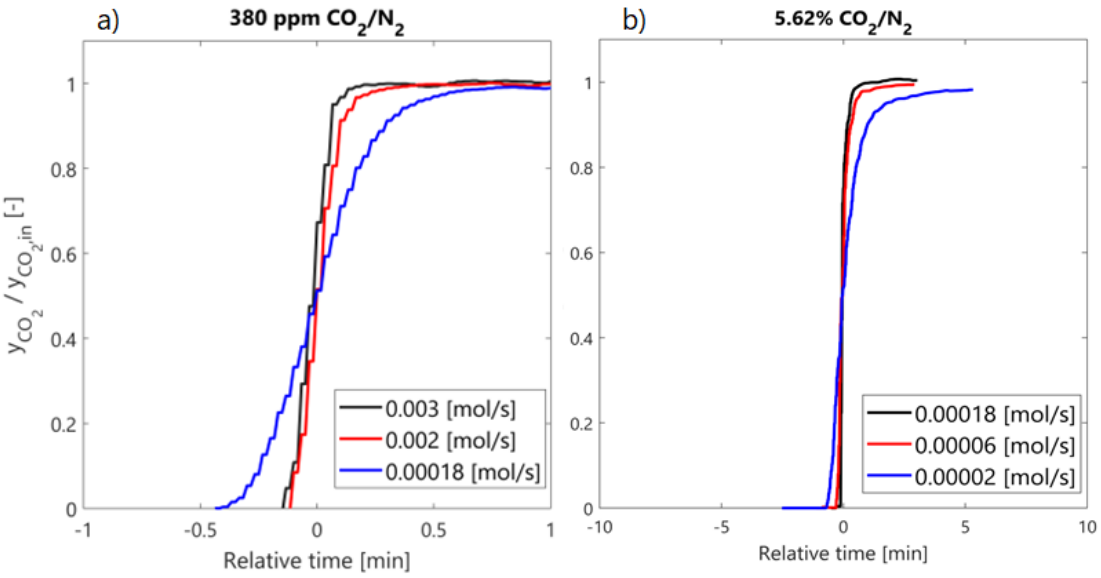

Figure 40: Total delay time at the main velocities and compositions employed for testing pellets and monolith.

Total delay (sensor response plus dead time) was measured at the main concentrations and velocities employed during the experiments on both the contactors.

The image shows the results as a function of a relative time to facilitate the comparison of the breakthrough front.

As one can see very sharp profiles can be achieved at the high and low flow rates, even though at low flow rates the flow requires significantly more time to reach the sensor.

Pipeline section and length were used to calculate the theoretical time required to reach the sensor to rule out any possibility that the delay could have been in part due to CO_2 uptake.

These calculations were repeated for all the flow rates and were found to follow absence of uptake.

For the case of monolith, axial dispersion results are reported for the same conditions in Fig. 41, while for pellets these data are not available due to the occurrence of adsorption phenomena during the testing of non-functionalized rings.

As evident from the discrepancies in the slope obtained at different velocities, at both composition axial dispersion contributes to the kinetic, even though in different extent depending on CO_2 concentration.

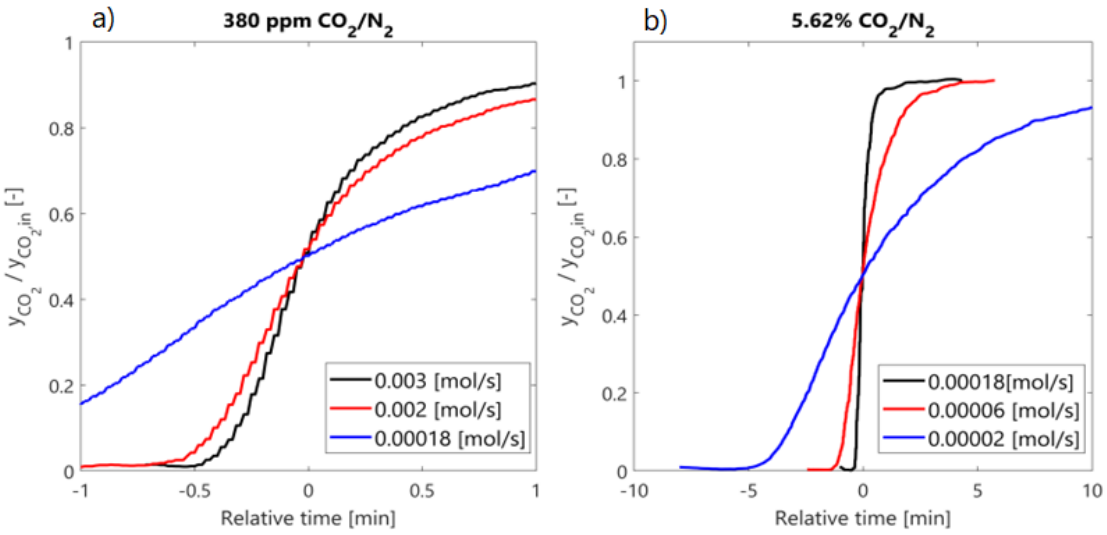

Figure 41: Axial dispersion results for monolith.

A visual representation of the impact of its presence on the experiments is provided at the higher composition, where the effect is predominant, in Fig. 42.

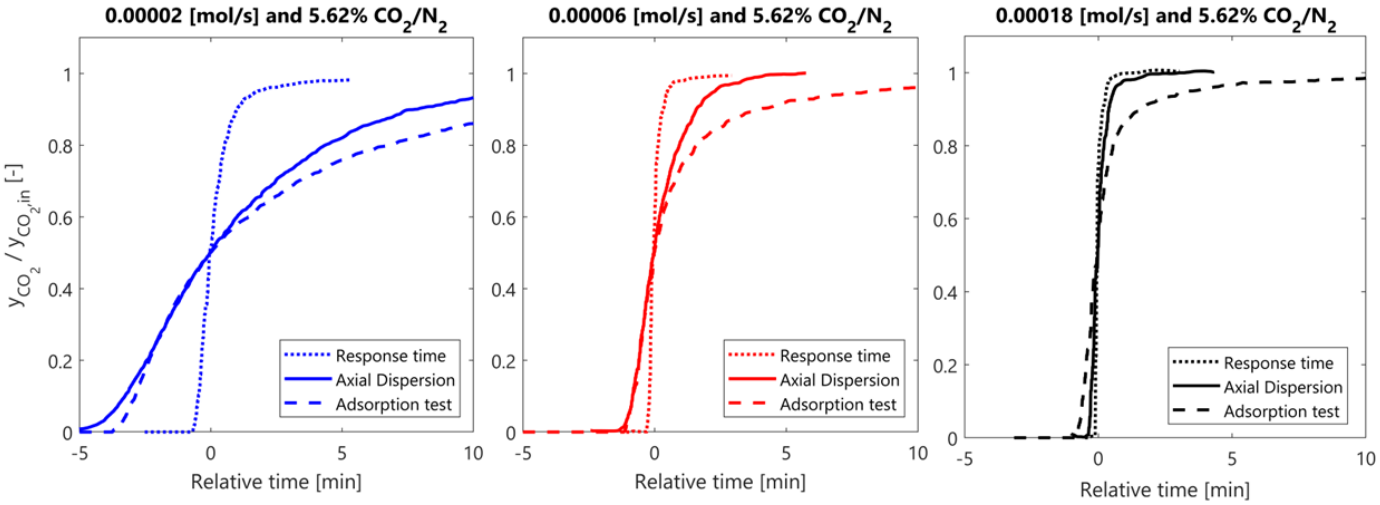

Figure 42: Contribution of axial dispersion in adsorption test at different velocities related to a monolithic contactor.

As shown in the image the response time has not influence on the overall resistance while axial dispersion accounts in all cases, slightly at the higher velocity but significantly at the lower flow rates.

Axial dispersion contribution could be seen as the difference between its curve and the one of the response times while the mass transfer effect is visible from the divergence of adsorption and axial dispersion curve.

Interestingly the behavior is quite different for the case of 382 ppm where adsorption is so slow that axial dispersion (AD) is no longer the main contributor and mass transfer becomes the limiting step (Fig. 43).

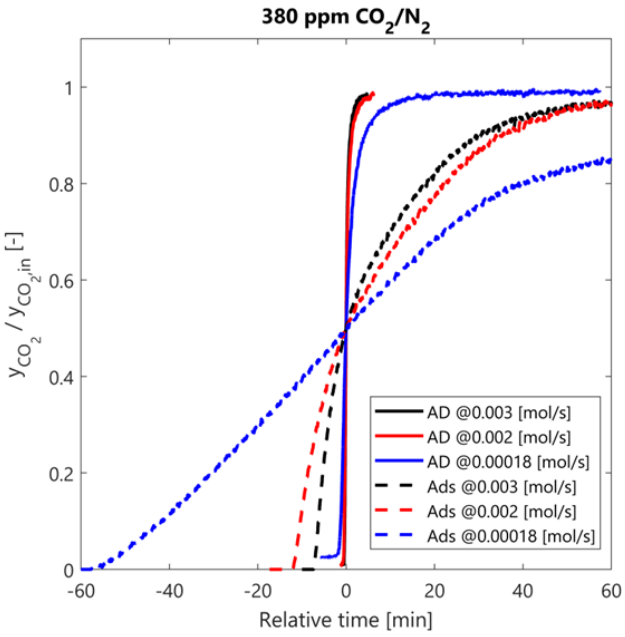

Figure 43: Effect of axial dispersion at low CO_2 concentrations.

Adsorption experiments for pellets are reported in Fig. 44.

Despite these trends, it is not possible to make complete statements due to the lack of axial dispersion data, it is reasonable to exclude the presence of film resistance, due to the slight differences in the slope of the breakthrough curve at higher flow rates and to the literature background on the limiting phenomena on packed bed.

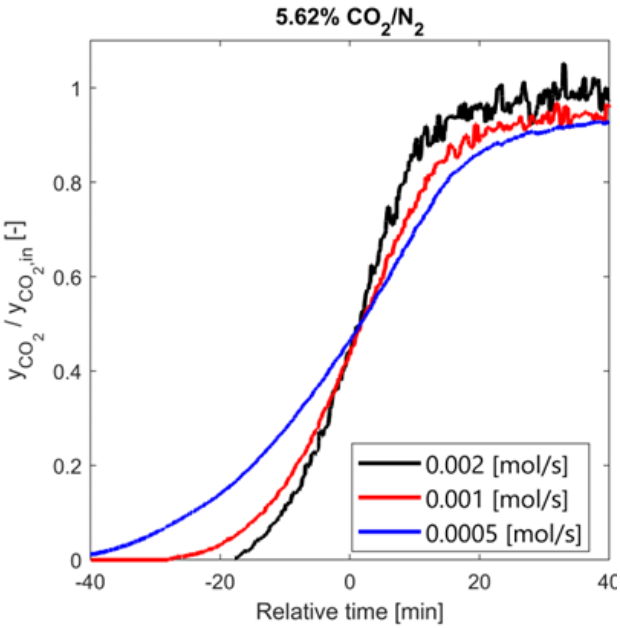

Figure 44: Adsorption measurements on pellets at different flow rates.

The discrepancy observed between the curve at low and high flow rate is most likely due to axial dispersion. However, experiments on non-functionalized pellets of an inert material of similar dimensions are necessary to confirm these considerations.

Tests at equal flow rates and different concentrations, on both contactors, were done at the highest flow rates possible between the ones employed.

Particularly, 0.002 mol/s was selected based on the maximum flow rate provided by the MFC to reach acceptable experimental times for pellets, while 0.00018 mol/s was employed for monolith using the maximum flow rate to avoid immediate breakthrough at the 5.62% of CO_2 and to decrease the influence of film resistance at the same time.

In the two cases the pores contribution acts similar on the curves being the contactor the same, so influence of resistance in the pores can be considered negligible in this comparison.

In Fig. 45a are reported the results obtained on pellets while in Fig. 45b are shown the trends achieved for monolith, at the concentration tested (5.62% and 382 ppm CO_2 in N_2).

The plots show that at low concentrations the kinetics are severely slowed in both cases with a decrease in the mass transfer that can be considered proportional to the c_{in}/q_{in}* ratio.

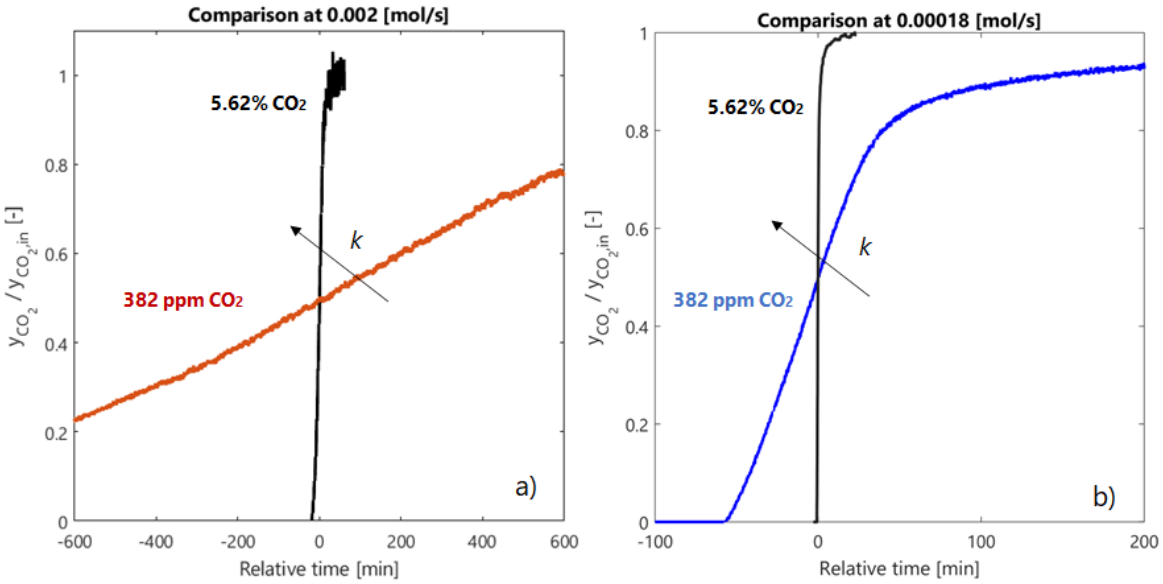

Figure 45: Effect of concentration on a) pellets and b) monolith.

The fall of the mass transfer coefficient was estimated through the calculation of the gas-solid ratio, where the gas concentration (c) was obtained by the ideal gas law at the inlet condition of pressure and temperature while the concentration of the adsorbed CO_2 (q) was derived from the isotherm.

The ratio results of ~ 60 for both cases since the inlet concentrations used are the same and the isotherm ratio was proved to be the same between the contactors.

In Fig. 46 the effect on kinetics induced by the low CO_2 concentration was looked specifically on pellets and monolith in a comparison at equal flow rate and composition.

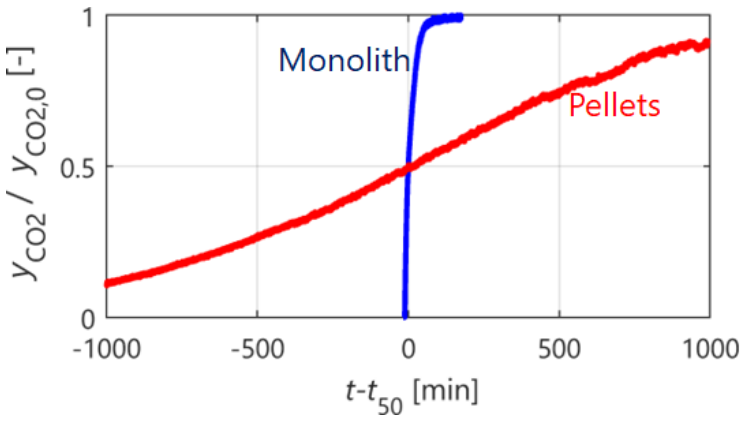

Figure 46: Comparison between pellets and monolith at equal flow rate [0.002 mol/s] and CO_2 concentration [382ppm].

The steeper curve achieved for monolith testifies a more effective mass transfer with respect to pellets.

The reasons behind this behavior were explained by the higher gas solid ratio and the different porosities of the two contactors.

Indeed, in this case, the inlet concentration is the same but the adsorption sites available for the uptake are less on the monolith due to the lower sorbent deposited on its walls.

This implies that the same amount of gas must occupy fewer adsorption sites and consequently this takes less.

Also, while pellets only have mesopores, the mullite, which constitutes the monolith, has macro and mesopores allowing for better gas diffusions and it offers shorter paths to the gas as well. Indeed, the CO_2 molecules must pass through a wall of 0.4 mm instead of a pellet of 3 mm.

Up to this point experiments made varying the feed concentration and flow rate allowed to gain knowledge on how $K_f, K_p, \frac{C_{in}}{q^*_{in}}$ influence the adsorption kinetics.

On monolith the stronger limitations on mass transfer appeared to come from film resistance therefore a more effective configuration of the monolith was proposed to overcome these limitations and further increase the kinetic in a prospective to boost the capture rate enough to adsorb as much as pellets at shorter times.

Indeed, the experiments showed that the kinetic of pellets appears to be limited mainly by the low CO_2 concentration fed rather than from film resistance, while for monolith this latter contribution seems to play a strong role.

This could be explain considering that the film formation results favored in the empty channels which constitute the monolith itself due to the higher probability to have a laminar flow regime, which is instead generally not the case of packed bed columns where turbulent regime are more common.

To disturb the laminar flow inside the monolith, a new configuration of the contactor was proposed and tested for the first time in this work.

A 3D printer plug was designed and applied to both the external sides of the monolith closing each channel alternately and taking care of applying the plug complementary on the ends of the contactor. In such a

configuration the flow enters the channel from which cannot exit and is forced to pass through the wall (Fig. 47).

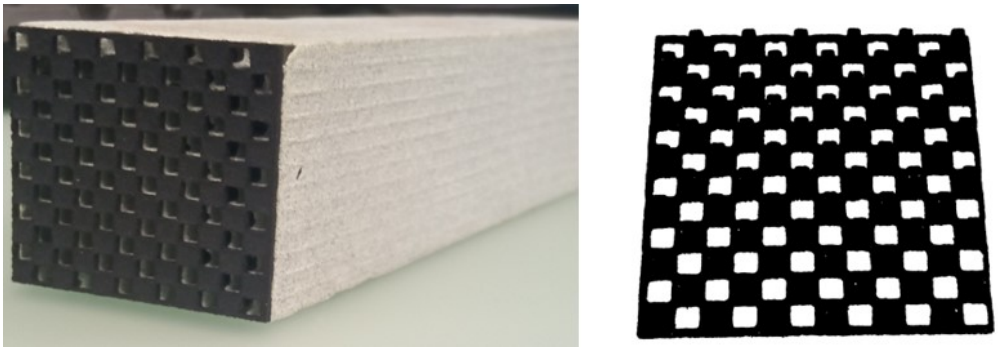

Figure 47: Monolith with the 3D printed plug (Nylon 12).

Also, in this condition the effective velocity inside each channel increases and a laminar regime is less favored.

Experiments at the same flow rates tested before on the monolith were repeated in presence of the plug to evaluate the impact on the breakthrough shape and compare it with the case of the unplugged monolith.

The same contactor was employed for testing since the plug was printed to perfectly fit the monolith and to ensure absence of leakages. A thin layer of a thermal resistant resin was applied between the plug and the monolith to avoid any movement of the plug.

The curves obtained with the plug are shown by dash line in Fig. 48. The shape of the breakthrough curves testifies that plug addition brings steeper profiles for all cases and consequently faster kinetics.

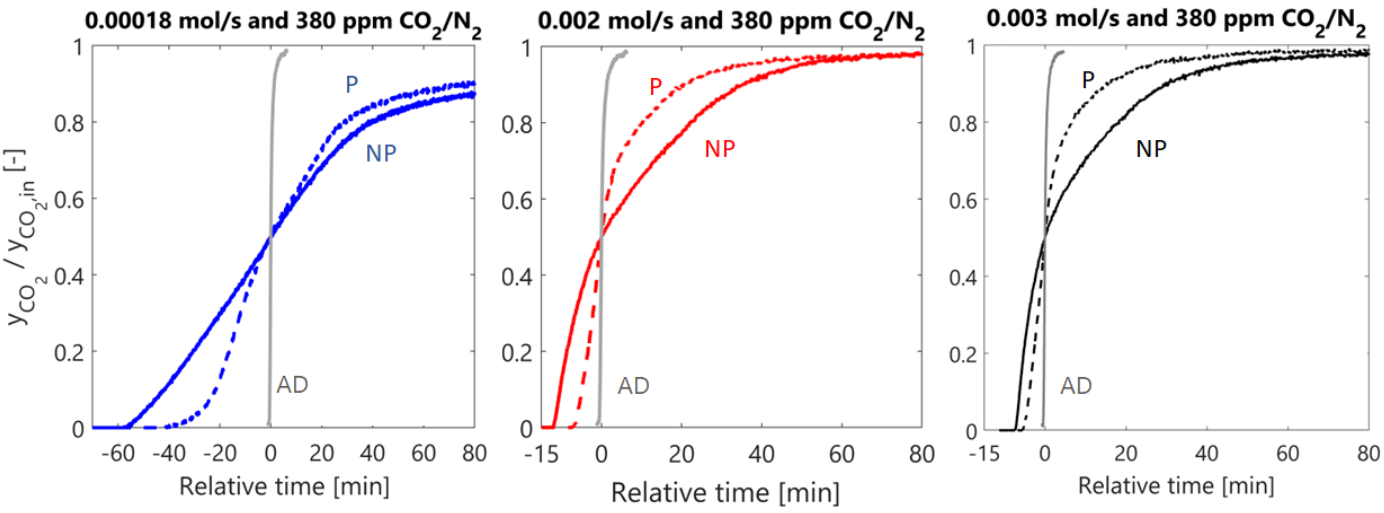

Figure 48: Influence of plug addition on the kinetic of the monolith at different flow rates.

The relevance, on an industrial scale, of productivity and cost effectiveness led us to represent the results in terms of these indexes.

The general performance of the contractors was therefore evaluated in terms of productivity and specific energy demand. All the specific energy contributions were calculated as follow:

$$W = \frac{\int_0^{t_{sat}} \frac{1}{\eta} \dot{V} \Delta P dt}{n_{\mathrm{ads}}}$$

As clear from the formula, the pressure profile which develops within the contactor largely impacts on the energetic demand of the blower, responsible to feed the air through the DAC module, and consequently on the cost effectiveness of the overall process.

Depending on the pressure drop that develops along the column the consumptions will be higher or lower.

The evaluation of this contribution is related to the knowledge of the flow regime since the pressure depends differently to the flow rate according to the regime that is being established.

In general rule turbulent regime brings to a quadratic increase of the pressure with the flow rate while laminar regime determines only a linear rise. Therefore, higher consumptions are expected for pellets.

Energy penalty (W) was calculated considering an efficiency of the fan (η) equal to 0.5 while the pressure difference was read on the manometer located on the conic flange of the monolith for this contactor and on the manometer at the column inlet for pellets.

The values were read on the same manometers at the end of experiments since when the experiment ends and there is no inlet flow in the column the manometer reads the atmospheric pressure.

The productivity was obtained as the ratio between the CO_2 mol captured up to 90% of CO_2 breakthrough and the time needed to reach this adsorption without constrains on recovery.

Indeed, in DAC applications the un-adsorbed CO_2 is re-emitted in ppm and not as concentrated stream as occurs in the processing of flue gas.

The results at different flow rates are depicted in Fig 49.

The analysis of the energy consumptions as a function of the productivity showed that, at the same flow rate, the monolith results favored over pellets and that the presence of the plug brings to an increase in the velocity of adsorption.

In all the conditions explored the plugged monolith appears to be less energy demanding than the corresponding unplugged (Fig. 49a). A slight trade-off is visible at the lower flow rate, but this is not particularly relevant since higher flow rates result in a much more convenient way to achieve good productivity.

These differences are also more substantial if the results are plotted normalized on the active sorbent, how is evident from the widening of the gap in the productivity of pellets and monolith (Fig. 49b).

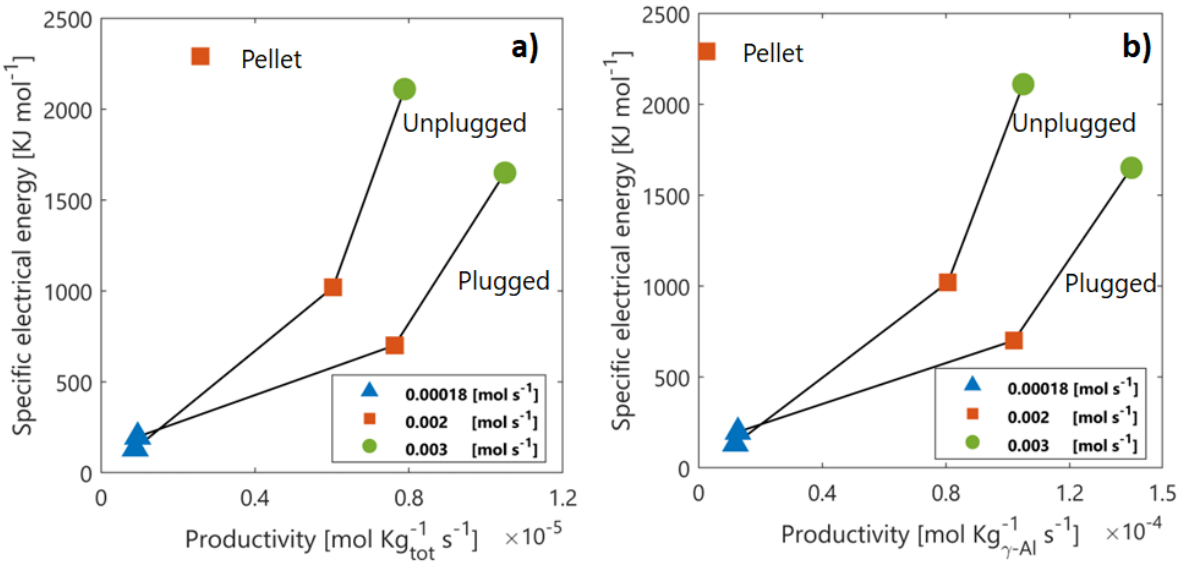

Figure 49: Specific energy demand as a function of productivity for pellet, monolith and plugged monolith normalized on a) contactor overall mass and on b) mass of active sorbent.

In conclusion, this study has led to the awareness that despite packed bed column being allowed to work with higher loading, in presence of such low concentrations, the utilization of monolith results favored due to strong kinetic limitations over pellets.

This places monolith as a more promising contactor than pellet at DAC concentration, at least relative to the adsorption stage. However, only a study that considers a whole cycle can allow us to determine the better contactor.

8 Bibliography

(1) Bereiter, B.; Eggleston, S.; Schmitt, J.; Nehrbass-Ahles, C.; Stocker, T. F.; Fischer, H.; Kipfstuhl, S.; Chappellaz, J. Revision of the EPICA Dome C CO_2 Record from 800 to 600 Kyr before Present: Analytical Bias in the EDC CO2 Record. *Geophys. Res. Lett.* **2015**, *42* (2), 542–549. https://doi.org/10.1002/2014GL061957.

(2) Hashemi, S. M.; Sedghkerdar, M. H.; Mahinpey, N. Calcium Looping Carbon Capture: Progress and Prospects. *Can J Chem Eng* **2022**, *100* (9), 2140–2171. https://doi.org/10.1002/cjce.24480.

(3) Dong, C.; Dong, X.; Jiang, Q.; Dong, K.; Liu, G. What Is the Probability of Achieving the Carbon Dioxide Emission Targets of the Paris Agreement? Evidence from the Top Ten Emitters. *Science of The Total Environment* **2018**, *622–623*, 1294–1303. https://doi.org/10.1016/j.scitotenv.2017.12.093.

(4) Hannah Ritchie, Max Roser, Pablo Rosado. our word in data. 'https://ourworldindata.org/co2-and-other-greenhouse-gas-emissions'.

(5) Christian Holter. Solar CEO:'Heating Electrification Is One of the Biggest Mistakes of the Energy Transition', 2019. https://www.euractiv.com/section/energy/interview/solar-ceo-heating-electrification-is-one-of-the-biggest-mistakes-of-the-energy-transition/.

(6) Zhang, R.; Fujimori, S. The Role of Transport Electrification in Global Climate Change Mitigation Scenarios. *Environ. Res. Lett.* **2020**, *15* (3), 034019. https://doi.org/10.1088/1748-9326/ab6658.

(7) Rüstemoğlu, H. Analysis of the Drivers of CO2 Emissions and Ecological Footprint Growth in Australia. *Energy Efficiency* **2022**, *15* (1), 1. https://doi.org/10.1007/s12053-021-10014-9.

(8) Rozzi, E.; Minuto, F. D.; Lanzini, A.; Leone, P. Green Synthetic Fuels: Renewable Routes for the Conversion of Non-Fossil Feedstocks into Gaseous Fuels and Their End Uses. *Energies* **2020**, *13* (2), 420. https://doi.org/10.3390/en13020420.

(9) Liu, Z.; Deng, Z.; Davis, S. J.; Giron, C.; Ciais, P. Monitoring Global Carbon Emissions in 2021. *Nat Rev Earth Environ* **2022**, *3* (4), 217–219. https://doi.org/10.1038/s43017-022-00285-w.

(10) Hannah Ritchie, Max Roser and Pablo Rosado. our word in data. 'https://ourworldindata.org/energy'.

(11) Economides, M. J.; Wood, D. A. The State of Natural Gas. *Journal of Natural Gas Science and Engineering* **2009**, *1* (1–2), 1–13. https://doi.org/10.1016/j.jngse.2009.03.005.

(12) Lunsford, J. H. Catalytic Conversion of Methane to More Useful Chemicals and Fuels: A Challenge for the 21st Century. *Catalysis Today* **2000**, *63* (2–4), 165–174. https://doi.org/10.1016/S0920-5861(00)00456-9.

(13) Tim Gould, Christophe McGlade. The Environmental Case for Natural Gas, IEA, Paris, 2017. https://www.iea.org/commentaries/the-environmental-case-for-natural-gas.

(14) IEA. *WEO Special Report: Are We Entering a Golden Age?*; 2011. https://www.iea.org/reports/weo-special-report-are-we-entering-a-golden-age.

(15) Global Industry. *Syngas and Derivatives Market (Feedstock: Coal, Petroleum, Biomass Waste, and Others; Production Technology: Partial Oxidation, Steam Reforming, Biomass Gasification, and Others; and End-User: Chemicals, Power Generation, Liquid Fuels, and Gaseous Fuels)- Global Industry Analysis, Size, Share, Growth, Trends, and Forecast, 2021-2031*. https://www.transparencymarketresearch.com/syngas-derivatives-market.html.

(16) Hernández, S.; Amin Farkhondehfal, M.; Sastre, F.; Makkee, M.; Saracco, G.; Russo, N. Syngas Production from Electrochemical Reduction of CO_2 : Current Status and Prospective Implementation. *Green Chem.* **2017**, *19* (10), 2326–2346. https://doi.org/10.1039/C7GC00398F.

(17) Abdin, Z.; Zafaranloo, A.; Rafiee, A.; Mérida, W.; Lipiński, W.; Khalilpour, K. R. Hydrogen as an Energy Vector. *Renewable and Sustainable Energy Reviews* **2020**, *120*, 109620. https://doi.org/10.1016/j.rser.2019.109620.

(18) Sun, Q.; Li, H.; Yan, J.; Liu, L.; Yu, Z.; Yu, X. Selection of Appropriate Biogas Upgrading Technology-a Review of Biogas Cleaning, Upgrading and Utilisation. *Renewable and Sustainable Energy Reviews* **2015**, *51*, 521–532. https://doi.org/10.1016/j.rser.2015.06.029.

(19) Baena-Moreno, F. M.; Sebastia-Saez, D.; Pastor-Pérez, L.; Reina, T. R. Analysis of the Potential for Biogas Upgrading to Syngas via Catalytic Reforming in the United Kingdom. *Renewable and Sustainable Energy Reviews* **2021**, *144*, 110939. https://doi.org/10.1016/j.rser.2021.110939.

(20) *Sorgenia:your next energy*. https://www.sorgenia.it/guida-energia/impianto-biogas-come-funziona.

(21) Santos, R. G. dos; Alencar, A. C. Biomass-Derived Syngas Production via Gasification Process and Its Catalytic Conversion into Fuels by Fischer Tropsch Synthesis: A Review. *International Journal of Hydrogen Energy* **2020**, *45* (36), 18114–18132. https://doi.org/10.1016/j.ijhydene.2019.07.133.

(22) Solarte-Toro, J. C.; Chacón-Pérez, Y.; Cardona-Alzate, C. A. Evaluation of Biogas and Syngas as Energy Vectors for Heat and Power Generation Using Lignocellulosic Biomass as Raw Material. *Electronic Journal of Biotechnology* **2018**, *33*, 52–62. https://doi.org/10.1016/j.ejbt.2018.03.005.

(23) Noh, Y.-G.; Lee, Y. J.; Kim, J.; Kim, Y. K.; Ha, J.; Kalanur, S. S.; Seo, H. Enhanced Efficiency in CO2-Free Hydrogen Production from Methane in a Molten Liquid Alloy Bubble Column Reactor with Zirconia Beads. *Chemical Engineering Journal* **2022**, *428*, 131095. https://doi.org/10.1016/j.cej.2021.131095.

(24) Vita, A.; Italiano, C. Fuel and Hydrogen Related Problems for Conventional Steam Reforming of Natural Gas. In *Current Trends and Future Developments on (Bio-) Membranes*; Elsevier, 2020; pp 71–89. https://doi.org/10.1016/B978-0-12-816778-6.00004-7.

(25) Arora, S.; Prasad, R. An Overview on Dry Reforming of Methane: Strategies to Reduce Carbonaceous Deactivation of Catalysts. *RSC Adv.* **2016**, *6* (110), 108668–108688. https://doi.org/10.1039/C6RA20450C.

(26) Zhao, Z.; Uddi, M.; Tsvetkov, N.; Yildiz, B.; Ghoniem, A. F. Redox Kinetics Study of Fuel Reduced Ceria for Chemical-Looping Water Splitting. *J. Phys. Chem. C* **2016**, *120* (30), 16271–16289. https://doi.org/10.1021/acs.jpcc.6b01847.

(27) Mantripragada, H. C.; Veser, G. Hydrogen Production via Chemical Looping Dry Reforming of Methane: Process Modeling and Systems Analysis. *AIChE Journal* **2022**, *68* (5). https://doi.org/10.1002/aic.17612.

(28) Ma, J.; Li, L.; Wang, H.; Du, Y.; Ma, J.; Zhang, X.; Wang, Z. Carbon Capture and Storage: History and the Road Ahead. *Engineering* **2022**, *14*, 33–43. https://doi.org/10.1016/j.eng.2021.11.024.

(29) Meylan, F. D.; Moreau, V.; Erkman, S. CO2 Utilization in the Perspective of Industrial Ecology, an Overview. *Journal of CO2 Utilization* **2015**, *12*, 101–108. https://doi.org/10.1016/j.jcou.2015.05.003.

(30) Muratori, M.; Calvin, K.; Wise, M.; Kyle, P.; Edmonds, J. Global Economic Consequences of Deploying Bioenergy with Carbon Capture and Storage (BECCS). *Environ. Res. Lett.* **2016**, *11* (9), 095004. https://doi.org/10.1088/1748-9326/11/9/095004.

(31) Mander, S.; Anderson, K.; Larkin, A.; Gough, C.; Vaughan, N. The Role of Bio-Energy with Carbon Capture and Storage in Meeting the Climate Mitigation Challenge: A Whole System Perspective. *Energy Procedia* **2017**, *114*, 6036–6043. https://doi.org/10.1016/j.egypro.2017.03.1739.

(32) Kanniche, M.; Gros-Bonnivard, R.; Jaud, P.; Valle-Marcos, J.; Amann, J.-M.; Bouallou, C. Pre-Combustion, Post-Combustion and Oxy-Combustion in Thermal Power Plant for CO2 Capture. *Applied Thermal Engineering* **2010**, *30* (1), 53–62. https://doi.org/10.1016/j.applthermaleng.2009.05.005.

(33) Stanger, R.; Wall, T.; Spörl, R.; Paneru, M.; Grathwohl, S.; Weidmann, M.; Scheffknecht, G.; McDonald, D.; Myöhänen, K.; Ritvanen, J.; Rahiala, S.; Hyppänen, T.; Mletzko, J.; Kather, A.; Santos, S. Oxyfuel Combustion for CO2 Capture in Power Plants. *International Journal of Greenhouse Gas Control* **2015**, *40*, 55–125. https://doi.org/10.1016/j.ijggc.2015.06.010.

(34) Farrelly, D. J.; Everard, C. D.; Fagan, C. C.; McDonnell, K. P. Carbon Sequestration and the Role of Biological Carbon Mitigation: A Review. *Renewable and Sustainable Energy Reviews* **2013**, *21*, 712–727. https://doi.org/10.1016/j.rser.2012.12.038.

(35) Blamey, J.; Anthony, E. J.; Wang, J.; Fennell, P. S. The Calcium Looping Cycle for Large-Scale CO2 Capture. *Progress in Energy and Combustion Science* **2010**, *36* (2), 260–279. https://doi.org/10.1016/j.pecs.2009.10.001.

(36) Stampi-Bombelli, V.; van der Spek, M.; Mazzotti, M. Analysis of Direct Capture of $${\hbox {CO}}_{2}$$ from Ambient Air via Steam-Assisted Temperature–Vacuum Swing Adsorption. *Adsorption* **2020**, *26* (7), 1183–1197. https://doi.org/10.1007/s10450-020-00249-w.

(37) Fasihi, M.; Efimova, O.; Breyer, C. Techno-Economic Assessment of CO2 Direct Air Capture Plants. *Journal of Cleaner Production* **2019**, *224*, 957–980. https://doi.org/10.1016/j.jclepro.2019.03.086.

(38) Lackner, K. S. The Thermodynamics of Direct Air Capture of Carbon Dioxide. *Energy* **2013**, *50*, 38–46. https://doi.org/10.1016/j.energy.2012.09.012.

(39) Darunte, L. A.; Terada, Y.; Murdock, C. R.; Walton, K. S.; Sholl, D. S.; Jones, C. W. Monolith-Supported Amine-Functionalized Mg $_2$ (Dobpdc) Adsorbents for CO $_2$ Capture. *ACS Appl. Mater. Interfaces* **2017**, *9* (20), 17042–17050. https://doi.org/10.1021/acsami.7b02035.

(40) DeWitt, S. J. A.; Sinha, A.; Kalyanaraman, J.; Zhang, F.; Realff, M. J.; Lively, R. P. Critical Comparison of Structured Contactors for Adsorption-Based Gas Separations. *Annu. Rev. Chem. Biomol. Eng.* **2018**, *9* (1), 129–152. https://doi.org/10.1146/annurev-chembioeng-060817-084120.

(41) Rezaei, F.; Webley, P. Optimum Structured Adsorbents for Gas Separation Processes. *Chemical Engineering Science* **2009**, *64* (24), 5182–5191. https://doi.org/10.1016/j.ces.2009.08.029.

(42) Marchese, M.; Buffo, G.; Santarelli, M.; Lanzini, A. CO2 from Direct Air Capture as Carbon Feedstock for Fischer-Tropsch Chemicals and Fuels: Energy and Economic Analysis. *Journal of CO2 Utilization* **2021**, *46*, 101487. https://doi.org/10.1016/j.jcou.2021.101487.

(43) Tregambi, C.; Bareschino, P.; Hanak, D. P.; Montagnaro, F.; Pepe, F.; Mancusi, E. Modelling of an Integrated Process for Atmospheric Carbon Dioxide Capture and Methanation. *Journal of Cleaner Production* **2022**, *356*, 131827. https://doi.org/10.1016/j.jclepro.2022.131827.

(44) Drechsler, C.; Agar, D. W. Intensified Integrated Direct Air Capture - Power-to-Gas Process Based on H2O and CO2 from Ambient Air. *Applied Energy* **2020**, *273*, 115076. https://doi.org/10.1016/j.apenergy.2020.115076.

(45) Sovacool, B. K.; Baum, C. M.; Low, S.; Roberts, C.; Steinhauser, J. Climate Policy for a Net-Zero Future: Ten Recommendations for Direct Air Capture. *Environ. Res. Lett.* **2022**, *17* (7), 074014. https://doi.org/10.1088/1748-9326/ac77a4.

(46) Godin, J.; Liu, W.; Ren, S.; Xu, C. C. Advances in Recovery and Utilization of Carbon Dioxide: A Brief Review. *Journal of Environmental Chemical Engineering* **2021**, *9* (4), 105644. https://doi.org/10.1016/j.jece.2021.105644.

(47) Forutan, H. R.; Karimi, E.; Hafizi, A.; Rahimpour, M. R.; Keshavarz, P. Expert Representation Chemical Looping Reforming: A Comparative Study of Fe, Mn, Co and Cu as Oxygen Carriers Supported on Al 2 O 3. *Journal of Industrial and Engineering Chemistry* **2015**, *21*, 900–911. https://doi.org/10.1016/j.jiec.2014.04.031.

(48) Löfberg, A.; Guerrero-Caballero, J.; Kane, T.; Rubbens, A.; Jalowiecki-Duhamel, L. Ni/CeO 2 Based Catalysts as Oxygen Vectors for the Chemical Looping Dry Reforming of Methane for Syngas Production. *Applied Catalysis B: Environmental* **2017**, *212*, 159–174. https://doi.org/10.1016/j.apcatb.2017.04.048.

(49) Guerrero-Caballero, J.; Kane, T.; Haidar, N.; Jalowiecki-Duhamel, L.; Löfberg, A. Ni, Co, Fe Supported on Ceria and Zr Doped Ceria as Oxygen Carriers for Chemical Looping Dry Reforming of Methane. *Catalysis Today* **2019**, *333*, 251–258. https://doi.org/10.1016/j.cattod.2018.11.064.

(50) Zhao, X.; Zhou, H.; Sikarwar, V. S.; Zhao, M.; Park, A.-H. A.; Fennell, P. S.; Shen, L.; Fan, L.-S. Biomass-Based Chemical Looping Technologies: The Good, the Bad and the Future. *Energy Environ. Sci.* **2017**, *10* (9), 1885–1910. https://doi.org/10.1039/C6EE03718F.

(51) Alvarez-Galvan, C.; Melian, M.; Ruiz-Matas, L.; Eslava, J. L.; Navarro, R. M.; Ahmadi, M.; Roldan Cuenya, B.; Fierro, J. L. G. Partial Oxidation of Methane to Syngas Over Nickel-Based Catalysts: Influence of Support Type, Addition of Rhodium, and Preparation Method. *Front. Chem.* **2019**, *7*, 104. https://doi.org/10.3389/fchem.2019.00104.

(52) Alipour, Z.; Babu Borugadda, V.; Wang, H.; Dalai, A. K. Syngas Production through Dry Reforming: A Review on Catalysts and Their Materials, Preparation Methods and Reactor Type. *Chemical Engineering Journal* **2023**, *452*, 139416. https://doi.org/10.1016/j.cej.2022.139416.

(53) Zhu, M.; Song, Y.; Chen, S.; Li, M.; Zhang, L.; Xiang, W. Chemical Looping Dry Reforming of Methane with Hydrogen Generation on Fe2O3/Al2O3 Oxygen Carrier. *Chemical Engineering Journal* **2019**, *368*, 812–823. https://doi.org/10.1016/j.cej.2019.02.197.

(54) Abanades, S.; Flamant, G. Thermochemical Hydrogen Production from a Two-Step Solar-Driven Water-Splitting Cycle Based on Cerium Oxides. *Solar Energy* **2006**, *80* (12), 1611–1623. https://doi.org/10.1016/j.solener.2005.12.005.

(55) Nolan, M.; Parker, S. C.; Watson, G. W. The Electronic Structure of Oxygen Vacancy Defects at the Low Index Surfaces of Ceria. *Surface Science* **2005**, *595* (1–3), 223–232. https://doi.org/10.1016/j.susc.2005.08.015.

(56) Haeussler, A.; Abanades, S.; Julbe, A.; Jouannaux, J.; Cartoixa, B. Two-Step CO2 and H2O Splitting Using Perovskite-Coated Ceria Foam for Enhanced Green Fuel Production in a Porous Volumetric Solar Reactor. *Journal of CO2 Utilization* **2020**, *41*, 101257. https://doi.org/10.1016/j.jcou.2020.101257.

(57) Jeong, H. H.; Kwak, J. H.; Han, G. Y.; Yoon, K. J. Stepwise Production of Syngas and Hydrogen through Methane Reforming and Water Splitting by Using a Cerium Oxide Redox System. *International Journal of Hydrogen Energy* **2011**, *36* (23), 15221–15230. https://doi.org/10.1016/j.ijhydene.2011.08.079.

(58) Zheng, Y.; Li, K.; Wang, H.; Tian, D.; Wang, Y.; Zhu, X.; Wei, Y.; Zheng, M.; Luo, Y. Designed Oxygen Carriers from Macroporous LaFeO3 Supported CeO2 for Chemical-Looping Reforming of Methane. *Applied Catalysis B: Environmental* **2017**, *202*, 51–63. https://doi.org/10.1016/j.apcatb.2016.08.024.

(59) Miccio, F.; Landi, E.; Murri, A. N.; Minelli, M.; Doghieri, F.; Storione, A. Fluidized Bed Reforming of Methane by Chemical Looping with Cerium Oxide Oxygen Carriers. *Chemical Engineering Research and Design* **2023**, *191*, 568–577. https://doi.org/10.1016/j.cherd.2023.02.007.

(60) Chuayboon, S.; Abanades, S.; Rodat, S. Solar Chemical Looping Reforming of Methane Combined with Isothermal H2O/CO2 Splitting Using Ceria Oxygen Carrier for Syngas Production. *Journal of Energy Chemistry* **2020**, *41*, 60–72. https://doi.org/10.1016/j.jechem.2019.05.004.

(61) Krenzke, P. T.; Fosheim, J. R.; Zheng, J.; Davidson, J. H. Synthesis Gas Production via the Solar Partial Oxidation of Methane-Ceria Redox Cycle: Conversion, Selectivity, and Efficiency. *International Journal of Hydrogen Energy* **2016**, *41* (30), 12799–12811. https://doi.org/10.1016/j.ijhydene.2016.06.095.

(62) Warren, K. J.; Carrillo, R. J.; Greek, B.; Hill, C. M.; Scheffe, J. R. Solar Reactor Demonstration of Efficient and Selective Syngas Production via Chemical-Looping Dry Reforming of Methane over Ceria. *Energy Technol.* **2020**, *8* (6), 2000053. https://doi.org/10.1002/ente.202000053.

(63) Warren, K. J.; Scheffe, J. R. Kinetic Insights into the Reduction of Ceria Facilitated via the Partial Oxidation of Methane. *Materials Today Energy* **2018**, *9*, 39–48. https://doi.org/10.1016/j.mtener.2018.05.001.

(64) Chuayboon, S.; Abanades, S.; Rodat, S. Syngas Production via Solar-Driven Chemical Looping Methane Reforming from Redox Cycling of Ceria Porous Foam in a Volumetric Solar Reactor. *Chemical Engineering Journal* **2019**, *356*, 756–770. https://doi.org/10.1016/j.cej.2018.09.072.

(65) Hill, C.; Robbins, R.; Furler, P.; Ackermann, S.; Scheffe, J. Kinetic Investigation of Solar Chemical Looping Reforming of Methane over Ni–CeO_2 at Low Temperature. *Sustainable Energy Fuels* **2023**, *7* (2), 574–584. https://doi.org/10.1039/D2SE01452A.

(66) Han, Y.; Tian, M.; Wang, C.; Kang, Y.; Kang, L.; Su, Y.; Huang, C.; Zong, T.; Lin, J.; Hou, B.; Pan, X.; Wang, X. Highly Active and Anticoke Ni/CeO_2 with Ultralow Ni Loading in Chemical Looping Dry Reforming via the Strong Metal–Support Interaction. *ACS Sustainable Chem. Eng.* **2021**, *9* (51), 17276–17288. https://doi.org/10.1021/acssuschemeng.1c06079.

Acknowledgments

Incredibly these three years of PhD flew by, and it is already time to start remembering them from the beginning to thank all the many people who made this path so worth noting it.

I would like to start with all of those who initially have directed me down to this path.

I thank Prof Alessandro Paglianti and Prof Giuseppina Montante for have being great teachers who made me passionate about the topics of chemical engineering helping me to find my road, and I thank Eng. Francesco Miccio for introducing me to the people I work with and for always bring good vibes in the group.

I would like to thank my advisor, Prof. Ferruccio Doghieri, for believing in my abilities over my PhD and after. I also thank him for everything he taught me and for always listening to me when I needed it.

Thanks to Prof Grazia de Angelis for her kindness, that make me feel at home since day one.

And definitely thanks to Prof. Matteo Minelli, more fundamental than everything, for guiding me along this path with great patience and for his constant availability. Thank you, Matteo, for all you taught me and for being a reference point for me over the years.

I sincerely thank Prof Marco Mazzotti and all the SPL group of ETH, especially Valentina. I lived some of the best months of my life in Zurich thanks to all of them. Thank you, Marco, for the opportunity you gave me to stay there longer.

I thank all the colleagues I have had over the years, most of whom are now dear friends.

First of all, thank you Kseniya for all our time together, I really appreciate how much you trust in me, and the esteem you have always shown me has been of great support to me, also during my PhD.

Thanks to Francesco, Eleonora, and Riccardo, “the seniors” for all the help, the advice, and the support they gave me.

Thanks to Elena, Miquel, Carla, Sara G, Marco, Sara C, Omar, Elisa, Virginia, Enrico, Mattia, Giacomo, Lorenzo and to all the professors and technicians of my research group for making Labic, a special place where to go work every day, a second home (Let’s say second...).

Thanks to my friends Giulia, Charles, Francesca, Erica, Lin, Michelle, Baptiste, Carla for the support in the most difficult times and for all the good moments spent together.

Thanks to my family. It is obvious to say that without them I would not have arrived here.